
Simulating inflation and phase transitions with *CosmoLattice*

by

Joel Wesenberg

October 2024

Master's thesis in Physics

Prepared at:

Institute for Theoretical Particle Physics and Cosmology,
RWTH Aachen University

Submitted to:

The Faculty of Mathematics, Computer Science and Natural Science,
RWTH Aachen University

Under the supervision of:

1st Examiner: Prof. Dr. Julien Lesgourgues, **RWTH Aachen University**
2nd Examiner: Dr. Christian Fidler, **RWTH Aachen University**

Abstract

RWTH Aachen University
Institute for Theoretical Particle Physics and Cosmology
Master of Science
by Joel Wesenberg

The early universe has always been a fascinating epoch for cosmologists, as it offers insights into many previously unknown physical processes and potential shortcomings in the Λ CDM model. The most prominent approach to describing this era is the model of cosmic inflation, which posits that the universe underwent a phase of exponential expansion. This thesis explores the foundational principles of cosmic inflation, focusing on two specific inflationary models: a single-field model with a quadratic potential and a hybrid inflation model. The work derives the key theoretical equations governing each model and evaluates the accuracy of these equations through numerical simulations. Using the software *CosmoLattice*, the study compares the theoretical predictions with simulated data to assess the validity of *CosmoLattice* as a reliable tool for simulating different inflationary scenarios.

Acknowledgements

I would like to take this opportunity to express my deepest gratitude to all those who have accompanied and supported me both in my academic journey and in my personal life over the past few years. First and foremost, I wish to extend my heartfelt thanks to my supervisor, Julien Lesgourgues, for giving me the opportunity to work on this project and for allowing me to be part of the scientific process within this wonderful research group. He was always available to answer my questions and made time for me, no matter how many times I might have annoyed him with my interim results and questions during his work. I would also like to offer a special thanks to Devanshu Sharma, who was always ready to assist me with questions and contributed valuable ideas and suggestions during our discussions. A huge thank you also goes to my fellow students and office colleagues Simon Neuland, Tyler Jeitz, and Erik de la Haye. Not only did you help me with general questions about programming or physics, but you also became true friends over this past year. No matter how things were going, I always looked forward to seeing you, and I am incredibly grateful for the experiences we shared. I sincerely hope that our paths will cross again in the future. I would also like to thank the rest of the research group – it has been a pleasure getting to know each and every one of you.

The greatest thanks, however, go to my family. Mom, Dad, all the successes I've had in life are thanks to you, as you've always done everything in your power to make my dreams possible. Mom, I know how much you sacrificed for me, and for all of us, to give me the life that no one ever wanted to give you. You've spent countless hours helping me with all sorts of problems, taking them on as if they were your own. I can't even put into words what an incredibly strong person you are. With your help, I always knew I could achieve anything, and I knew that you and Dad would always be there for me, for which I am endlessly grateful. Dad, like Mom, you have always given everything for me without asking for anything in return because it was natural to you. I know you may sometimes think I don't appreciate it, but I want you to know how thankful I am for everything you've done for me and for the entire family. I am also incredibly proud to call you my father. I dedicate this thesis to both of you and hope that it can give something back, showing that I've made you proud.

Finally, I want to thank my brother, who has always stood by me in so many challenges. Marvin, you are not just my brother, but over the past few years, you've become the person I trust most. I hope now that my work is done, we can spend more time together, and I'm really looking forward to it! The love and support you all have given me, I hope to shape into something great and share it with the world.

Contents

Abstract	iii
Acknowledgements	v
1 Introduction to inflation	1
1.1 Basics of general relativity	1
1.2 The homogeneous and isotropic universe	3
1.2.1 Basics of the standard cosmological model	4
1.2.2 The horizon problem	6
1.2.3 The flatness problem	10
1.3 The problem of initial conditions	11
2 Mathematical description of single-field inflation	13
2.1 Background evolution: scalar field dynamics	13
2.2 Cosmological perturbation theory	18
2.2.1 General metric of first order	19
2.2.2 Gauge transformations	20
2.2.3 Fourier space description and SVT decomposition	24
2.3 Einstein equations for SVT perturbations	30
2.3.1 Scalar perturbations	30
2.3.2 Vector perturbations	36
2.3.3 Tensor perturbations	37
3 Measurable quantities of inflation	39
3.1 Introduction of the power spectrum	39
3.2 Power spectrum of curvature perturbation	40
3.3 Model parameters of inflaton	42
4 Lattice simulation of single-field Inflation	45
4.1 Introduction to <i>CosmoLattice</i>	45
4.2 Simulation of quadratic model	48
5 Theory and simulation of hybrid inflation model	53
5.1 Inflaton background dynamics	55
5.2 Waterfall field dynamics	56
5.3 Calculation of curvature perturbation	59
5.4 Results	62

5.4.1	Results for background	62
5.4.2	Results for curvature power spectrum	65
6	Conclusion and outlook	73
A	Scalar perturbations	75
A.1	Gauge transformation of scalar perturbation	75
A.2	Conservation of curvature perturbation	76
B	Single field model	77
B.1	Plots for single field	77
C	Hybrid inflation model	79
C.1	Curvature perturbation for multiple fields	79
C.2	Simulations versus 1-loop power spectra	80
	Bibliography	83

Chapter 1

Introduction to inflation

In the field of cosmology, the theory of "cosmic inflation" broadly describes the exponential expansion of space in the early universe. It involves a class of models that enable a rapid expansion of space within fractions of a second after the Big Bang. The theory was developed in the late 1970s and early 1980s by various theoretical physicists such as Starobinsky [1], Guth [2], and Linde [3] to explain several observations like the large-scale structures in the cosmos, the cosmic microwave background (CMB), and other phenomena. The idea behind this work is to clarify the fundamental concept of inflation, understand the nonlinear dynamics of the early universe using the simulation program *CosmoLattice*, and compare the predictions of two inflationary models. A significant part of the paper will therefore also address the limitations and possibilities of *CosmoLattice* as a tool for understanding the early universe. This chapter serves as an introduction to the theory and motivation behind inflation.

1.1 Basics of general relativity

In general, Cosmology deals with the nature and development of the observable universe, the understanding and dynamics of its structures, and its ultimate fate. For this description, a mathematical framework is required, which is provided by Einstein's general theory of relativity. This theory describes, through the Einstein field equations [4]

$$R_{\mu\nu} - \frac{1}{2}Rg_{\mu\nu} = \frac{8\pi G}{c^4}T_{\mu\nu} \quad (1.1)$$

the non-linear evolution of the metric tensor field $g_{\mu\nu}$. They explain how spacetime curvature responds to the presence of energy and momentum.

Here, $T_{\mu\nu}$, also known as the energy-momentum tensor, describes the matter content of the physical system under consideration, and $g_{\mu\nu}$ represents the corresponding geometry of spacetime. R is the Ricci scalar given by $R \equiv R_{\mu\nu}g^{\mu\nu}$, where $R_{\mu\nu}$ is called the Ricci tensor, which is given by

$$R_{\mu\nu} \equiv R_{\mu\alpha\nu}^{\alpha} = \Gamma_{\mu\nu,\alpha}^{\alpha} - \Gamma_{\mu\alpha,\nu}^{\alpha} + \Gamma_{\delta\alpha}^{\alpha}\Gamma_{\nu\mu}^{\delta} - \Gamma_{\delta\nu}^{\alpha}\Gamma_{\alpha\mu}^{\delta}. \quad (1.2)$$

The Ricci tensor can be broadly understood as a way to quantify how much the geometry of a given metric tensor $g_{\mu\nu}$ deviates from the flat geometry of Euclidean space in a localized region and is linked to the Christoffel symbols $\Gamma_{\mu\nu}^{\alpha}$, which themselves are directly linked to the metric tensor $g_{\mu\nu}$ through the following relationship:

$$\Gamma_{\mu\nu}^{\alpha} = \frac{1}{2}g^{\alpha\beta}(g_{\mu\beta,\nu} + g_{\beta\nu,\mu} - g_{\mu\nu,\beta}). \quad (1.3)$$

In general, the methodology for solving the Einstein equations involves choosing an appropriate ansatz for the metric suitable for the given problem, substituting it into the left-hand side of the equations, and then matching it with the energy-momentum distribution of the system through an appropriate choice of $T_{\mu\nu}$.

This method will also be crucial in addressing cosmological questions in the next section, which is why the general approach will be briefly explained below.

1. Setting Symmetries:

- First, one needs to determine the symmetries of the physical system (e.g., spherical symmetry)
 - ⇒ These symmetries then simplify the form of the metric and reduce the number of independent functions in the Einstein equations

2. Choosing a Metric:

- Based on the symmetries, one has to select an appropriate metric (e.g., Schwarzschild metric for spherical symmetry)
- The metric should describe the geometry of spacetime respecting the imposed symmetries

3. Calculating Connection and Curvature Tensors:

- Next, one needs to compute the Christoffel symbols $\Gamma_{\mu\nu}^{\alpha}$, Ricci tensor $R_{\mu\nu}$ and Ricci scalar R for the chosen metric
 - ⇒ These calculations provide the left-hand side for the Einstein equations

4. Formulating the Einstein Equations:

- The right-hand side of the Einstein equations is given by the energy-momentum tensor $T_{\mu\nu}$ which can be chosen arbitrarily, as long as it respects the symmetry of the metric
- In cosmology, fields that describe elementary particles are commonly used to characterize the matter content of our cosmos

5. Solving the Equations:

- At last, the resulting equations, which are typically coupled nonlinear partial differential equations, have to be solved
 \Rightarrow There are analytical solutions in some cases, but numerical methods are often required for more complex or less symmetric scenarios

1.2 The homogeneous and isotropic universe

Albert Einstein's paper published in 1917 is considered the birth of modern cosmology, as it provides a description of the relativistic dynamics of the entire universe, as discussed in [5].

He attempted to find a solution to his field equations that would allow for a static and spatially closed universe, which is also homogeneous and isotropic on large scales. His considerations led him to the following expression for the so-called line element in spherical coordinates:

$$ds^2 \equiv dx^\mu g_{\mu\nu} dx^\nu = -c^2 dt^2 - R_{rad.}^2 \left(\frac{dr^2}{1 - kr^2} + r^2 d\theta^2 + r^2 \sin^2(\theta) d\phi^2 \right), \quad (1.4)$$

where $R_{rad.}$ can be thought of the radius of the cosmos, whereas k describes the spatial curvature of the universe.

Here, the line element can be understood as the infinitesimal square distance in four-dimensional spacetime, associated with an infinitesimal displacement vector at each coordinate point in this metric space. Therefore, it contains information about the structure of spacetime and is thus linked to the metric tensor through the above relation.

Einstein chose to model the energy-momentum tensor $T_{\mu\nu}$ as that of a perfect fluid filling the entire cosmos,

$$T_{\mu\nu} = \text{diag}(-\rho, p, p, p) \quad (1.5)$$

albeit with a negligible pressure $p = 0$. However, to resolve inconsistencies regarding the radius R , he had to augment the left-hand side of the Einstein Equations 1.1 by a constant value coupled to the metric: $-\Lambda g_{\mu\nu}$. This extension led to a static universe with a finite radius $R_{rad.} = \frac{1}{\sqrt{\Lambda}}$ and a value of the so-called cosmological constant of $\Lambda = \frac{4\pi G\rho}{c^2}$. Over time, however, some physicists recognized that his model was unstable with respect to small perturbations in the matter density field.

The next major development in applying general relativity to the entire universe came from Friedmann's paper published in 1922 [6]. Taking into account the isotropy and homogeneity of space, now known as the cosmological principle, he derived the most general solution to Einstein's field equations:

$$ds^2 = -c^2 dt^2 + a(t)^2 \left(\frac{dr^2}{1 - kr^2} + r^2 d\theta^2 + r^2 \sin^2(\theta) d\phi^2 \right). \quad (1.6)$$

This solution allowed for a time-varying scale factor $a(t)$, which characterizes the relative size of spacelike hypersurfaces at different times, instead of having a constant factor $R_{rad.}$. As an approach for the energy-momentum tensor, he also used the model of a perfect fluid, as in equation 1.5, which gives rise to the well-known Friedman equations that describe the dynamics of an expanding universe (even when $\Lambda \neq 0$)

$$H^2 \equiv \frac{\dot{a}^2}{a^2} = \frac{8\pi G\rho}{3} - \frac{kc^2}{a^2} + \frac{\Lambda c^2}{3}, \quad (1.7)$$

$$\dot{H} + H^2 = \frac{\ddot{a}}{a} = -\frac{4\pi G}{3c^2} (\rho c^2 + 3p) + \frac{\Lambda c^2}{3}. \quad (1.8)$$

From the second equation, it can be seen that in an expanding universe ($\dot{a} > 0$) with ordinary matter that satisfies the strong energy condition ($\rho c^2 + 3p \geq 0$), no accelerated expansion of the universe occurs, unless $\Lambda \neq 0$.

1.2.1 Basics of the standard cosmological model

The previous equations 1.7 and 1.8 can be used to make statements about the time evolution of the homogeneous universe, as shown in [7]. Initially, these can be simplified by considering that the measured curvature of the universe is relatively small, $k \approx 0$. Furthermore, with a clever choice of unit system where $8\pi G = 1$ and $c = 1$, the following equation results after combining the two:

$$\frac{d\rho}{dt} + 3H(\rho + p) = 0. \quad (1.9)$$

This can also be written as

$$\frac{d \ln \rho}{d \ln a} = -3(1 + \omega), \quad (1.10)$$

where the equation of state parameter ω was defined via $\omega \equiv \frac{p}{\rho}$.

For most of the history of the universe, a single type of matter or radiation dominated at any given time, each with constant but different equation of state parameters ω . This allows the above differential equation to be analytically solved by integration. Substituting the solution into 1.7 yields the following functional dependence for the scale factor:

$$a(t) \propto \begin{cases} t^{2/3(1+\omega)} & \omega \neq -1, \\ e^{Ht} & \omega = -1. \end{cases} \quad (1.11)$$

	ω	$\rho(a)$	$a(t)$
matter dom. (MD)	0	a^{-3}	$t^{2/3}$
radiation dom. (RD)	$\frac{1}{3}$	a^{-4}	$t^{1/2}$
Λ dom. (Λ AD)	-1	a^0	e^{Ht}

TABLE 1.1: Solution of Friedman equations with $k=0$ for matter-, radiation- and cosmological constant domination

The solution of Equation 1.10 for various types of matter species indicates that their energy densities dilute at different rates throughout the universe's evolution. This results in various epochs where different matter species have dominated the cosmological expansion (cosmological hierarchy), as illustrated in Figure 1.1.

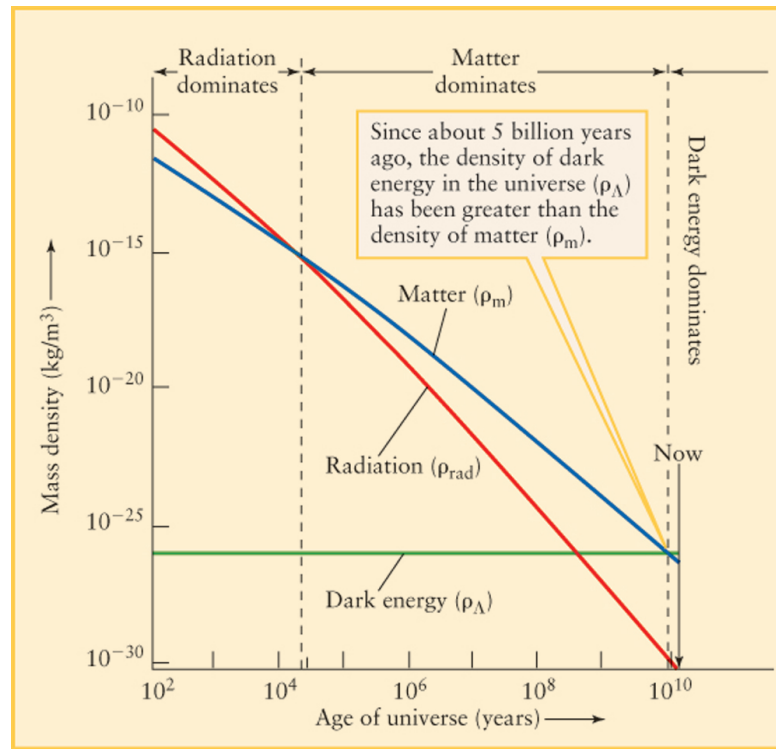


FIGURE 1.1: Evolution of the cosmological hierarchy of our universe without curvature.

1.2.2 The horizon problem

It is an exceedingly important philosophical question whether the Standard Cosmological Model, with its cosmological hierarchy, should be able to explain the initial conditions of the universe. The following discussion on this topic in this chapter is mainly based on [7].

On one hand, one can argue that initial conditions do not necessarily have to be part of the given theory, as it depends on whether a specific theory can satisfactorily explain a physical phenomenon with a given set of initial conditions. On the other hand, the fundamental task of physics is to explain natural events, including the choice of parameters within a theory. Fundamentally, this issue can be summarized as a fine-tuning problem. From a scientific perspective, it is highly unsatisfying that the universe could evolve to its current state solely due to strongly fine-tuned parameters.

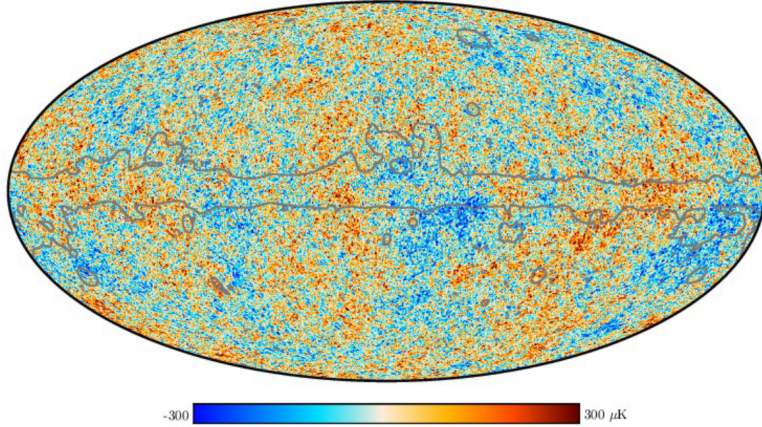


FIGURE 1.2: Map of the CMB anisotropies $\delta T(\theta, \phi)$ in units of micro-Kelvin, taken from [8]. The data represents temperature differences on a sphere (last scattering surface) projected on an ellipse.

Such a problem arises in the Standard Cosmological Model concerning relative density fluctuations, as one can see in Figure 1.2. The picture illustrates that the universe, in an early phase, was in a very homogeneous state with density fluctuations of the order of $\mathcal{O}(10^{-4})$. Since inhomogeneities are gravitationally unstable, implying that the universe was in an even more homogeneous state in an earlier phase, the question arises as to why this smoothness occurred and how it can be explained.

To better describe this issue mathematically, one must first recognize that the causal structure of FLRW-spacetime, given in 1.6, is determined by the propagation of light. Photons are massless and therefore follow trajectories with $ds^2 = 0$. This means that they represent the fastest possible way to transmit information between two spatially separated points.

It is thus useful to define the so-called *comoving horizon*

$$r_H \equiv \int_{t_{ini}}^{t_{end}} \frac{dt'}{a(t')} = \int_{a_{ini}}^{a_{end}} \frac{da'}{Ha'^2} = \int_{a_{ini}}^{a_{end}} d\ln a' \left(\frac{1}{Ha'} \right), \quad (1.12)$$

which indicates the maximum coordinate distance that light can travel between the emission of a signal t_{ini} and the time $t_{end} > t_{ini}$. The difference between comoving and physical quantities lies in the fact that the former do not account for the expansion of the universe and therefore do not describe directly measurable quantities. For example, to obtain the *physical horizon*, the comoving horizon r_H must be multiplied by the scale factor at time t_{end} . Nevertheless, these quantities are of immense importance in cosmology, as they offer a way to represent many complex processes with greater mathematical simplicity, as shown in Figure 1.3. This Figure specifically uses what is known as *conformal time* $\tau = \int \frac{dt}{a(t)}$, which quantifies the amount of time a photon would need to travel a given distance if the expansion of the universe were to stop.

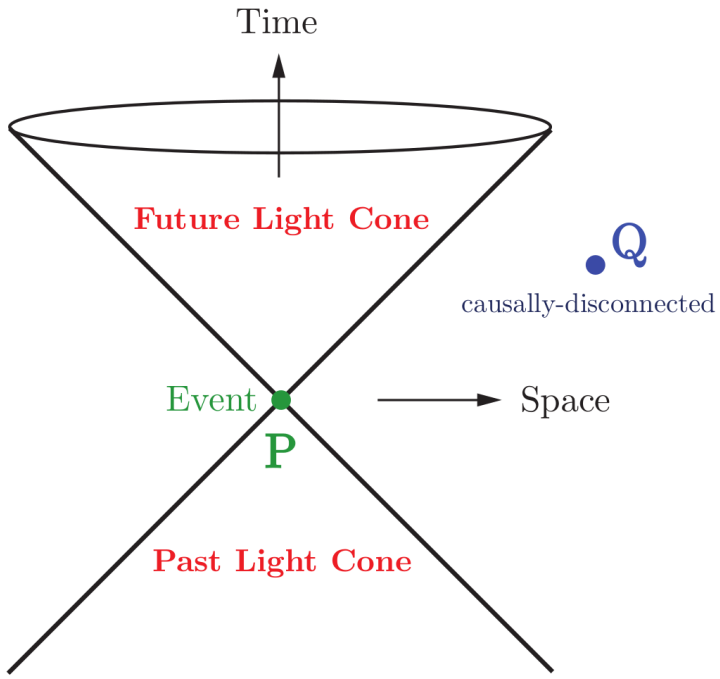


FIGURE 1.3: A light cone in comoving coordinates, used from [7]. Photons move along world lines with zero proper time ($ds^2 = 0$), known as *null geodesics*. Massive particles follow world lines with positive proper time ($ds^2 > 0$), referred to as *timelike geodesics*. Spacetime regions that are causally disconnected are separated by *spacelike intervals* ($ds^2 > 0$). The collection of all null geodesics passing through a specific point in spacetime forms the *light cone*. The interior of the light cone, comprising all null and timelike geodesics, defines the region of spacetime causally connected to that event.

In 1.12 the comoving horizon r_H was defined as an integral of the comoving Hubble radius, $(aH)^{-1}$, which will play an important role in inflation. By substituting the

solution in 1.11 for $\omega \neq -1$ into Equation 1.12, r_H is obtained as follows:

$$r_H \propto a^{\frac{1}{2}(1+3\omega)}. \quad (1.13)$$

This means that the comoving Hubble radius $(aH)^{-1}$, and consequently the comoving horizon r_H , grows monotonically in the standard cosmological model. In particular, during matter domination (MD) and radiation domination (RD), the following behavior is observed:

$$r_H = \int_{a_{ini}}^{a_{end}} \frac{da'}{Ha'^2} \propto \begin{cases} a & RD, \\ a^{1/2} & MD. \end{cases} \quad (1.14)$$

During RD and MD, the scale factor $a(t)$ grows according to a power law, and therefore, a Big Bang singularity exists at $t_{ini} = 0$. Thus, the comoving causal horizon for CMB photons is given by the integral of the comoving Hubble radius from the value of $a(t)$ at $t_{ini} = 0$ to its value at the time t_{LSS} , when the last scattering surface forms. t_{LSS} is the point in time when the fluctuations in the universe should be distributed as shown in Figure 1.2.

Figure 1.4 presents the conformal diagram for the standard Big Bang cosmology. Each point within this diagram has an associated past light cone, defining its causal history. Two points on a given surface with constant conformal time $\tau = const.$ are in causal contact if their past light cones intersect at the Big Bang, $\tau_i = 0$. Consequently, the surface of last scattering (τ_{LSS}) comprised numerous causally disconnected regions that could not exchange information to enable a smoothing of perturbations, illustrating the horizon problem.

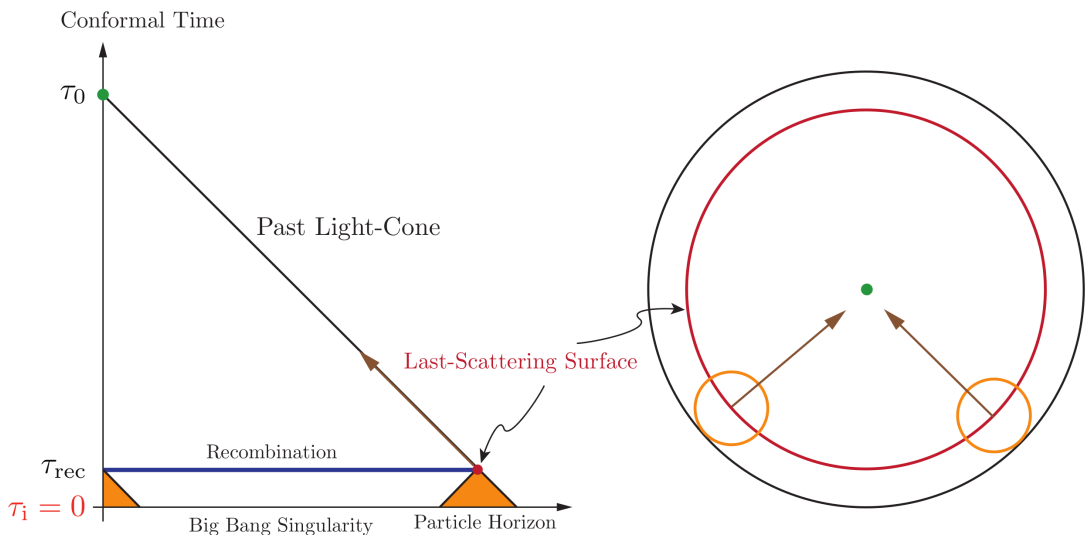


FIGURE 1.4: Conformal diagram of the standard cosmological model [7]. The CMB at last-scattering (τ_{rec}) consists of 10^5 causally disconnected regions.

The problem can be resolved by first understanding the difference between the comoving horizon r_H and the comoving Hubble radius $(aH)^{-1}$. If particles are separated by distances greater than r_H , they could never have interacted; if they are separated by distances greater than $(aH)^{-1}$, they cannot interact now. This distinction is crucial for resolving the horizon problem, which hinges on the possibility that r_H is much larger than $(aH)^{-1}$ today, implying that particles cannot interact now but were in causal contact early on. This scenario arises if the comoving Hubble radius was significantly larger in the early universe than it is now, necessitating a phase of decreasing Hubble radius. During inflation, H remains approximately constant while $a(t)$ grows exponentially, leading to a decreasing comoving Hubble radius, consistent with this requirement.

Since H remains approximately constant during inflation, the scale factor $a(\tau)$, expressed in conformal time, evolves like

$$a(\tau) = -\frac{1}{H\tau}, \quad (1.15)$$

and the singularity at $a = 0$ is pushed into the distant past as $\tau \rightarrow -\infty$.

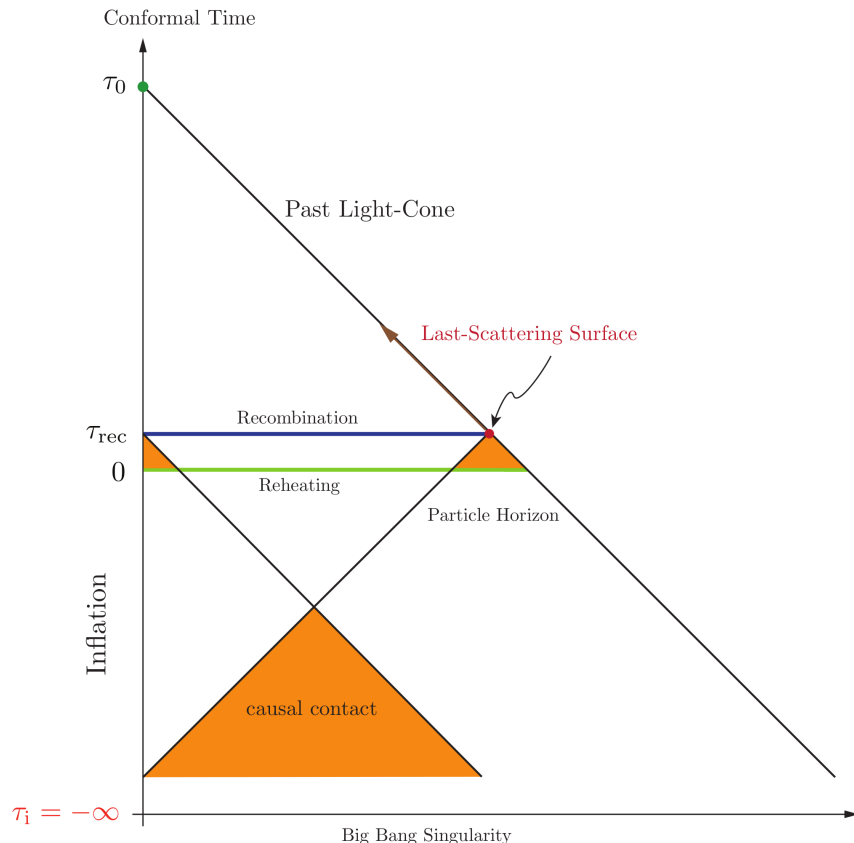


FIGURE 1.5: Conformal diagram of inflationary cosmology [7]. Inflation pushes conformal time into negative values, and the end of inflation creates an ‘apparent’ Big Bang at $\tau = 0$. However, there is no singularity at $\tau = 0$; if inflation persists long enough, light cones intersect at an earlier time.

In this model, $\tau = 0$ does not correspond to the Big Bang singularity but rather marks the end of inflation. Consequently, with $H \approx \text{const.}$, the initial singularity can be shifted arbitrarily far into the past in conformal time, allowing for more conformal time between the singularity and the time of recombination (LSS). This enables light cones to extend through the apparent Big Bang, bringing seemingly disconnected points into causal contact. This process is illustrated in Figure 1.5.

In summary, the following equivalent conditions are required in the early universe to solve the horizon problem:

$$\boxed{\frac{d}{dt} \left(\frac{1}{aH} \right) < 0 \quad \Leftrightarrow \quad \ddot{a} > 0 \quad \Leftrightarrow \quad \rho + 3p < 0.} \quad (1.16)$$

1.2.3 The flatness problem

The so-called flatness problem addresses the question of why the observable universe appears nearly flat, despite expectations from the standard cosmological model that curvature k should have influenced the universe's evolution for non-fine-tuned values. To quantify this problem mathematically, the Friedmann equation, taking curvature into account, can be used:

$$H^2 = \frac{1}{3}\rho(a) - \frac{k}{a^2}. \quad (1.17)$$

It can also be written as

$$\boxed{1 - \Omega(a) = \frac{-k}{(aH)^2}}, \quad (1.18)$$

where $\Omega(a)$ is given by

$$\Omega(a) \equiv \frac{\rho(a)}{\rho_{\text{crit}}(a)}, \quad \rho_{\text{crit}}(a) \equiv 3H(a)^2. \quad (1.19)$$

From Equation 1.18 one can see that flatness of the universe today corresponds to $\Omega(a_0) \approx 1$. However, in standard Big Bang cosmology the comoving Hubble radius $(aH)^{-1}$ grows with time and therefore the left-hand side of Equation 1.18 diverges, which implies that the critical value $\Omega = 1$ is an unstable fixed point. Therefore, without inflation the near-flatness observed today requires an extreme fine-tuning of Ω very close to 1 in the early universe. At the Planck scale, for example, the following condition must be satisfied to ensure the present-day flatness of the universe:

$$|\Omega(a_{\text{pl}}) - 1| \leq \mathcal{O}(10^{-61}). \quad (1.20)$$

Another way of formulating the horizon problem is looking at the following equation

$$\frac{d\Omega}{d \ln a} = (1 + 3\omega)\Omega(\Omega - 1), \quad (1.21)$$

which was derived by differentiating Equation 1.18 and making use of Equation 1.10. This makes clear that $\Omega = 1$ is indeed an unstable fixed point if the strong energy condition is fulfilled

$$\frac{d|\Omega - 1|}{d \ln a} > 0 \Leftrightarrow 1 + 3\omega > 0. \quad (1.22)$$

The solution to this problem is quite simple based on the knowledge from the last subsection. Assuming that there was a phase in the early universe that caused the Hubble radius to shrink, any initial values for the curvature k can be used, as a sufficiently long inflationary phase can always make the universe flat. The solution $\Omega = 1$ is now an attractor solution during inflation, when the strong energy condition is violated.

1.3 The problem of initial conditions

It is important to note that the flatness and horizon problems are not strict inconsistencies within the framework of the standard cosmological model. The model can accommodate a universe that evolves homogeneously if one assumes that the initial value of Ω was very close to unity and that the universe began with a high degree of homogeneity even beyond causal scales, combined with just the right level of inhomogeneity to account for structure formation. Under these assumptions, the universe will continue to evolve in a manner consistent with current observational data.

Thus, the flatness and horizon problems highlight significant limitations in the predictive power of the standard cosmological model rather than fundamental flaws. The model cannot predict the early universe's dramatic flatness but instead requires it as an initial condition. Similarly, the model does not explain the observed large-scale homogeneity of the universe but assumes it as a given. Consequently, a theory that provides a dynamic explanation for these initial conditions is highly appealing.

Chapter 2

Mathematical description of single-field inflation

Inflation is an extremely counter-intuitive physical process, as it causes the universe to expand by many orders of magnitude in fractions of a second, but it requires a violation of the strong energy condition. Therefore, a model must be sought that provides a negative pressure source. This chapter will address the physical conditions necessary to enable such an inflationary model, with Section 2.1 still following [7]. The focus will first be on the specific model that allows for a homogeneous and isotropic universe while addressing both the horizon and flatness problems. Subsequently, the theory of cosmological perturbations will be introduced, which enables the formation of structures in the universe and also serves as a means to satisfactorily explain the CMB data.

2.1 Background evolution: scalar field dynamics

One might assume that the simplest way to achieve an inflationary phase in the early universe is to allow the energy density of the universe to be dominated by a cosmological constant. This would result in $\omega = -1$, leading to negative pressure and thus a violation of the strong energy condition. The key issue, however, is that this constant energy density would cause the inflationary phase to persist indefinitely, preventing it from ever coming to an end. Therefore, conditions must be established that bring inflation to an end and lead to structure formation in the universe.

It turns out that the simplest model involves the early universe being filled with a scalar field, φ , which exhibits the properties of a perfect fluid. The physical nature of the field φ does not need to be specified. Instead, it is used as an order parameter to describe the

time evolution of the inflationary energy density. The dynamics of a (scalar) field that is (minimally) coupled to gravity can best be described through the so-called action:

$$S = \int d^4x \sqrt{-g} \left[\frac{1}{2}R - \frac{1}{2}g^{\mu\nu}\partial_\mu\varphi\partial_\nu\varphi - V(\varphi) \right]. \quad (2.1)$$

The advantage of formulating the physical model through the action lies in the ease with which simple modifications can be made by altering the corresponding terms. For instance, replacing R with a function $f(R)$ can change the geometry of spacetime, while adjusting the kinetic or potential terms modifies the form or structure of the energy-momentum tensor $T_{\mu\nu}$. The corresponding field equations are then obtained through the principle of least action by varying the action S with respect to the metric tensor $g_{\mu\nu}$, and the equation of motion for the field is derived through variation with respect to the field φ . This approach also facilitates generalizations to multiple fields.

In the case of a scalar field that is minimally coupled to standard Einstein gravity and possesses a canonical kinetic term, the following equations of motion arise for a spatially homogeneous field $\varphi(t, \mathbf{x}) \equiv \varphi(t)$ with dependence on cosmic time t

$$\frac{\delta S}{\delta \varphi} \Rightarrow \frac{1}{\sqrt{-g}}\partial_\mu(\sqrt{-g}\partial^\mu\varphi) + V_{,\varphi} = 0 \Leftrightarrow \ddot{\varphi} + 3H\dot{\varphi} + V_{,\varphi} = 0, \quad (2.2)$$

$$H^2 = \frac{1}{3M_{pl}^2} \left(\frac{1}{2}\dot{\varphi}^2 + V(\varphi) \right), \quad (2.3)$$

where the Planck mass was defined as $M_{pl}^2 \equiv \frac{1}{8\pi G}$ and the derivatives of potential and field are written as $V_{,\varphi} \equiv \frac{dV}{d\varphi}$ and $\dot{\varphi} \equiv \frac{d\varphi}{dt}$. The variation of the action with respect to the metric tensor $g_{\mu\nu}$ gives an expression for the energy-momentum tensor

$$T_{\mu\nu} = \partial_\mu\varphi\partial_\nu\varphi - g_{\mu\nu} \left(\frac{1}{2}\partial_\alpha\varphi\partial^\alpha\varphi + V(\varphi) \right). \quad (2.4)$$

Again, assuming the FLRW metric, given in Equation 1.6, for $g_{\mu\nu}$ and restricting to the case of a spatially homogeneous field $\varphi(t, \mathbf{x}) \equiv \varphi(t)$, the metric takes the form of a perfect fluid with the following values for the energy density ρ and the pressure p :

$$\rho = \frac{1}{2}\dot{\varphi}^2 + V(\varphi), \quad (2.5)$$

$$p = \frac{1}{2}\dot{\varphi}^2 - V(\varphi). \quad (2.6)$$

This results in a equation of state of

$$\omega = \frac{p}{\rho} = \frac{\frac{1}{2}\dot{\varphi}^2 - V(\varphi)}{\frac{1}{2}\dot{\varphi}^2 + V(\varphi)}, \quad (2.7)$$

which demonstrates that a scalar field can lead to a negative pressure ($\omega < 0$) and especially to accelerated expansion, if the potential energy $V(\varphi)$ dominates over the kinetic energy $\frac{1}{2}\dot{\varphi}^2$. Thus, the first condition for accelerated expansion driven by a scalar field can be expressed as

$$\frac{1}{2}\dot{\varphi}^2 \ll V(\varphi). \quad (2.8)$$

However, this condition is not sufficient for a prolonged phase of inflation, as it may be initially satisfied but can also be quickly violated. Therefore, it is necessary to additionally require that the time derivative of this inequality condition is also satisfied:

$$|\ddot{\varphi}| \ll |V_{,\varphi}|. \quad (2.9)$$

These two conditions can also be written in the form of the so-called *slow-roll parameters* ϵ and η

$$\varepsilon \equiv -\frac{\dot{H}}{H^2} = -\frac{d \ln H}{dN} < 1, \quad (2.10)$$

$$\eta \equiv -\frac{\ddot{\varphi}}{H\dot{\varphi}} = \varepsilon - \frac{1}{2\varepsilon} \frac{d\varepsilon}{dN} < 1, \quad (2.11)$$

where $dN = Hdt$ with N being referred to as the e-folding number, a crucial concept in inflation theory, which will be further discussed on the following page. Here, ϵ ensures that the relative change in the Hubble parameter is small, while η ensures that the fractional change of ϵ per e-fold is small. This guarantees a prolonged, approximately De Sitter expansion ($H = \text{const.}$).

By using these conditions, one can approximate the equations of motion as follows

$$H^2 \approx \frac{1}{3M_{\text{pl}}^2} V(\varphi) \approx \text{const.}, \quad (2.12)$$

$$\dot{\varphi} \approx -\frac{V_{,\varphi}}{3H}. \quad (2.13)$$

The slow-roll conditions can then be re-expressed in a manner that places constraints on the shape of the inflationary potential:

$$\boxed{\epsilon_v(\varphi) \equiv \frac{M_{\text{pl}}^2}{2} \left(\frac{V_{,\varphi}}{V} \right)^2}, \quad (2.14)$$

$$\boxed{\eta_v(\varphi) \equiv M_{\text{pl}}^2 \frac{V_{,\varphi\varphi}}{V}}. \quad (2.15)$$

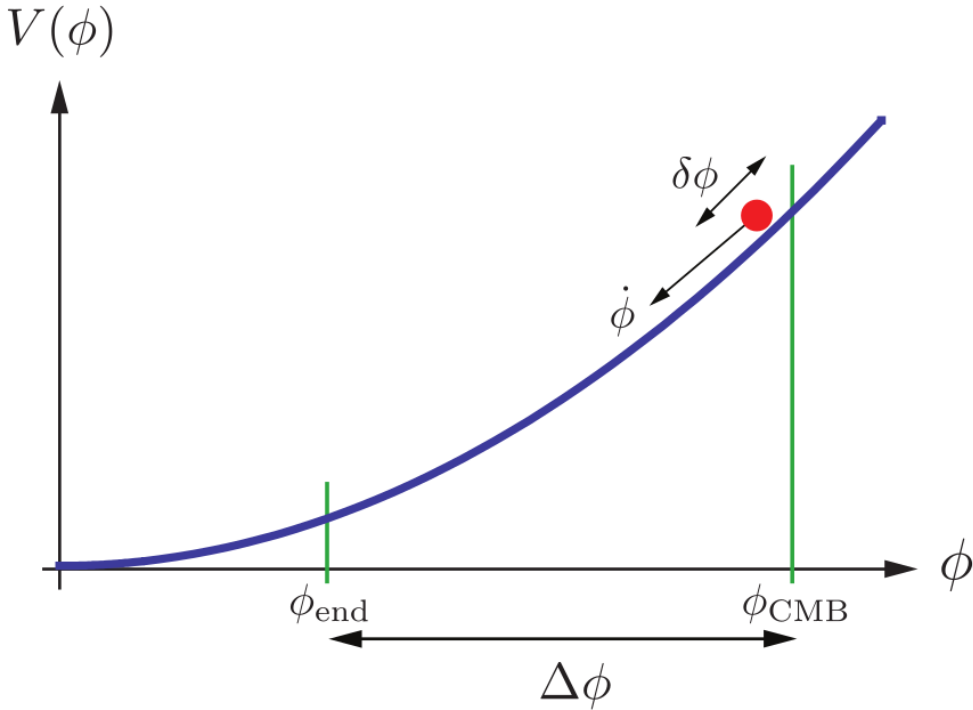


FIGURE 2.1: Example of an inflaton potential, taken from [7]. Accelerated expansion occurs, when the potential energy $V(\varphi)$ dominates over the kinetic term $\frac{1}{2}\dot{\varphi}^2$. Inflation ends at φ_{end} , when the slow-roll approximation breaks ($\epsilon_v, \eta_v = 1$). $\varphi_{start} = \varphi_{CMB}$ has to be chosen such that inflation last for about 50-60 e-folds.

The parameters ϵ_v and η_v are called the *potential slow-roll parameters*. As the name suggests, these conditions impose a certain flatness on the potential, allowing the field to start from high potential values and generate sufficient expansion of the universe before inflation abruptly ends at a certain potential value. Intuitively, this model can be understood as the scalar field slowly "rolling down" the potential starting from an initial value, as illustrated in Figure 2.1. This is why the terms ϵ_v and η_v have become known as slow-roll parameters. Inflation ends when the slow-roll conditions are violated

$$\epsilon_v(\varphi_{end}) \approx 1, \quad \eta_v(\varphi_{end}) \approx 1. \quad (2.16)$$

As already mentioned before, there is a quantity N called the *e-fold number*, which quantifies the expansion of the universe. The number of *e-folds* before the end of inflation is given by

$$N(\varphi) \equiv \ln \frac{a_{end}}{a} = \int_t^{t_{end}} H dt = \int_\varphi^{\varphi_{end}} \frac{H}{\dot{\varphi}} d\varphi \approx M_{pl} \int_{\varphi_{end}}^\varphi \frac{V}{V_{,\varphi}} d\varphi, \quad (2.17)$$

where the approximated Equations 2.12 and 2.13 were used. By noting that $\epsilon \approx \epsilon_v$, the result may also be written as

$$N(\varphi) = \int_{\varphi_{\text{end}}}^{\varphi} \frac{d\varphi}{\sqrt{2\varepsilon}} \approx \int_{\varphi_{\text{end}}}^{\varphi} \frac{d\varphi}{\sqrt{2\epsilon_v}}. \quad (2.18)$$

To solve the horizon and flatness problems it is required that the initial field value φ_{ini} is chosen such that the total number of inflationary e -folds exceeds 50-60 ,

$$N_{\text{tot}} \equiv N(\varphi_{ini}) = \ln \frac{a_{\text{end}}}{a_{\text{start}}} \gtrsim 50 - 60. \quad (2.19)$$

The exact value of the number of e -folds during inflation is influenced by the specific inflation model or energy scale, as well as the details of post-inflationary processes such as reheating. In this context, a mathematical framework has been established to describe the exponential expansion of the early universe, effectively addressing both the flatness and horizon problems, provided this expansion continues for approximately 50 to 60 e -folds. The homogeneous scalar field $\varphi(t)$ acts as the key driver of this rapid expansion.

As will be discussed in the next chapter, this field also plays a crucial role in explaining the cosmic microwave background (CMB) and the formation of large-scale structures in the universe by generating small local fluctuations, denoted as $\delta\varphi(t, \mathbf{x})$. Consequently, the inflaton φ serves as more than just a theoretical construct for resolving the flatness and horizon problems. It is deeply connected to the generation of observable structures in the universe and its matter content. This connection emphasizes the significance of the inflationary mechanism in understanding the evolution of the cosmos and the intricate interplay between the early universe and its subsequent development.

2.2 Cosmological perturbation theory

While the mathematical model discussed in the last section serves to solve critical cosmological problems such as the horizon and flatness problems, it still exhibits significant weaknesses at this point. One obvious limitation of this model is that it does not provide a mechanism for the generation of structure. In this model, the universe remains completely homogeneous and isotropic, offering no explanation for the density fluctuations illustrated in Figure 1.2.

One approach to addressing this problem is to solve it perturbatively. In this case, one considers a spacetime, the *perturbed spacetime*, that is close to a homogeneous and isotropic spacetime, known as the *background spacetime*, which was discussed in the previous chapter. The metric can then be expanded in the following way [9]:

$$g_{\mu\nu}^{full}(\eta, \mathbf{x}) = g_{\mu\nu}^{(0)}(\eta) + \sum_{n=1}^{\infty} \frac{\epsilon^n}{n!} g_{\mu\nu}^{(n)}(\eta, \mathbf{x}), \quad (2.20)$$

where $g_{\mu\nu}^{(0)}$ describes the background spacetime, ϵ is assumed to be a small parameter, which is necessary for a perturbative approach, and η denotes the conformal time, in order to be consistent with the notation in [9]. The choice of conformal time as the time variable is made solely to simplify the solution of later equations. At this point, it is also important to note that in the course of this work, background quantities will be interchangeably referred to as e.g. $g_{\mu\nu}$ or simply $g_{\mu\nu}$, instead of just $g_{\mu\nu}^{(0)}$. However, they can always be distinguished from perturbations by their simple time dependence. Since Figure 1.2 shows that relative density perturbations in the early universe are at most on the order of $\mathcal{O}(10^{-4})$, the following can be assumed:

$$\left| \frac{\epsilon^n}{n!} g_{\mu\nu}^{(n)}(\eta, \mathbf{x}) \right| \ll g_{\mu\nu}^{(0)}(\eta). \quad (2.21)$$

This justifies treating the problem to linear order in perturbation theory, which is why the expansion of the metric can be written as follows:

$$g_{\mu\nu}^{full}(\eta, \mathbf{x}) \approx g_{\mu\nu}^{(0)}(\eta) + \delta g_{\mu\nu}(\eta, \mathbf{x}), \quad (2.22)$$

with $\delta g_{\mu\nu}$ being a small perturbation of linear order. This perturbative expansion of the metric can then be carried forward into the Einstein equations, leading to the following expansions of the energy-momentum tensor, the Ricci tensor, and the Ricci scalar:

$$T_{\mu\nu}^{full}(\eta, \mathbf{x}) = T_{\mu\nu}^{(0)}(\eta) + \sum_{n=1}^{\infty} \frac{\epsilon^n}{n!} T_{\mu\nu}^{(n)}(\eta, \mathbf{x}) \approx T_{\mu\nu}^{(0)}(\eta) + \delta T_{\mu\nu}(\eta, \mathbf{x}), \quad (2.23)$$

$$R_{\mu\nu}^{full}(\eta, \mathbf{x}) = R_{\mu\nu}^{(0)}(\eta) + \sum_{n=1}^{\infty} \frac{\epsilon^n}{n!} R_{\mu\nu}^{(n)}(\eta, \mathbf{x}) \approx R_{\mu\nu}^{(0)}(\eta) + \delta R_{\mu\nu}(\eta, \mathbf{x}), \quad (2.24)$$

$$R^{full}(\eta, \mathbf{x}) = R^{(0)}(\eta) + \sum_{n=1}^{\infty} \frac{\epsilon^n}{n!} R^{(n)}(\eta, \mathbf{x}) \approx R^{(0)}(\eta) + \delta R(\eta, \mathbf{x}). \quad (2.25)$$

The main motivation behind this approach is to linearize the Einstein equations by first perturbing them and then identifying the terms, order by order. Since the early universe was highly homogeneous, the background equations can be solved independently of the perturbation equations, which themselves, due to their linearity, are much easier to solve than the unperturbed Einstein equations.

2.2.1 General metric of first order

As shown in [10] the most general first-order perturbed metric (line element) can be expressed as:

$$ds^2 = a^2(\eta) \left\{ -(1 + 2\phi)d\eta^2 - 2B_i d\eta dx^i + [(1 - 2\psi)\delta_{ij} + 2E_{ij}] dx^i dx^j \right\}. \quad (2.26)$$

The term in the square brackets specifies the *curvature perturbation* $2(E_{ij} - \psi\delta_{ij})$, and E_{ij} is taken to be traceless ($E_{ii} = 0$) such that the separation between the two is unique. B_i is called the *shift vector* and ϕ is called the *lapse function*.

By substituting this metric into the left side of the Einstein equations and the ansatz $\varphi^{full}(\eta, \mathbf{x}) \approx \varphi^{(0)}(\eta) + \delta\varphi(\eta, \mathbf{x})$ into the stress-energy tensor in Equation 2.4, one obtains the evolution equations for the metric components and the field φ^{full} up to first order. This formulation mathematically defines the problem, leaving only the task of solving the corresponding coupled differential equations. However, it can also be shown that the resulting equations can be significantly simplified through additional steps, such as exploiting the symmetries of the background. Therefore, the steps needed to simplify this physical problem will be addressed first before formulating the respective equations of motion.

2.2.2 Gauge transformations

One question that arises is whether the separation between the background and perturbations is uniquely defined. The answer to this question becomes relatively clear when one realizes that the background spacetime and the complete system with perturbations (the physical system) are defined on different manifolds [11]. To explore this, one considers a physical manifold \mathcal{M} and a background manifold \mathcal{N} , where the coordinates x_b^α are rigidly fixed, with the index b standing for ‘background’. These manifolds can be linked by a so-called diffeomorphism, which describes a smooth, bijective map between two manifolds that has a smooth inverse. In other words, it’s a function that provides a one-to-one correspondence between points on two manifolds, preserving the smooth structure of both. Every diffeomorphism $\mathcal{D} : \mathcal{N} \rightarrow \mathcal{M}$ also induces a coordinate system on \mathcal{M} via $\mathcal{D} : x_b^\alpha \rightarrow x^\alpha$; see Figure 2.2 for reference.

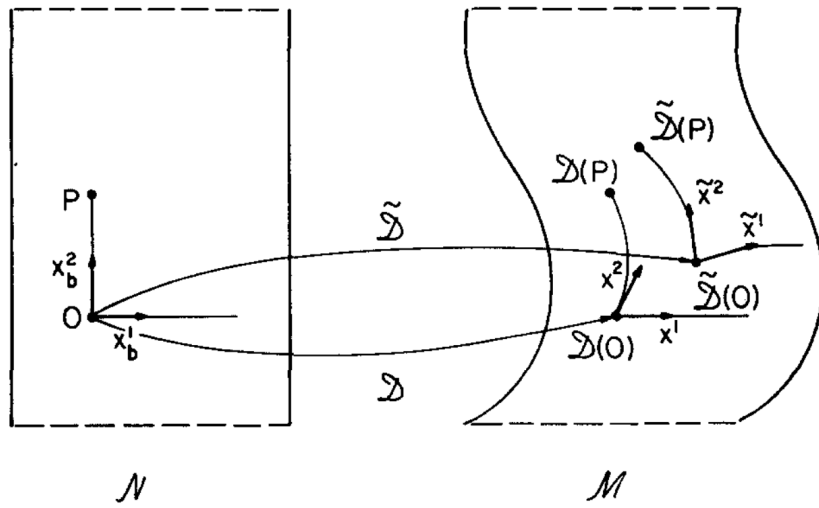


FIGURE 2.2: Illustration of two diffeomorphisms, \mathcal{D} and $\tilde{\mathcal{D}}$, which map a homogeneous background manifold \mathcal{N} onto an inhomogeneous manifold \mathcal{M} , inferred from [11]. Given fixed background coordinates x_b^α on \mathcal{N} , the diffeomorphisms \mathcal{D} and $\tilde{\mathcal{D}}$ define two coordinate systems, x^α and \tilde{x}^α , on \mathcal{M} .

For a given diffeomorphism \mathcal{D} the perturbation δQ of any function Q defined on \mathcal{M} can be expressed as

$$\delta Q(p) = Q(p) - Q^{(0)}(\mathcal{D}^{-1}(p)), \quad (2.27)$$

where $Q^{(0)}$ is a fixed function defined on the background space-time and $p \in \mathcal{M}$. A second diffeomorphism $\tilde{\mathcal{D}} : \mathcal{N} \rightarrow \mathcal{M}$ will then induce a different set of coordinates \tilde{x}^α on \mathcal{M} via $\tilde{\mathcal{D}} : x_b^\alpha \rightarrow \tilde{x}^\alpha$. In this case the perturbation at the given point p is defined as

$$\widetilde{\delta Q}(p) = \tilde{Q}(p) - Q^{(0)}(\tilde{\mathcal{D}}^{-1}(p)), \quad (2.28)$$

where \tilde{Q} is defined as the value of Q in the \tilde{x}^α coordinates. One can immediately see that $\delta\tilde{Q}(p)$ and $\delta Q(p)$ are different and that the difference between them is caused by the change of correspondence $\mathcal{D} \rightarrow \tilde{\mathcal{D}}$ between the manifolds \mathcal{N} and \mathcal{M} , which is called *gauge transformation*. This change of correspondence can be associated with a change of coordinates $x^\alpha \rightarrow \tilde{x}^\alpha$ induced on \mathcal{M} .

The coordinates x^α and \tilde{x}^α can then be related via

$$\tilde{x}^\alpha = x^\alpha + \xi^\alpha, \quad (2.29)$$

where ξ^α and its derivatives are of first order and small. The difference between $\frac{\partial \xi^\alpha}{\partial x^\alpha}$ and $\frac{\partial \xi^\alpha}{\partial \tilde{x}^\alpha}$ is second-order small and can be neglected. Therefore, one can just write $\xi^\alpha_{,\beta}$ and think of ξ^α as living on the background spacetime.

Equation 2.29 will be crucial for understanding how different quantities like scalars, vectors, or tensors behave under a small coordinate transformation induced by ξ^α . However, it is first necessary to clarify how different points on the manifolds relate to each other in different coordinate systems. The majority of this section discussing gauge transformations originates from sources [11] and [10]. A point p_b on the background manifold is described by the coordinate system $\{x_b^\alpha\}$. It is associated with a point p on the perturbed manifold by the coordinate system $\{x^\alpha\}$, while the coordinate system $\{\tilde{x}^\alpha\}$ associates it with another point \tilde{p} . Thus, there is the following relationship:

$$x_b^\alpha(p_b) = x^\alpha(p) = \tilde{x}^\alpha(\tilde{p}). \quad (2.30)$$

The gauge transformation then relates the coordinates of the *same point* in the perturbed manifold

$$\tilde{x}^\alpha(p) = x^\alpha(p) + \xi^\alpha(p), \quad (2.31)$$

$$\tilde{x}^\alpha(\tilde{p}) = x^\alpha(\tilde{p}) + \xi^\alpha(\tilde{p}). \quad (2.32)$$

Because the difference $\xi^\alpha(p) - \xi^\alpha(\tilde{p})$ is second-order small, it can be neglected and one can just write ξ^α . Therefore, ξ^α can be associated with a background point as mentioned before

$$\xi^\alpha \equiv \xi^\alpha(p_b) \equiv \xi^\alpha(x_b^\beta). \quad (2.33)$$

Plugging Equation 2.30 in Equations 2.31 and 2.32 gives the relation between two different points of the perturbed manifold in a given coordinate system

$$\tilde{x}^\alpha(p) = \tilde{x}^\alpha(\tilde{p}) + \xi^\alpha, \quad (2.34)$$

$$x^\alpha(\tilde{p}) = x^\alpha(p) - \xi^\alpha. \quad (2.35)$$

The transformation of scalars, vectors and tensors is then given by

$$\begin{aligned}
\text{Scalar: } & \tilde{\phi}(\tilde{x}) = \phi(x), \\
\text{Contravariant Vector: } & \tilde{V}^\alpha = \frac{\partial \tilde{x}^\alpha}{\partial x^\beta} V^\beta, \\
\text{Covariant Vector: } & \tilde{V}_\alpha = \frac{\partial x^\beta}{\partial \tilde{x}^\alpha} V_\beta, \\
\text{Contravariant Rank-2 Tensor: } & \tilde{T}^{\alpha\beta} = \frac{\partial \tilde{x}^\alpha}{\partial x^\gamma} \frac{\partial \tilde{x}^\beta}{\partial x^\delta} T^{\gamma\delta}, \\
\text{Covariant Rank-2 Tensor: } & \tilde{T}_{\alpha\beta} = \frac{\partial x^\gamma}{\partial \tilde{x}^\alpha} \frac{\partial x^\delta}{\partial \tilde{x}^\beta} T_{\gamma\delta}, \\
\text{Mixed Rank-2 Tensor: } & \tilde{T}^\alpha_\beta = \frac{\partial \tilde{x}^\alpha}{\partial x^\gamma} \frac{\partial x^\delta}{\partial \tilde{x}^\beta} T_\delta^\gamma,
\end{aligned} \tag{2.36}$$

where $\frac{\partial \tilde{x}^\alpha}{\partial x^\beta} = \delta_\beta^\alpha + \xi_{,\beta}^\alpha$ and $\frac{\partial x^\beta}{\partial \tilde{x}^\alpha} = \delta_\alpha^\beta - \xi_{,\alpha}^\beta$.

Focusing on the definition of metric perturbation $\delta g_{\mu\nu}$, one can see that it is defined as the difference between quantities residing on two different spacetimes.

$$\begin{aligned}
\delta g_{\mu\nu}(x_b^\alpha) &= g_{\mu\nu}(p) - g_{\mu\nu}^{(0)}(p_b), \\
\delta \tilde{g}_{\mu\nu}(x_b^\alpha) &= \tilde{g}_{\mu\nu}(\tilde{p}) - g_{\mu\nu}^{(0)}(p_b).
\end{aligned} \tag{2.37}$$

Consequently, it depends on how the background points are associated with the points on the perturbed manifold, which further illustrates that the value of its individual components is not unique but depends on the chosen gauge. Once a gauge has been selected, these quantities can be considered, through the corresponding association of the spacetimes, as if they *reside on the background spacetime*. This is also the reason why these were expressed as a function of a background point x_b^α in Equation 2.37.

Now one can finally relate $\delta \tilde{g}_{\mu\nu}$ to $\delta g_{\mu\nu}$ by first expanding $g_{\mu\nu}$ around point \tilde{p}

$$g_{\mu\nu}(\tilde{p}) = g_{\mu\nu}(p) + \frac{\partial g_{\mu\nu}}{\partial x^\alpha} [x^\alpha(\tilde{p}) - x^\alpha(p)] = g_{\mu\nu}(p) - \frac{\partial g_{\mu\nu}^{(0)}}{\partial x^\alpha}(p_b) \xi^\alpha \tag{2.38}$$

and

$$\begin{aligned}
\tilde{g}_{\mu\nu}(\tilde{p}) &= X_\mu^\rho X_\nu^\sigma g_{\rho\sigma}(\tilde{p}) = (\delta_\mu^\rho - \xi_{,\mu}^\rho)(\delta_\nu^\sigma - \xi_{,\nu}^\sigma) \left[g_{\rho\sigma}(p) - \frac{\partial g_{\rho\sigma}^{(0)}}{\partial x^\alpha}(p_b) \xi^\alpha \right] \\
&= g_{\mu\nu}(p) - \xi_{,\mu}^\rho g_{\rho\nu}(p) - \xi_{,\nu}^\sigma g_{\mu\sigma}(p) - \frac{\partial g_{\mu\nu}^{(0)}}{\partial x^\alpha}(p) \xi^\alpha \\
&= g_{\mu\nu}(p) - \xi_{,\mu}^\rho g_{\rho\nu}^{(0)}(p_b) - \xi_{,\nu}^\sigma g_{\mu\sigma}^{(0)}(p_b) - \frac{\partial g_{\mu\nu}^{(0)}}{\partial x^\alpha}(p_b) \xi^\alpha,
\end{aligned} \tag{2.39}$$

where the quantity $g_{\mu\nu}(p)$ can be replaced by the background quantity $g_{\mu\nu}^{(0)}(p_b)$ whenever it is multiplied by the first order quantity ξ^α . Subtracting the background value at p_b ,

one gets the gauge transformation rule for the tensor perturbation $\delta g_{\mu\nu}$

$$\begin{aligned}\delta \tilde{g}_{\mu\nu} &= \tilde{g}_{\mu\nu}(\tilde{p}) - g_{\mu\nu}^{(0)}(p_b) \\ \Rightarrow \delta \tilde{g}_{\mu\nu} &= \delta g_{\mu\nu} - \xi_{,\mu}^{\rho} g_{\rho\nu}^{(0)} - \xi_{,\nu}^{\sigma} g_{\mu\sigma}^{(0)} - g_{\mu\nu,\alpha}^{(0)} \xi^{\alpha}.\end{aligned}\quad (2.40)$$

The background metric can be decomposed as $g_{\mu\nu}^{(0)} = a^2(\eta) \eta_{\mu\nu}$ with

$$\eta_{\mu\nu} = \text{diag}(-1, 1, 1, 1), \quad (2.41)$$

which leads to only the time derivative $g_{\mu\nu,0}^{(0)} = 2a' a \eta_{\mu\nu}$ being non-zero. By taking the difference between Equations 2.26 and the decomposition for the background metric, one ultimately obtains the following expression for the perturbed metric:

$$[\delta g_{\mu\nu}] = a^2 \begin{bmatrix} -2\phi & -B_i \\ -B_i & -2\psi \delta_{ij} + 2E_{ij} \end{bmatrix}. \quad (2.42)$$

Applying the gauge transformation for the components δg_{00} , δg_{0i} and δg_{ij} separately leads to the following transformation behavior of the metric perturbation components

$$\begin{aligned}\tilde{\phi} &= \phi - \xi_{,0}^0 - \frac{a'}{a} \xi^0, \\ \tilde{B}_i &= B_i + \xi_{,0}^i - \xi_{,i}^0, \\ \tilde{\psi} &= \psi + \frac{1}{3} \xi_{,k}^k + \frac{a'}{a} \xi^0, \\ \tilde{E}_{ij} &= E_{ij} - \frac{1}{2} (\xi_{,j}^i + \xi_{,i}^j) + \frac{1}{3} \delta_{ij} \xi_{,k}^k,\end{aligned}\quad (2.43)$$

with the transformation of $\tilde{\psi}$ and \tilde{E}_{ij} being unique, because it was imposed that E_{ij} is traceless.

The gauge transformation is a mathematically useful tool in that it demonstrates that not every perturbation is physical, as some can be set to zero in a specific coordinate system through an appropriate gauge transformation. However, it turns out that certain linear combinations of perturbations, known as *gauge-invariant perturbations*, remain invariant under a gauge transformation. These represent the physical perturbations and will play a significant role in the following sections.

2.2.3 Fourier space description and SVT decomposition

Before deriving the equations of motion in the next section, it is necessary to first prove or demonstrate two essential concepts that significantly simplify the description of the dynamics of perturbations. The first concept involves describing the dynamics using the wave number $|\mathbf{k}| = k$ instead of the spatial variable \mathbf{x} , which are related through a Fourier transformation. The advantage of this approach is that, in first-order perturbation theory, different modes k can be described independently, which will be proven below. The proof follows the approach in reference [7].

The Fourier space decomposition of an arbitrary perturbation $\delta Q(t, \mathbf{x})$ can be written as follows

$$\delta Q(t, \mathbf{k}) = \int d^3 \mathbf{x} \delta Q(t, \mathbf{x}) e^{-i\mathbf{k}\cdot\mathbf{x}}. \quad (2.44)$$

Lemma: Translation invariance of the background implies that different Fourier modes of arbitrary perturbations decouple in first order

Proof: Consider the most general linear evolution of N arbitrary perturbations $\delta Q_I, I = 1, \dots, N$ from an initial time t_1 to a final time t_2

$$\delta Q_I(t_2, \mathbf{k}) = \sum_{J=1}^N \int d^3 \bar{\mathbf{k}} T_{IJ}(t_2, t_1, \mathbf{k}, \bar{\mathbf{k}}) \delta Q_J(t_1, \bar{\mathbf{k}}). \quad (2.45)$$

Here, the transfer matrix $T_{IJ}(t_2, t_1, \mathbf{k}, \bar{\mathbf{k}})$ follows from the Einstein Equations and the possibility of a mixing of \mathbf{k} -modes has been allowed for. Translation invariance of the background implies that T_{IJ} remains invariant under a constant spatial shift, because, to first order, the δQ_I couple only linearly to background quantities, which themselves do not depend on position, and they do not mix (such mixing would be a second-order term). As a result, the equations of motion are invariant under this transformation, meaning the solution in the shifted coordinate system can also be described by the exact same transfer function T_{IJ} . With this information one can consider the coordinate transformation

$$\tilde{x}^i = x^i + \Delta x^i, \quad \text{where} \quad \Delta x^i = \text{const.} \quad (2.46)$$

This transformation leads to the following shift of the respective Fourier amplitude

$$\widetilde{\delta Q_I}(t, \mathbf{k}) = e^{-ik_j \Delta x^j} \delta Q_I(t, \mathbf{k}). \quad (2.47)$$

Thus the evolution equation in the coordinate system with a tilde becomes

$$\delta\widetilde{Q}_I(t_2, \mathbf{k}) = \sum_{J=1}^N \int d^3\bar{\mathbf{k}} e^{-ik_j \Delta x^j} T_{IJ}(t_2, t_1, \mathbf{k}, \bar{\mathbf{k}}) e^{i\bar{k}_j \Delta x^j} \delta\widetilde{Q}_J(t_1, \bar{\mathbf{k}}) \quad (2.48)$$

$$\equiv \sum_{J=1}^N \int d^3\bar{\mathbf{k}} \widetilde{T}_{IJ}(t_2, t_1, \mathbf{k}, \bar{\mathbf{k}}) \delta\widetilde{Q}_J(t_1, \bar{\mathbf{k}}). \quad (2.49)$$

As mentioned before, by translation invariance the equations of motion must be the same in both coordinate systems. This implies that the transfer matrices T_{IJ} and \widetilde{T}_{IJ} must be the same:

$$T_{IJ}(t_2, t_1, \mathbf{k}, \bar{\mathbf{k}}) = e^{i(\bar{k}_j - k_j)\Delta x^j} T_{IJ}(t_2, t_1, \mathbf{k}, \bar{\mathbf{k}}). \quad (2.50)$$

This must hold for all Δx^j . Hence, either $\bar{\mathbf{k}} = \mathbf{k}$ or $T_{IJ}(t_2, t_1; \mathbf{k}, \bar{\mathbf{k}}) = 0$. The latter describes a spacetime without any fluctuations, so the only possibility left is that the arbitrary perturbation $\delta Q_I(t_2, \mathbf{k})$ of wave vector \mathbf{k} depends only on the initial perturbations of wave vector \mathbf{k} . Therefore, at linear order there is no coupling of different k -modes. \square

In cosmological perturbation theory, two types of coordinate transformations are of particular interest. The treatment of these in this chapter is based on source [10]. The first is the gauge transformation previously discussed, where the coordinates of the background remain fixed while those in the perturbed spacetime are altered, thereby changing the correspondence between points in the background and the perturbed spacetime.

The second type involves keeping the gauge, meaning the correspondence between background and perturbed spacetime points, unchanged while performing a coordinate transformation in the background spacetime. This transformation then induces a corresponding change in the perturbed spacetime coordinates. The background coordinate system is typically chosen to respect the symmetries of the background spacetime, and preserving this property is crucial. In cosmological perturbation theory, the background coordinates are selected to maintain the homogeneity of the spacetime, providing a unique slicing of the spacetime into homogeneous, time-constant spacelike slices. It is important to maintain this slicing to ensure the consistency of the perturbative framework.

This only leaves rotations in 3D space with the full transformation matrices:

$$X_{\rho'}^{\mu'} = \begin{bmatrix} 1 & 0 \\ 0 & R_{k'}^{i'} \end{bmatrix} \quad \text{and} \quad X_{\rho'}^{\mu} = \begin{bmatrix} 1 & 0 \\ 0 & R_{k'}^i \end{bmatrix} \quad (2.51)$$

This coordinate transformation in the background induces the corresponding transformations

$$\begin{aligned} x^\mu' &= X_\rho^\mu x^\rho, \\ g_{\rho'\sigma'} &= X_{\rho'}^\mu X_{\sigma'}^\nu g_{\mu\nu}, \end{aligned} \tag{2.52}$$

in the perturbed spacetime. Transforming the different components of the metric gives the perturbations in the new coordinate system

$$\begin{aligned} \phi' &= \phi, \\ \psi' &= \psi, \\ B_{l'} &= R^j{}_{l'} B_j, \\ E_{k'l'} &= R^i{}_{k'} R^j{}_{l'} E_{ij}. \end{aligned} \tag{2.53}$$

Consequently, ϕ and ψ behave as scalars under rotations in the background spacetime coordinates, B_i transforms as a 3-vector, and E_{ij} as a 3D tensor. When working within a fixed gauge, these quantities can be interpreted as scalar, vector, and tensor fields on the 3D Euclidean background space. However, this classification is not yet complete. It is possible to extract two additional scalar quantities and one additional vector quantity from B_i and E_{ij} . According to principles from Euclidean 3D vector calculus, a vector field can be decomposed into two components: one with zero curl and the other with zero divergence:

$$\vec{B} = \vec{B}^S + \vec{B}^V, \quad \text{with} \quad \vec{\nabla} \times \vec{B}^S = 0 \quad \text{and} \quad \vec{\nabla} \cdot \vec{B}^V = 0. \tag{2.54}$$

The component with zero curl can be represented as the negative gradient of a scalar field

$$\vec{B}^S = -\vec{\nabla} B. \tag{2.55}$$

In component notation this reads

$$B_i = -B_{,i} + B_i^V, \quad \text{where} \quad \delta^{ij} B_{i,j}^V = 0. \tag{2.56}$$

In the same way, the tensor E_{ij} , which by definition is symmetric and traceless, can be decomposed into three parts

$$E_{ij} = E_{ij}^S + E_{ij}^V + E_{ij}^T, \tag{2.57}$$

where E_{ij}^T describes the tensor part and E_{ij}^S and E_{ij}^V can be expressed in terms of a scalar field E and a vector field E_i ,

$$E_{ij}^S = \left(\partial_i \partial_j - \frac{1}{3} \delta_{ij} \Delta \right) \hat{E} \equiv E_{,ij}, \quad \text{where } \delta^{ij} E_{,ij} = \Delta E = 0, \quad (2.58)$$

$$E_{ij}^V = -\frac{1}{2} (E_{i,j} + E_{j,i}), \quad \text{where } \delta^{ij} E_{i,j} = \nabla \cdot \vec{E} = 0, \quad (2.59)$$

$$E_{ij}^T = E_{ij}, \quad \text{where } \delta^{ik} E_{ij,k} = 0, \quad \delta^{ij} E_{ij} = 0. \quad (2.60)$$

Every component is assumed to be symmetric and traceless. Therefore, the metric perturbations can be divided into

1. a scalar part, consisting of ϕ, B, ψ , and E , (4 d.o.f.)
2. a vector part, consisting of B_i^V and E_i , (4 d.o.f.)
3. a tensor part E_{ij}^T . (2 d.o.f.)

It is important to notice that the names "scalar", "vector" and "tensor" refer to their *transformation properties under rotation in the background space* and have nothing to do with their behaviour under a gauge-transformation. An important aspect of this division is that the scalar, vector, and tensor components do not interact with each other in first order perturbation theory but instead evolve independently. This will be demonstrated at the end of this section. This separation allows each component to be treated individually, with the overall evolution of the perturbation being the linear superposition of the independent evolutions of the scalar, vector, and tensor components.

A constraint is imposed on each of the 3-vectors B_i and E_i , along with $3+1=4$ constraints on the symmetric 3-dimensional tensor E_{ij}^T , leaving two independent components for each. Consequently, the 10 degrees of freedom correspond to the 10 components of the metric perturbation $g_{\mu\nu}$, although not all of these are physical. This can be seen if one looks at the spatial part of the four-vector $\xi^\alpha = (\xi^0, \xi^i)$, which also can be written like

$$\xi^i = \xi_{tr.}^i + g^{(0)ij} \xi_{,j}, \quad (2.61)$$

where the "transverse" vector $\xi_{tr.}^i$ and the scalar function ξ satisfy the conditions

$$\xi_{tr. ,i}^i = 0 \quad \text{and} \quad \xi_{,i}^i = \xi_{,i}^i. \quad (2.62)$$

Hence, due to a gauge transformation the two components ξ^0 and ξ can eliminate up to 2 scalar perturbations and will leave 2 physical scalar degrees of freedom. The same principle applies to the vector perturbations, which are reduced from four to two physical perturbations due to the two independent components of $\xi_{tr.}^i$.

Tensor perturbations remain invariant under gauge transformations, as these transformations only generate scalar and vector perturbations. This can be seen if one looks at Equations 2.43. Therefore, there are a total of six physical degrees of freedom: two scalar, two vector, and two tensor. The remaining four degrees of freedom are not physical, representing perturbations of the coordinates rather than the spacetime itself.

To fully understand the rationale behind the decomposition of perturbations into scalar, vector, and tensor components, these perturbations are first transformed from real space to Fourier space, characterized by the wavevector \mathbf{k} :

$$\begin{aligned}\phi^S &= \phi, \\ \psi^S &= \psi, \\ B_i^S &= -ik_i B, \\ B_i^V &= B_i \quad \text{with} \quad k_i B_i = 0, \\ E_{ij}^S &= (-k_i k_j + \frac{1}{3} \delta_{ij} k^2) \hat{E}, \\ E_{ij}^V &= -\frac{i}{2} (k_i E_j + k_j E_i), \quad \text{with} \quad k_i E_i = 0, \\ E_{ij}^T &= E_{ij}, \quad \text{with} \quad k_i E_{ij} = 0 \quad \text{and} \quad E_{ii} = 0.\end{aligned}\tag{2.63}$$

This transformation allows for an analysis of how the perturbations behave under rotations by an angle θ about the Fourier vector \mathbf{k} . Without loss of generality, $\mathbf{k} = (0, 0, k)$ can be assumed, given that the background is rotationally invariant. Consequently, it suffices to consider a rotation about the z-axis, described by the following rotation matrix:

$$\mathbf{R} = \begin{pmatrix} 1 & 0 & 0 & 0 \\ 0 & \cos \theta & \sin \theta & 0 \\ 0 & -\sin \theta & \cos \theta & 0 \\ 0 & 0 & 0 & 1 \end{pmatrix}.\tag{2.64}$$

This rotation matrix \mathbf{R} then transforms the metric via $\mathbf{R}^T \mathbf{g} \mathbf{R}$ and leads to the transformation of the individual metric components (scalar, vector, tensor). With tedious calculations one can show that the Fourier-space perturbations can then be classified according to their helicity m , where a perturbation with helicity m has its amplitude multiplied by $e^{im\theta}$ under such a rotation. Scalar, vector, and tensor perturbations correspond to helicities 0, ± 1 , and ± 2 , respectively. This classification underscores the natural distinction between these types of perturbations based on their rotational properties.

This leads to the most important mathematical statement of this section, which asserts that scalar, vector, and tensor perturbations decouple at linear order and can thus be

described independently. The proof, taken from [7], leverages the rotational invariance of the background spacetime.

Theorem: Rotational invariance of the background implies that helicity scalars, vectors and tensors evolve independently

Proof: Consider N arbitrary perturbations $\delta Q_I, I = 1, \dots, N$ of helicity m_I . The linear evolution is

$$\delta Q_I(t_2, \mathbf{k}) = \sum_{J=1}^N T_{IJ}(t_2, t_1, \mathbf{k}) \delta Q_J(t_1, \mathbf{k}), \quad (2.65)$$

where the transfer matrix $T_{IJ}(t_2, t_1, \mathbf{k})$ follows from the Einstein Equations and it is already assumed that different modes \mathbf{k} evolve independently. As already mentioned, under rotation the perturbations transform as

$$\widetilde{\delta Q_I}(t, \mathbf{k}) = e^{im_I\theta} \delta Q_I(t, \mathbf{k}) \quad (2.66)$$

and therefore the linear evolution transforms as

$$\widetilde{\delta Q_I}(t_2, \mathbf{k}) = \sum_{J=1}^N e^{im_I\theta} T_{IJ}(t_2, t_1, \mathbf{k}) e^{-im_J\theta} \delta Q'_J(t_1, \mathbf{k}). \quad (2.67)$$

Like in the proof of decoupling of different Fourier modes \mathbf{k} , the rotational invariance of the background spacetime implies that the solution T_{IJ} of the equations of motion has to be invariant under such transformation:

$$T_{IJ}(t_2, t_1, \mathbf{k}) = e^{im_I\theta} T_{IJ}(t_2, t_1, \mathbf{k}) e^{-im_J\theta} = e^{i(m_I - m_J)\theta} T_{IJ}(t_2, t_1, \mathbf{k}), \quad (2.68)$$

which has to hold for any angle θ . It follows that either $m_I = m_J$, i.e. δQ_I and δQ_J have the same helicity or $T_{IJ}(t_2, t_1, \mathbf{k}) = 0$, which corresponds to a trivial theory without perturbations. Therefore, this proves that the equations of motion don't mix modes of different helicity. \square

With this groundwork laid, in the next section the Einstein equations for the various perturbations will be individually formulated and solved. Special attention will be given to scalar perturbations, as they play a crucial role in the cosmological evolution of the universe, as will become evident in the following chapters. For simplicity, the subsequent calculations will initially be carried out in real space, with key equations then transformed into Fourier space. Thanks to the results of this section, this can be done easily without violating the essential principles of decomposition, allowing for a clearer understanding of the physics underlying the corresponding equations.

2.3 Einstein equations for SVT perturbations

In this chapter the equations of motion for scalar, vector, and tensor perturbations will be derived separately. It will become apparent that both vector and tensor perturbations play a subordinate role in cosmological evolution, whereas the study of scalar perturbations offers a means to understand the structure of the observable universe, as will be demonstrated later. The introduction of so-called *gauge-invariant quantities* will also play a central role in this analysis. The derivation of various equations in this section was based on [11].

2.3.1 Scalar perturbations

After the decomposition made in the last section, the general first-order metric 2.26 for just scalar perturbations can be written as

$$\begin{aligned} ds^2 &= a^2(\eta) \left\{ -(1 + 2\phi)d\eta^2 + 2B_{,i}d\eta dx^i + [(1 - 2\psi)\delta_{ij} + 2E_{,ij}] dx^i dx^j \right\} \\ &\equiv a^2(\eta)dx^\mu [\eta_{\mu\nu} + h_{\mu\nu}] dx^\nu, \end{aligned} \quad (2.69)$$

where $\eta_{\mu\nu}$ describes flat Minkowski space and $h_{\mu\nu}$ consists of all perturbations. The main task now is to find an expression for the Einstein equations up to first order. For this purpose, the Christoffel symbols $\Gamma_{\mu\nu}^\alpha$ must first be perturbed to first order. These depend not only on $g_{\mu\nu} = g_{\mu\nu}^{(0)} + \delta g_{\mu\nu}$ (with $\delta g_{\mu\nu} = a^2(\eta)h_{\mu\nu}$), but are also dependent on $g^{\mu\nu} = g^{(0)\mu\nu} + \delta g^{\mu\nu}$, where $\delta g^{\mu\nu}$ describes the inverse of $\delta g_{\mu\nu}$ to first order, for which an expression still needs to be found. It can be derived very easily from the following ansatz

$$\begin{aligned} \delta_\nu^\mu &= g^{\mu\rho}g_{\rho\nu} = \left(g^{(0)\mu\rho} + \delta g^{(\mu\rho)} \right) \left(g_{\rho\nu}^{(0)} + \delta g_{\rho\nu} \right) \\ &= g^{(0)\mu\rho}g_{\rho\nu}^{(0)} + g^{(0)\mu\rho}\delta g_{\rho\nu} + \delta g^{\mu\rho}g_{\rho\nu}^{(0)} + \mathcal{O}(\delta g^2) \\ &\approx \delta_\nu^\mu + g^{(0)\mu\rho}\delta g_{\rho\nu} + \delta g^{\mu\rho}g_{\rho\nu}^{(0)} \\ \Rightarrow \quad \delta g^{\mu\rho}g_{\rho\nu}^{(0)}g^{(0)\nu\sigma} &= -g^{(0)\mu\rho}\delta g_{\rho\nu}g^{(0)\nu\sigma} \\ \Rightarrow \quad \boxed{\delta g^{\mu\nu} = -g^{(0)\mu\rho}\delta g_{\rho\sigma}g^{(0)\sigma\nu}.} \end{aligned}$$

Using this decomposition for the metric, the Christoffel symbols can also be perturbed to first order $\Gamma_{\mu\nu}^\alpha = \Gamma_{\mu\nu}^{(0)\alpha} + \delta\Gamma_{\mu\nu}^\alpha$, resulting in the following expression

$$\delta\Gamma_{\mu\nu}^\alpha = \frac{1}{2}g^{(0)\alpha\sigma} \left(\delta g_{\sigma\mu,\nu} + \delta g_{\sigma\nu,\mu} - \delta g_{\mu\nu,\sigma} - 2\delta g_{\sigma\beta}\Gamma_{\mu\nu}^{(0)\beta} \right). \quad (2.70)$$

This yields the following expressions for the background values and the corresponding perturbations of each component.

Background Christoffel symbols:

$$\boxed{\begin{aligned}\Gamma_{00}^{0(0)} &= \mathcal{H}, \\ \Gamma_{ij}^{0(0)} &= \mathcal{H}\delta_{ij}, \\ \Gamma_{0j}^{i(0)} &= \mathcal{H}\delta_j^i,\end{aligned}} \quad (2.71)$$

where $\mathcal{H} \equiv \frac{a'}{a}$, and a' is defined as a derivative with respect to conformal time: $a' \equiv \frac{da}{d\eta}$.

Perturbations of Christoffel symbols:

$$\boxed{\begin{aligned}\delta\Gamma_{00}^0 &= -\frac{1}{2}h'_{00}, \quad \delta\Gamma_{i0}^0 = -\frac{1}{2}(h_{00,i} - 2\mathcal{H}h_{0i}), \\ \delta\Gamma_{00}^i &= h'_{i0} + \mathcal{H}h_{i0} - \frac{1}{2}h_{00,i}, \\ \delta\Gamma_{ij}^0 &= -\frac{1}{2}(h_{0i,j} + h_{0j,i} - h'_{ij} - 2\mathcal{H}h_{ij} - 2\mathcal{H}\delta_{ij}h_{00}), \\ \delta\Gamma_{j0}^i &= \frac{1}{2}h'_{ij} + \frac{1}{2}(h_{i0,j} - h_{0j,i}), \\ \delta\Gamma_{jk}^i &= \frac{1}{2}(h_{ij,k} + h_{ik,j} - h_{jk,i} - 2\mathcal{H}\delta_{jk}h_{i0}).\end{aligned}} \quad (2.72)$$

This perturbative description can now be extended to the Ricci tensor $R_{\mu\nu}$, defined in Equation 1.2, which is separated into background and perturbation components by the following equations:

$$\begin{aligned}R_{\mu\nu}^{(0)} &= \Gamma_{\mu\nu}^{(0)\rho} - \Gamma_{\mu\rho,\nu}^{(0)\rho} + \Gamma_{\mu\nu}^{(0)\rho}\Gamma_{\rho\sigma}^{(0)\sigma} - \Gamma_{\mu\sigma}^{(0)\rho}\Gamma_{\nu\rho}^{(0)\sigma} \\ \delta R_{\mu\nu} &= \delta\Gamma_{\mu\nu,\rho}^{(0)} - \delta\Gamma_{\mu\rho,\nu}^{(0)\rho} + \Gamma_{\mu\nu}^{(0)\rho}\delta\Gamma_{\rho\sigma}^{(0)\sigma} + \delta\Gamma_{\mu\nu}^{(0)\rho}\Gamma_{\rho\sigma}^{(0)\sigma} - \Gamma_{\mu\sigma}^{(0)\rho}\delta\Gamma_{\nu\rho}^{(0)\sigma} - \delta\Gamma_{\mu\sigma}^{(0)\rho}\Gamma_{\nu\rho}^{(0)\sigma}.\end{aligned} \quad (2.73)$$

As before, this leads to the following expressions for both the background and the perturbations.

Background Ricci tensor:

$$\boxed{\begin{aligned}R_{00}^{(0)} &= 3\left(\mathcal{H}^2 - \frac{a''}{a}\right), \\ R_{ij}^{(0)} &= \delta_{ij}\left(\mathcal{H}^2 + \frac{a''}{a}\right), \\ R_{0i}^{(0)} &= 0.\end{aligned}} \quad (2.74)$$

Perturbations of Ricci tensor:

$$\begin{aligned}
 \delta R_{00} &= -\frac{1}{2}\Delta h_{00} - \frac{3}{2}\mathcal{H}h'_{00} + h'_{k0,k} + \mathcal{H}h_{k0,k} - \frac{1}{2}(h''_{kk} + \mathcal{H}h'_{kk}), \\
 \delta R_{0i} &= -\mathcal{H}h_{00,i} - \frac{1}{2}(\Delta h_{0i} - h_{k0,ik}) + \left(\mathcal{H}^2 + \frac{a''}{a}\right)h_{0i} - \frac{1}{2}(h'_{kk,i} - h'_{ki,k}), \\
 \delta R_{ij} &= \frac{1}{2}h_{00,ij} + \frac{\mathcal{H}}{2}h'_{00}\delta_{ij} + \left(\mathcal{H}^2 + \frac{a''}{a}\right)h_{00}\delta_{ij} + \frac{1}{2}(h_{ki,kj} + h_{kj,ki} - h_{kk,ij}) \\
 &\quad - \frac{1}{2}\Delta h_{ij} + \frac{1}{2}h''_{ij} + \mathcal{H}h'_{ij} + \left(\mathcal{H}^2 + \frac{a''}{a}\right)h_{ij} + \frac{\mathcal{H}}{2}h'_{kk}\delta_{ij} - \mathcal{H}h_{k0,k}\delta_{ij} \\
 &\quad - \frac{1}{2}(h'_{0i,j} + h'_{0j,i}) - \mathcal{H}(h_{0i,j} + h_{0j,i}).
 \end{aligned} \tag{2.75}$$

Finally, these results can be combined to get an expression for the left-hand side of the Einstein equations

$$\begin{aligned}
 G_\nu^\mu &= g^{\mu\rho}R_{\rho\nu} - \frac{1}{2}\delta_\nu^\mu R \\
 \Rightarrow G_\nu^{(0)\mu} &= R_\nu^{(0)\mu} - \frac{1}{2}\delta_\nu^\mu R^{(0)} \\
 \Rightarrow \delta G_\nu^\mu &= g^{(0)\mu\rho}\delta R_{\rho\nu} + \delta g^{\mu\rho}R_{\rho\nu}^{(0)} - \frac{1}{2}\delta_\nu^\mu\delta R.
 \end{aligned} \tag{2.76}$$

Here, the subsequent equations for $R^{(0)}$ and δR were used

$$\begin{aligned}
 a^2 R^{(0)} &= 6\frac{a''}{a}, \\
 a^2 \delta R &= \Delta h_{00} + 3\mathcal{H}h'_{00} + 6\frac{a''}{a}h_{00} - 2h'_{k0,k} - 6\mathcal{H}h_{k0,k} \\
 &\quad + h''_{kk} + 3\mathcal{H}h'_{kk} - \Delta h_{kk} + h_{kl,kl}.
 \end{aligned} \tag{2.77}$$

This ultimately leads to the ensuing derivations for the components of the **first-order perturbed Einstein tensor**:

$$\begin{aligned}
 2a^2\delta G_0^0 &= -6\mathcal{H}^2h_{00} + 4\mathcal{H}h_{k0,k} - 2\mathcal{H}h'_{kk} + \Delta h_{kk} - h_{kl,kl}, \\
 2a^2\delta G_i^0 &= 2\mathcal{H}h_{00,i} + \Delta h_{0i} - h_{k0,ki} + h'_{kk,i} - h'_{ki,k}, \\
 2a^2\delta G_j^i &= \left[-4\frac{a''}{a}h_{00} - 2\mathcal{H}h'_{00} - \Delta h_{00} + 2\mathcal{H}^2h_{00} - 2\mathcal{H}h'_{kk} + \Delta h_{kk} - h_{kl,kl} \right. \\
 &\quad \left. + 2h'_{k0,k} + 4\mathcal{H}h_{k0,k} - h''_{kk}\right]\delta_j^i + h_{00,ij} - \Delta h_{ij} + h_{ki,kj} + h_{kj,ki} - h_{kk,ij} \\
 &\quad + h''_{ij} + 2\mathcal{H}h'_{ij} - (h'_{0i,j} + h'_{0j,i}) - 2\mathcal{H}(h_{0i,j} + h_{0j,i}).
 \end{aligned} \tag{2.78}$$

The final step is now to find an expression for the right-hand side of the Einstein equations, and thus for T_ν^μ . The energy-momentum tensor can generally be expressed as follows:

$$T_\nu^\mu \equiv g^{\mu\alpha} T_{\alpha\nu} = \partial^\mu \varphi \partial_\nu \varphi - \delta_\nu^\mu \left[\frac{1}{2} g^{\alpha\beta} \partial_\alpha \varphi \partial_\beta \varphi V(\varphi) \right]. \quad (2.79)$$

The perturbation of this tensor to first order is simply achieved by perturbing the metric tensor $g_{\mu\nu}$ and the scalar field φ to first order. This leads to the following expressions for the components of the **energy-momentum tensor for the background and at first order**, derived through straightforward calculations:

$$\begin{aligned} T_0^{0(0)} &= - \left[\frac{1}{2a^2} \bar{\varphi}'^2 + V \right], & a^2 \delta T_0^0 &= - [\bar{\varphi}' (\delta\varphi' - \phi\bar{\varphi}') + V_{,\varphi} a^2 \delta\varphi], \\ T_i^{0(0)} &= 0, & a^2 \delta T_i^0 &= -\bar{\varphi}' \delta\varphi_i, \\ T_j^{i(0)} &= \delta_j^i \left[\frac{1}{2a^2} \bar{\varphi}'^2 - V \right], & a^2 \delta T_j^i &= [\bar{\varphi}' (\delta\varphi' - \phi\bar{\varphi}') + V_{,\varphi} a^2 \delta\varphi] \delta_j^i. \end{aligned} \quad (2.80)$$

Before formulating the Einstein equations, it is reasonable to consider whether the gauge freedom for scalar perturbations should be utilized. This would allow the equations to be described using only 2 physical scalar metric perturbations instead of 4 scalar metric perturbations. One way to reduce the number of parameters is to define so-called *gauge-invariant perturbations*:

$$\begin{aligned} \Phi &= \phi + \frac{1}{a} [(B - E') a]' = \phi + (B - E')' + \mathcal{H}(B - E'), \\ \Psi &= \psi - \mathcal{H}(B - E'). \end{aligned} \quad (2.81)$$

The name comes from the fact that both of them are invariant under a gauge transformation, which can be proven quite easily with the scalar parts of Equations 2.43. By introducing these quantities, the perturbed Einstein tensor can be written in a gauge-invariant form. Now, it is only necessary to formulate the perturbed energy-momentum tensor in a gauge-invariant form. This tensor depends on the field fluctuation $\delta\varphi$, which, as shown in [Appendix A](#), transforms under a gauge transformation as a scalar perturbation as follows:

$$\delta\tilde{\varphi} = \delta\varphi - \bar{\varphi}' \xi^0. \quad (2.82)$$

Once the transformation behavior of $\delta\varphi$ is known, it is straightforward to construct a gauge-invariant quantity from it. It can be shown, as before, that the following quantity, also called *the inflaton perturbation on spatially flat slices*, is indeed gauge-invariant:

$$\delta Q = \delta\varphi + \bar{\varphi}' (B - E'). \quad (2.83)$$

This allows the Einstein equations to be formulated separately for the background evolution and the perturbations in a gauge-invariant manner using

$$G_\nu^{\mu(0)} = \frac{1}{M_{pl}^2} T_\nu^{\mu(0)}, \quad a^2 \delta G_{gi.\nu}^\mu = \frac{1}{M_{pl}^2} a^2 \delta T_{gi.\nu}^\mu. \quad (2.84)$$

Since the background equations are already known from the first chapter, only the equations for the perturbations will be provided. These are obtained by substituting $h_{\mu\nu}$ into the individual components of G_ν^μ and are detailed below:

$$\begin{aligned} \Delta\Phi - 3\mathcal{H}(\Psi' + \mathcal{H}\Phi) &= \frac{1}{2M_{pl}^2} [\bar{\varphi}' (\delta Q' - \Phi\bar{\varphi}') + V_{,\varphi} a^2 \delta Q], \\ [\mathcal{H}\Phi + \Psi']_{,i} &= \frac{1}{2M_{pl}^2} \bar{\varphi}' \delta Q_{,i}, \\ \left[(2\mathcal{H}' + \mathcal{H}^2) \Phi + \mathcal{H}\Phi' + \Psi'' + 2\mathcal{H}\Psi' - \mathcal{H}\Psi + \frac{1}{2} \Delta D \right] \delta_j^i \\ - \frac{1}{2} \eta^{ik} D_{,kj} &= \frac{1}{2M_{pl}^2} [\bar{\varphi}' (\delta Q' - \Phi\bar{\varphi}') + V_{,\varphi} a^2 \delta Q] \delta_j^i, \end{aligned} \quad (2.85)$$

where D is defined as $D \equiv \Phi - \Psi$. The absence of non-diagonal spacial components in the energy-momentum tensor considerably simplifies this set of equations. The equations for $i \neq j$ imply that all mixed spatial derivatives of $D = \Phi - \Psi$ must vanish. Therefore, $D(x_1, x_2, x_3)$ must be expressed as a sum of three separate functions $D_i(x_i)$. The only way this structure remains invariant under coordinate transformations is if the D_i are linear functions. Since the spatial average is required to be zero, D must necessarily be zero, which implies $\Phi = \Psi$. In conjunction with Equations 2.2 and 2.3 for the background, the perturbation equations can be simplified as follows:

$$\begin{aligned} \Delta\Phi - 3\mathcal{H}\Phi' - (\mathcal{H}' + 2\mathcal{H}^2) \Phi &= \frac{1}{2M_{pl}^2} (\bar{\varphi}' \delta Q' + V_{,\varphi} a^2 \delta Q), \\ \mathcal{H}\Phi + \Phi' &= \frac{1}{2M_{pl}^2} \bar{\varphi}' \delta Q, \\ \Phi'' + 3\mathcal{H}\Phi' + (\mathcal{H}' + 2\mathcal{H}') \Phi &= \frac{1}{2M_{pl}^2} (\bar{\varphi}' \delta Q' - V_{,\varphi} a^2 \delta Q). \end{aligned} \quad (2.86)$$

The first and third equations can be added and the remaining term proportional to $\delta Q'$ can be eliminated with the second equation. This gives the evolution equation for Φ :

$$\Phi'' + 2 \left(\mathcal{H} - \frac{\bar{\varphi}''}{\bar{\varphi}'} \right) \Phi' - \Delta\Phi + 2 \left(\mathcal{H}' - \mathcal{H} \frac{\bar{\varphi}''}{\bar{\varphi}'} \right) \Phi = 0. \quad (2.87)$$

This equation describes the evolution of the only remaining degree of freedom of the perturbed metric. To fully describe the system of scalar perturbations, it is now necessary to obtain the equation of motion for δQ . This is provided by the 0-component of the energy-momentum conservation equation:

$$T_{\nu;\mu}^\mu \equiv \partial_\mu T_\nu^\mu + \Gamma_{\mu\alpha}^\mu T_\nu^\alpha - \Gamma_{\nu\mu}^\beta T_\beta^\mu = 0 \quad (2.88)$$

In first-order perturbation theory, the following gauge-invariant equation for δQ is obtained:

$$\delta Q'' + 2\mathcal{H}\delta Q' - \Delta\delta Q + V_{\varphi\varphi}a^2\delta Q - 4\dot{\varphi}'\Phi' + 2V_\varphi a^2\Phi = 0. \quad (2.89)$$

It becomes quite apparent that in the equation of motion for δQ , there are source terms involving Φ , indicating that these two quantities cannot be described independently of each other. This raises the question of whether there exists a linear combination of both perturbations that is also gauge-invariant and evolves independently as the only degree of freedom, without any source terms from other quantities. Indeed, such a perturbation exists, called the *comoving curvature perturbation* \mathcal{R} , is given by the following expression:

$$\boxed{\mathcal{R} = \psi + \frac{\mathcal{H}}{\dot{\varphi}'}\delta\varphi = \Psi + \frac{\mathcal{H}}{\dot{\varphi}'}\delta Q = \Phi + \frac{\mathcal{H}}{\dot{\varphi}'}\delta Q.} \quad (2.90)$$

By substituting $v = z\mathcal{R}$, with $z \equiv \frac{a\dot{\varphi}'}{\mathcal{H}}$, into the equation of motion for δQ and utilizing the background equations 2.2 and 2.3, using the constraint equations 2.86, and the equation of motion for Φ , the final so-called *Mukhanov-Sasaki equation* can be derived:

$$\boxed{v'' - \Delta v - \frac{z''}{z}v = 0.} \quad (2.91)$$

This equation plays a central role in the study of scalar perturbations. The solution to this equation reveals the behavior of $v \sim \mathcal{R}$, which has two significant properties. First, it can be shown that \mathcal{R} remains constant on super-Hubble scales in Fourier space. Specifically, it satisfies the following relation, which is derived in [Appendix A](#):

$$\mathcal{R}'(\eta, \mathbf{x}) = \frac{2M_{pl}^2\mathcal{H}}{\dot{\varphi}'^2}\Delta\Phi \implies \dot{\mathcal{R}}(t, \mathbf{k}) = -\frac{2M_{pl}^2H^3}{\dot{\varphi}'^2}\left(\frac{k}{aH}\right)^2\Phi. \quad (2.92)$$

Moreover, it can also be demonstrated that on super-Hubble scales, \mathcal{R} can be equated, up to a constant numerical factor, with, for example, the relative temperature fluctuations of photons after inflation. Thus, an inflationary model provides initial conditions for perturbations of the standard cosmological model and is able to give a direct prediction for phenomena such as the CMB, which will be discussed in more detail in the next chapter.

2.3.2 Vector perturbations

In case of vector perturbations, the general first-order metric 2.26 can be written as

$$\begin{aligned} ds^2 &= a^2(\eta) \left\{ -d\eta^2 - 2B_i d\eta dx^i + [\delta_{ij} - (E_{i,j} + E_{j,i})] dx^i dx^j \right\} \\ &\equiv a^2(\eta) dx^\mu [\eta_{\mu\nu} + h_{\mu\nu}^V] dx^\nu, \end{aligned} \quad (2.93)$$

where $h_{\mu\nu}^V$ consists of all vector perturbations. Plugging this into the equations for the Einstein tensor 2.78 and the perturbed stress-energy tensor 2.80 gives the corresponding equations of motion for vector perturbations. Using the additional conditions $B_{i,i}^V = E_{i,i} = 0$ and the fact that scalar-, vector- and tensor perturbations decouple in linear order, one obtains the following non-trivial equations for the $(0, i)$ and (i, j) components of the Einstein equations:

$$\Delta A_i = 0, \quad (2.94)$$

$$\frac{d}{d\eta} \left[A_{i,j} + A_{j,i} \right] + 2\mathcal{H} \left[A_{i,j} + A_{j,i} \right] = 0, \quad (2.95)$$

where $A_i \equiv E'_i - B_i$ describes the only physical vector degree of freedom. From Equation 2.95, it follows that the quantity in parentheses decays exponentially due to the quasi-exponential expansion with $H \approx \text{const}$. Thus, approximately, the following holds:

$$A_{i,j} + A_{j,i} = 0 \quad \forall i, j. \quad (2.96)$$

It is evident that for $i = j$, the respective A_i cannot depend on x_i . The relations between the A_i given by the previous equation for $i \neq j$ then imply that only terms up to the quadratic order in x_i can appear. The gauge invariance of A_i and the fact that its spatial average vanishes further imply that $A_i = 0$ must hold. This demonstrates that vector perturbations play a minor role in the cosmological evolution for a model without components for $i \neq j$ in the energy-momentum tensor.

2.3.3 Tensor perturbations

Lastly, in case of tensor perturbations, the general first-order metric 2.26 can be written as

$$\begin{aligned} ds^2 &= a^2(\eta) \left\{ -1 d\eta^2 + [1\delta_{ij} + h_{i,j}] dx^i dx^j \right\} \\ &\equiv a^2(\eta) dx^\mu [\eta_{\mu\nu} + h_{\mu\nu}^T] dx^\nu, \end{aligned} \quad (2.97)$$

where $h_{\mu\nu}^T$ consists of the two tensor degrees of freedom, which describe the propagation of gravitational waves. If one plugs $h_{\mu\nu}^T$ into the perturbed Einstein equations like before and makes use of the fact that $h_{ii} = h_{ij,i} = 0$, the only non-trivial equation comes from the (i, j) component and reads:

$$h_{ij}'' + 2\mathcal{H}h_{ij}' - \Delta h_{ij} = 0. \quad (2.98)$$

Performing a Fourier transformation on this equation gives

$$h_{ij}''(\eta, k) + 2\mathcal{H}h_{ij}'(\eta, k) + k^2 h_{ij}(\eta, k) = 0. \quad (2.99)$$

In the limit where a given mode k is deep in the sub-Hubble regime, the damping term proportional to \mathcal{H} can be neglected, resulting in the differential equation of a harmonic oscillator:

$$h_{ij}''(\eta, k) + k^2 h_{ij}(\eta, k) \approx 0. \quad (2.100)$$

The solution to this equation results in an oscillatory behavior for h_{ij}'' with a constant amplitude. When a given mode k grows to super-Hubble scales the last term is negligible and the equation reduces to

$$h_{ij}''(\eta, k) + 2\mathcal{H}h_{ij}'(\eta, k) \approx 0. \quad (2.101)$$

The general solution of this equation reads as follows:

$$h_{ij}(\eta, k) = \hat{h}_{ij}(k) - 2\mathcal{H}\tilde{h}_{ij}(\eta_*, k) e^{-\int_{\eta_*}^{\eta} 2\mathcal{H}d\eta'}, \quad (2.102)$$

where the second term decays over time and only the constant term remains. In conclusion, if the tensor perturbation is primordially created, then it remains as almost constant during the history of the Universe.

Chapter 3

Measurable quantities of inflation

This chapter focuses on how to derive measurable quantities from the inflation model and the previously derived equations, enabling physical predictions. It turns out that the introduction of so-called *power spectra* addresses this task effectively. Finally, it can be shown that a precise replication of the observable power spectrum for the curvature perturbation \mathcal{R} is possible through the appropriate choice of two model parameters. This chapter is mainly based on [7].

3.1 Introduction of the power spectrum

In cosmology (and astrophysics) one defines the power spectrum as the variance of the Fourier modes of an arbitrary field A :

$$P_A(t, k) = \left\langle |A(t, \vec{k})|^2 \right\rangle. \quad (3.1)$$

A wave vector appears on the right-hand side because it represents the variance for each mode \vec{k} . However, on the left-hand side, only the wave number is shown, since the assumption of a statistically isotropic universe ensures that the variance is identical for all modes \vec{k} sharing the same magnitude k . Although the power spectrum can be calculated at any specific time t , the time dependence will be omitted in the following discussion for brevity. Many measurable quantities in cosmology arise from the following type of integral:

$$Q = \int \frac{d^3 \vec{k}}{(2\pi)^3} P_A(k) K(k), \quad (3.2)$$

where $K(k)$ describes a dimensionless kernel. If the integrand depends only on the magnitude of \vec{k} , the integral can be decomposed as $d^3 \vec{k} = k^2 dk d\Omega$. This leads to the

following expression for the measurable quantity Q:

$$Q = \int d\ln k \left(\frac{k^3}{2\pi^2} P_A(k) \right) K(k). \quad (3.3)$$

The expression above was derived by performing an integration over the solid angle $d\theta$ and changing the integration variable from dk to $d\ln k$. If A is dimensionless, the expression within the parentheses must also be dimensionless. This expression is typically referred to as the *dimensionless power spectrum* \mathcal{P}_A :

$$\mathcal{P}_A(k) = \frac{k^3}{2\pi^2} P_A(k). \quad (3.4)$$

The power spectrum of a quantity Q describes the 'amount' of fluctuations of this quantity for each mode k. In the case of the curvature perturbation \mathcal{R} , it is particularly significant because, after inflation, it is related to the statistics of other perturbations.

3.2 Power spectrum of curvature perturbation

The Mukhanov-Sasaki equation 2.91 can also be transformed into the following form using a Fourier transformation:

$$v_k'' + \left(k^2 - \frac{z''}{z} \right) v_k = 0, \quad (3.5)$$

where the subscript for v_k denotes, that v only depends on the magnitude of \vec{k} . Starting from this point, it is reasonable to ask where the fluctuations in the early universe originate from and how exactly these should be initialized. At first glance, it might seem that the horizon problem is merely replaced by the problem of choosing the initial conditions for the fluctuations. However, it turns out that an elegant solution to this problem exists when one recognizes that the fluctuations of the inflaton field, like those of any field, are of a quantum nature. This means that one can promote the field v and its conjugate momentum v' to a quantum operator

$$v \rightarrow \hat{v} = \int \frac{d\vec{k}^3}{(2\pi)^3} \left[v_k(\eta) \hat{a}_{\vec{k}} e^{i\vec{k}\cdot\vec{x}} + v_k^*(\eta) \hat{a}_{\vec{k}}^\dagger e^{-i\vec{k}\cdot\vec{x}} \right], \quad (3.6)$$

$$\text{or } v_{\vec{k}} \rightarrow \hat{v}_{\vec{k}} = v_k(\eta) \hat{a}_{\vec{k}} + v_{-k}^*(\eta) \hat{a}_{-\vec{k}}^\dagger, \quad (3.7)$$

where $\hat{a}_{\vec{k}}^\dagger$ and $\hat{a}_{\vec{k}}$ are the creation and annihilation operators respectively and satisfy the canonical commutation relation

$$[\hat{a}_{\vec{k}}, \hat{a}_{\vec{k}'}^\dagger] = (2\pi)^3 \delta(\vec{k} - \vec{k}'), \quad (3.8)$$

only if the mode function v_k is normalized as follows

$$\langle v_k, v_k \rangle \equiv \frac{i}{\hbar} (v_k^* v'_k - v_k^{*\prime} v_k) = 1. \quad (3.9)$$

Equation 3.9 provides a boundary condition to the solution of equation 3.5. However, the mode function is not uniquely determined by this alone. A second boundary condition is required, the choice of which is equivalent to selecting a vacuum state, which is not uniquely defined in curved spacetime:

$$\hat{a}_{\vec{k}} |0\rangle = 0. \quad (3.10)$$

An intuitive choice for the vacuum is the *Minkowski vacuum of a comoving observer in the distant past*. In this limit, all comoving scales are within the sub-Hubble regime, $\eta \rightarrow -\infty$ or $k \gg aH$. This designation arises from the observation that when considering distances and timescales much smaller than the Hubble scale, the curvature of spacetime becomes negligible, and perturbations behave as they would in Minkowski space.

In this limit the Mukhanov-Sasaki equation reduces to

$$v''_k + k^2 v_k = 0. \quad (3.11)$$

This equation represents a simple harmonic oscillator with a constant frequency. In this scenario, a unique solution can be determined by requiring that the vacuum state corresponds to the state of minimum energy. Consequently, the following initial condition is imposed:

$$\boxed{\lim_{\eta \rightarrow -\infty} v_k = \frac{e^{-ik\eta}}{\sqrt{2k}}.} \quad (3.12)$$

The boundary conditions completely fix the mode function v_k on all scales. This makes it relatively straightforward to obtain a solution in the de-Sitter limit ($H = \text{const.}$), as the following holds:

$$\frac{z''}{z} = \frac{a''}{a} = \frac{2}{\eta^2}, \quad (3.13)$$

which leads to the following mode equation

$$v''_k + \left(k^2 - \frac{2}{\eta^2} \right) v_k = 0. \quad (3.14)$$

Considering the quantization condition 3.9 together with the sub-horizon limit 3.2 there is a unique expression for the mode function

$$\boxed{v_k = \frac{e^{-ik\eta}}{\sqrt{2k}} \left(1 - \frac{i}{k\eta} \right).} \quad (3.15)$$

This leads to the following expression for the power spectrum $\mathcal{P}_{\mathcal{R}}$

$$\mathcal{P}_{\mathcal{R}}(k) = \frac{k^3}{2\pi^2} \langle 0 | \hat{\mathcal{R}}_k^\dagger \hat{\mathcal{R}}_k | 0 \rangle = \frac{k^3}{2\pi^2} \frac{|v_k(\eta)|^2}{z^2} = \frac{k^3}{2\pi^2} \frac{H^2}{a^2 \dot{\varphi}^2} \frac{1}{2k} \left(1 + \frac{1}{k^2 \eta^2} \right) \quad (3.16)$$

$$= \frac{k^3}{2\pi^2} \frac{H^2}{a^2 \dot{\varphi}^2} \frac{1}{2k} \left(1 + \frac{a^2 H^2}{k^2} \right) \stackrel{k \ll aH}{\approx} \frac{k^3}{2\pi^2} \frac{H^2}{a^2 \dot{\varphi}^2} \frac{1}{2k^3} a^2 H^2 \quad (3.17)$$

$$= \frac{H^4}{(2\pi)^2 \dot{\varphi}^2}, \quad (3.18)$$

where the ensemble average $\langle \dots \rangle$ was replaced by a vacuum expectation value due to the quantization of the field $\hat{v}_k = z \hat{\mathcal{R}}_k$ and the calculation was performed in the super-Hubble regime $k \ll aH$. Additionally, it has been assumed, with reasonable approximation, that $\eta \approx -\frac{1}{aH}$ is valid for a quasi De Sitter expansion. This approach was taken because, as demonstrated in the Appendix, \mathcal{R} remains constant in the super-Hubble regime, which in turn causes the power spectrum to also become constant for each mode k once $k = aH$ is satisfied. Since the time t_k of the so-called Hubble crossing varies slightly for each mode, the power spectrum $\mathcal{P}_{\mathcal{R}}$ has a non-trivial feature and for modes in the super-Hubble regime is given by:

$$\mathcal{P}_{\mathcal{R}}(k) = \frac{H^4(t_k)}{(2\pi)^2 \dot{\varphi}^2(t_k)}. \quad (3.19)$$

3.3 Model parameters of inflaton

In the previous section, it was demonstrated that the power spectrum depends on the values of H and $\dot{\varphi}$ at the time t_k , when the corresponding mode k becomes super-Hubble. Since the field is in the slow-roll regime, H and $\dot{\varphi}$ should have a weak dependence on this time t_k , and thus also on k . Therefore, the leading order of the Taylor expansion of $\ln \mathcal{P}_{\mathcal{R}}$ with respect to $\ln k$ can be approximated as follows:

$$\mathcal{P}_{\mathcal{R}} = A_s (k/k_*)^{n_s - 1}, \quad (3.20)$$

where A_s represents the *amplitude of the power spectrum*, and n_s describes the *spectral tilt*. The variable k_* denotes an arbitrary *pivot scale* required for the expansion, which is typically set to a value within the CMB scale, often chosen as $k = 0.05 Mpc^{-1}$.

A_s and n_s can be calculated via the following equations

$$A_s = \frac{128\pi}{3} \frac{V(\varphi(t_{k_*}))^3}{M_{pl}^6 V'(\varphi(t_{k_*}))^2}, \quad (3.21)$$

$$n_s = 1 - 6\epsilon(t_{k_*}) + 2\eta(t_{k_*}). \quad (3.22)$$

By specifying A_s and n_s , the power spectrum is fully determined up to the point when the corresponding mode R_k re-enters the sub-Hubble region. After horizon re-entry, this serves as the initial condition for the evolution of perturbations, which is crucial for calculating the CMB power spectrum, as illustrated in Figure 3.1.

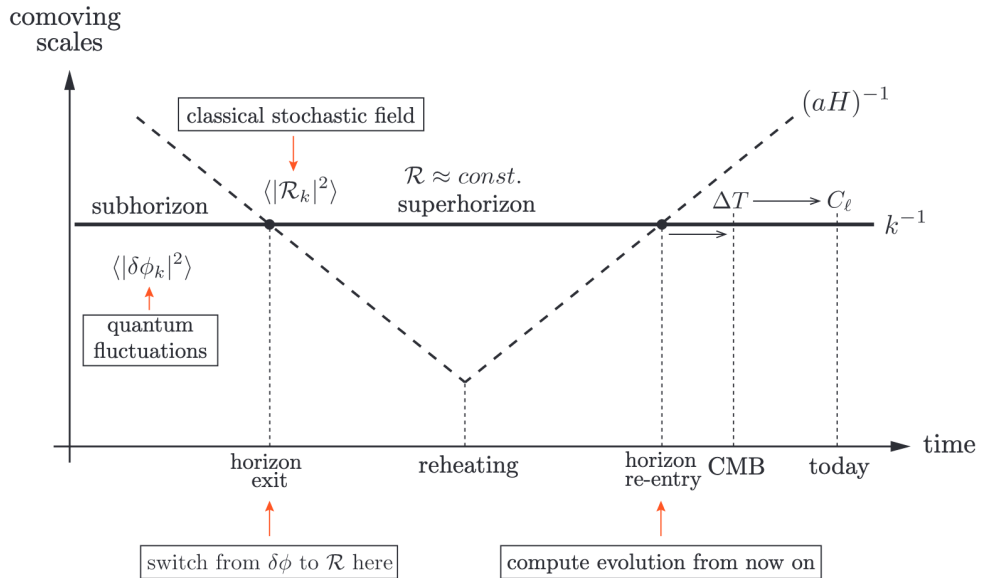


FIGURE 3.1: Illustrative representation of the evolution of a mode R_k from the beginning of inflation until the point when the corresponding mode re-enters the sub-Hubble regime. Afterward, these corresponding fluctuations R_k can be used as the initial conditions for the further evolution of the perturbations required to calculate the CMB power spectrum.

This approach provides predictive power, enabling a comparison between a given inflationary model with potential V and observational data. It turns out that $A = 2.1 \cdot 10^{-9}$ and $n = 0.9665$, which, for the $m^2\varphi^2$ -model, corresponds to the following parameters:

$$\begin{aligned} m &\approx 1.42 \cdot 10^{13} \text{ GeV}, \\ \varphi_{ini} &\approx 3.7885 \cdot 10^{19} \text{ GeV}. \end{aligned} \quad (3.23)$$

Chapter 4

Lattice simulation of single-field Inflation

This chapter focuses on the simulation of the first out of two inflationary models using the *CosmoLattice* program. The first section explains the principles and benefits of *CosmoLattice* for simulating inflationary physics in the early universe. Subsequently, the results of the simulation for a quadratic potential are compared with the corresponding analytical expressions. This comparison provides insight into the predictiveness and limitations of *CosmoLattice*, as it assesses how well the program can reproduce the predictions of this "simple" model. The final chapter then presents an analysis of a hybrid inflation model, which constitutes the core of this thesis. Unlike the quadratic potential, the hybrid model generally lacks analytical solutions. Building on the groundwork laid in the analysis of the quadratic potential in this chapter, the study demonstrates to what extent *CosmoLattice*, within its capabilities, can yield meaningful results for this more complex model.

4.1 Introduction to *CosmoLattice*

CosmoLattice [12] is a modern computational package designed for simulating the dynamics of interacting scalar and gauge fields in an expanding universe. It discretizes spacetime to simulate the non-linear evolution of such fields on a lattice. The equations implemented in *CosmoLattice* are grounded in the theoretical framework described in [13]. The package currently supports simulations of various scenarios, including singlet scalar fields and scalar fields charged under U(1) and/or SU(2) gauge symmetries, along with their corresponding Abelian and non-Abelian gauge vector fields. Simulations can

be conducted in either a flat spacetime or a homogeneous and isotropic expanding background. In the latter case, the fields can evolve over a fixed background (e.g., with a power-law scale factor) or self-consistently, where the expansion rate of the universe is determined by the fields themselves.

CosmoLattice is particularly suited for studying scenarios where the dynamics of the fields lead to large occupation numbers ($n_k \gg 1$), making the quantum nature of the fields negligible. In such cases, classical field theory becomes a powerful tool for analyzing complex field dynamics, including scenarios involving non-linear interactions, non-perturbative particle production, and out-of-equilibrium field distributions. The early universe, characterized by high-energy physics and rich non-linear dynamics, often cannot be described analytically. As a result, numerical techniques are essential for fully understanding these phenomena, particularly in post-inflationary scenarios such as reheating.

The program therefore adopts the approach of not expanding the underlying equations of motion for the fields in leading perturbative order, but rather retaining the full non-linearity of the equations and solving them numerically. These are then expressed by the following equations in case of an arbitrary number of scalar fields:

$$\begin{aligned} \tilde{\varphi}_i'' - a^{-2(1-\alpha)} \tilde{\nabla}^2 \tilde{\varphi}_i + (3 - \alpha) \frac{a'}{a} \tilde{\varphi}_i' &= -a^{2\alpha} \tilde{V}_{,\varphi_i}, \\ \tilde{\mathcal{H}} \equiv \left(\frac{a'}{a}\right)^2 &= \frac{a^{2\alpha} f_*^2}{3m_{pl}^2} \left\langle \frac{1}{2a^{2\alpha}} \sum_i \tilde{\varphi}_i^2 + \frac{1}{2a^2} \sum_i (\tilde{\nabla}_i \tilde{\varphi}_i)^2 + \tilde{V}(\tilde{\varphi}_i) \right\rangle. \end{aligned} \quad (4.1)$$

where $\tilde{\varphi}_i' \equiv \frac{d\tilde{\varphi}_i}{d\tilde{\eta}}$, $\langle \dots \rangle$ refers to an average in real space and both equations are written in dimensionless quantities, which are defined by the following relations:

$$\tilde{\varphi}_i \equiv \frac{\varphi_i}{f_*}, \quad d\tilde{\eta} \equiv a^{-\alpha} \omega_* dt, \quad d\tilde{x}^i \equiv \omega_* dx^i. \quad (4.2)$$

The primary motivation for normalizing by ω_* and f_* is twofold: firstly, to bring the input parameters of the equations, such as the fields φ_i , to an order of magnitude around $\mathcal{O}(1)$, ensuring numerical stability when solving the equations; and secondly, in conjunction with α , to set the timescale over which the system evolves and the relevant physical processes occur.

To numerically solve these equations, **CosmoLattice** discretizes and evolves the equations on a cubic lattice with N^d points, where N represents the number of lattice sites per dimension and d the number of spatial dimensions. By default, $d = 3$, although simulations with scalar fields in $d = 2$ or $d = 1$ dimensions are also possible.

In addition to N , the box length L must be specified, which determines the spacing between neighboring points as $\delta x \equiv \frac{L}{N}$. In this way, continuous functions $f(\mathbf{x})$ can be defined on the lattice, where they only have a value at the point $\mathbf{x} = \mathbf{n}\delta x$, with \mathbf{n} denoting the position of a lattice point. For a self-consistent expansion, determined by the corresponding evolution of the fields, the \mathbf{x} coordinates represent comoving spatial coordinates. To simulate an infinitely expanding universe within a finite lattice, periodic boundary conditions are also assumed. This means that for unit vectors \mathbf{e}_i with $i \in 1, 2, 3$ along the lattice edges and any point \mathbf{x}_p on the lattice, the following holds: $f(\mathbf{x}_p + \mathbf{e}_i \cdot N) = f(\mathbf{x}_p)$. These periodic boundary conditions in coordinate space imply that the momenta must be discretized. For each lattice one can always consider a reciprocal lattice representing Fourier modes, with its sites labeled as $\tilde{\mathbf{n}}$ and which are related through a discrete Fourier transformation (DFT) defined by

$$f(\mathbf{n}) \equiv \frac{1}{N^3} \sum_{\tilde{\mathbf{n}}} e^{-i\frac{2\pi}{N}\tilde{\mathbf{n}}\mathbf{n}} f(\tilde{\mathbf{n}}) \quad \Leftrightarrow \quad f(\tilde{\mathbf{n}}) \equiv \sum_{\mathbf{n}} e^{+i\frac{2\pi}{N}\mathbf{n}\tilde{\mathbf{n}}} f(\mathbf{n}). \quad (4.3)$$

As previously mentioned, the momenta are discretized in the reciprocal lattice, with the minimum and maximum momenta given by:

$$k_{IR} = \frac{2\pi}{L}, \quad k_{max} = \frac{\sqrt{3}}{2} N k_{IR}, \quad (4.4)$$

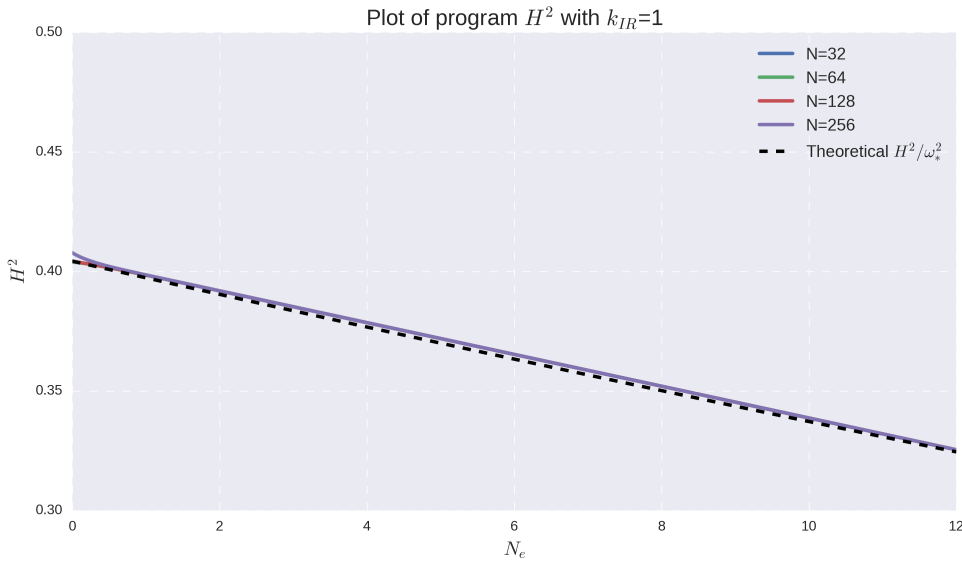
and hence $\tilde{\mathbf{n}}$ labels the discretized momentum values $\mathbf{k} = \tilde{\mathbf{n}}k_{IR}$. If one has a good a priori understanding of the typical momentum scales expected to be excited in the scenario to be simulated, k_{IR} can be specified instead of L . A time step $\delta\eta$ can then be chosen to evolve the system incrementally. To ensure the stability of the solution, the criterion $\delta\eta/\delta x < 1/\sqrt{d}$ must be met. By appropriately choosing φ_{ini} and $\dot{\varphi}_{ini}$, the system can be numerically evolved in real space up to a time t_{end} . However, before this, the fluctuations in Fourier space are initialized. These fluctuations are Gaussian-distributed around zero with a variance of

$$|\delta\tilde{\varphi}(\tilde{\mathbf{n}})|^2 \equiv \left(\frac{\omega_*}{f_*}\right)^2 \left(\frac{N}{\delta x}\right)^3 \frac{1}{2a^2 \sqrt{\tilde{k}^2(\tilde{\mathbf{n}}) + a^2 \tilde{m}_\varphi^2}}, \quad \tilde{m}_\varphi^2 \equiv \frac{\partial^2 \tilde{V}}{\partial \tilde{\varphi}^2}, \quad (4.5)$$

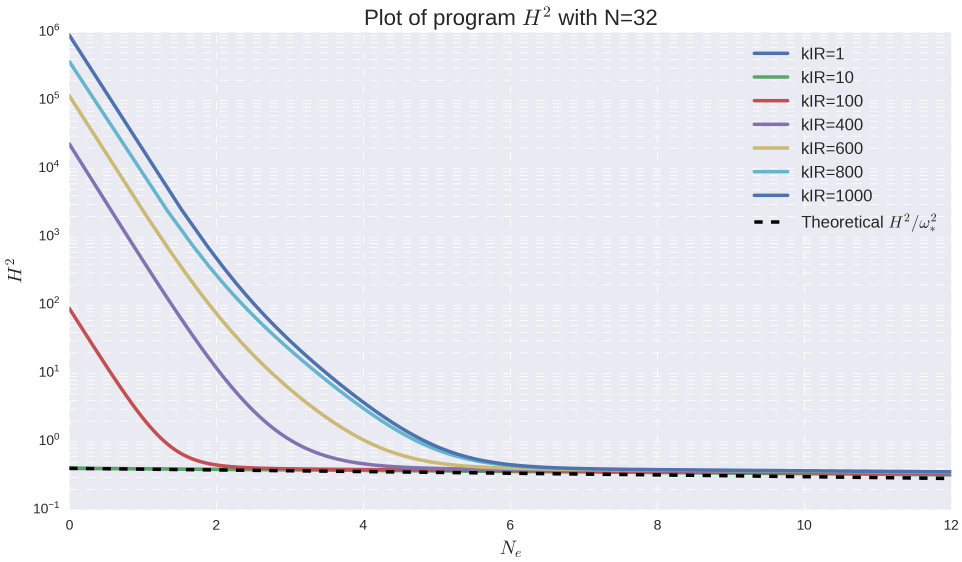
where $\tilde{k} \equiv k/\omega_*$ and $\tilde{m}_\varphi \equiv m_\varphi/\omega_*$ are momentum and effective mass in program variables. The variance of the fluctuations is set in such a way that the modes in the continuum reproduce the Bunch-Davies vacuum. This outlines the basic principle of the program and the most important part of its structure for this work. For further information on the mathematical treatment of discretization, the development of various evolvers for the evolution of the equations of motion, as well as general settings and technical details, references [12] and [13] are recommended.

4.2 Simulation of quadratic model

This section compares the theoretical predictions of the inflation model with a quadratic potential $V(\varphi) = \frac{1}{2}m^2\varphi^2$ to the corresponding simulations from *CosmoLattice*. The simulations use the same values for the initial condition $\varphi_{ini} \approx 3.7885 \cdot 10^{19}$ GeV and the mass $m \approx 1.42 \cdot 10^{13}$ GeV of the inflaton field, as mentioned at the end of Chapter 3, to allow for a direct comparison with background quantities φ , $\dot{\varphi}$ and H and the power spectrum \mathcal{P}_R .



(a) Simulations of the evolution of H^2 over 12 e-folds with varying grid resolutions N , compared to the analytic expression in the slow-roll approximation. The smallest mode was set to $k_{IR} = 1$.



(b) Simulations of the evolution of H^2 over 12 e-folds with different infrared modes k_{IR} , compared to the analytic expression in the slow-roll approximation. The grid resolution was fixed at $N = 32$.

Assuming slow-roll conditions, the background equations for φ and H can be solved relatively easily, taking the following form with respect to cosmic time:

$$\bar{\varphi}(t) = \varphi_{ini} + \dot{\varphi}_{init} t, \quad \dot{\varphi}_{ini} \equiv -\sqrt{\frac{m^2}{12\pi G}}, \quad (4.6)$$

$$H^2 = \frac{4\pi G}{3} \left[\dot{\varphi}_{ini}^2 + m^2 (\varphi_{ini} + \dot{\varphi}_{init} t)^2 \right]. \quad (4.7)$$

The dimensionless quantities H/ω_* and $\dot{\varphi}/(\omega_* f_*)$ can then be compared with the simulations for different box parameters N and k_{IR} in dependence of the e-fold number $N_e(t)$, as shown in Figure 4.1(a) and 4.1(b) for the former. For the latter, the plots can be found in Appendix B. The plots clearly demonstrate that `CosmoLattice` successfully reproduces the background evolution for this model, as long as N and, in particular, k_{IR} are not chosen too large. Since the plots for $\dot{\varphi}/(\omega_* f_*)$ exhibit the same behavior, they have been included in the appendix.

Otherwise, back-reaction effects dominate, caused by the large number of modes deep in the sub-Hubble regime. While these specific simulations approach the theoretical curve over the course of the evolution, they still significantly influence the evolution of other quantities such as \mathcal{P}_R . Thus, their impact should be minimized by choosing appropriate values for N and k_{IR} . The influence of back-reactions arises from the fact that the average is performed over quadratic quantities such as $\langle \varphi^2 \rangle$, leading the fluctuations to provide the following additional contribution for a spherically symmetric geometry [14]:

$$\langle \delta\varphi^2 \rangle = \int d\log(k) \frac{k^3}{2\pi^2} P_R(k) \sim \int_{k_{IR}}^{\frac{\sqrt{3}}{2} k_{IR} N} dk k \sim \left(\frac{3}{4} N^2 - 1 \right) k_{IR}^2. \quad (4.8)$$

The expression above exhibits a divergence in the ultraviolet region. The ultraviolet divergence is the typical one found in free quantum field theory, which can be addressed by introducing an ultraviolet cutoff, k_{cut} . In the infrared, all modes with $k < k_{IR}$, corresponding to wavelengths larger than the Hubble radius at the onset of inflation, are excluded, as these modes are governed by pre-inflationary physics. These are considered to contribute to the background. However, the relationship can not be entirely accurate and was only assumed to illustrate the dependence of back-reactions on k_{IR} and N , as the lattice only allows discrete modes and has the geometry of a cube. This implies that, in addition to the quadratic dependence on k_{IR} , a cubic dependence on N is expected for the back-reactions, as shown in Figure 4.1. In this rather symbolic 'fit,' it is demonstrated that the magnitude of the back-reactions scales quadratically with the parameter k_{IR} and cubically with N . To minimize the effect of the back-reactions and ensure reasonable runtime for the simulation, the parameters were limited to $k_{IR} = 1$ and $N = 128$ in the following analysis.

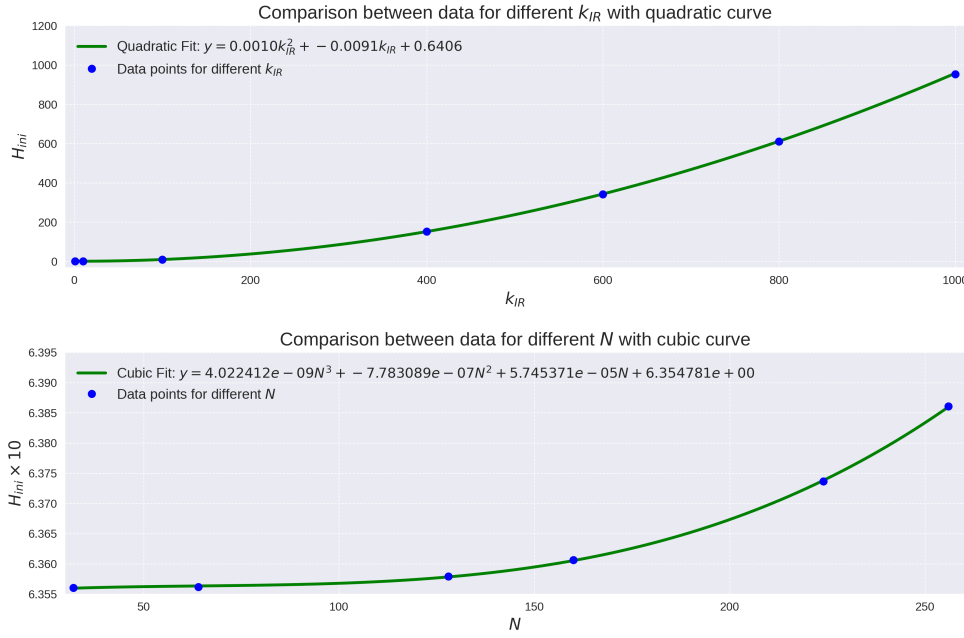


FIGURE 4.1: Symbolic fits of data points for H_{ini} for different values of k_{IR} and N . Since the errors of the data points are not known, the corresponding curves serve only to illustrate the polynomial behavior of the back-reactions with respect to k_{IR} and N .

Since *CosmoLattice* provides not only the background quantities but also the power spectrum for the field φ , it allows one to also track the time evolution of the curvature power spectrum \mathcal{P}_R shown in Figure 4.2, which is given by the following relation:

$$\mathcal{P}_R(k, N_e) = \frac{H^2(N_e)}{\dot{\varphi}^2(N_e)} \mathcal{P}_{\delta\varphi}(k, N_e). \quad (4.9)$$

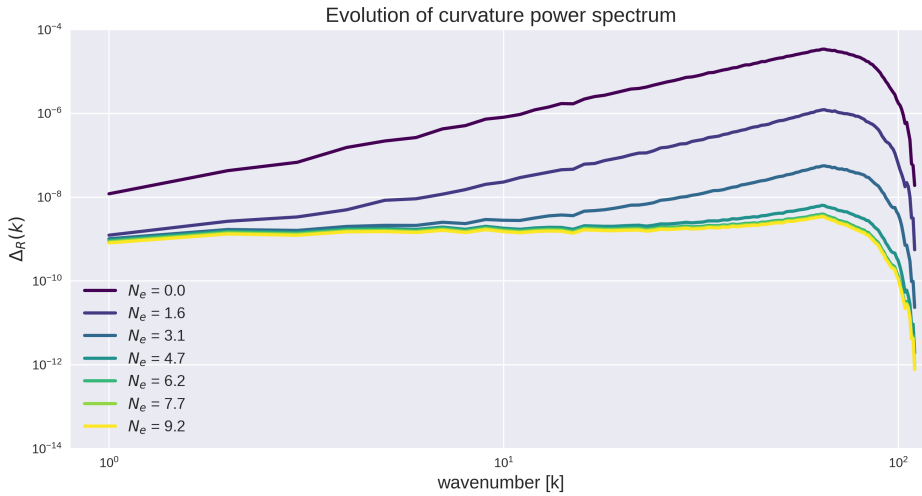


FIGURE 4.2: Time evolution of the curvature power spectrum from the Bunch-Davies vacuum to the nearly scaleless power spectrum. The time dependence is expressed in terms of the e-fold number N_e .

Comparing equation 4.9 with the definition of \mathcal{R} in equation 2.90, it becomes evident that the contribution from the metric perturbation Φ has been neglected. This is because *CosmoLattice* does not currently account for metric perturbations, as they play a minor role in the early universe, as shown in [11]. This omission allows for a direct comparison between the *CosmoLattice* simulation, up to the point where all modes are in the super-Hubble regime, and the theoretical expectation for $\mathcal{P}_{\mathcal{R}}$. This comparison is shown in Figure 4.3, where it is clear that *CosmoLattice* can mostly reproduce the amplitude of the power spectrum in a specific wavelength range, with the exception of the scalar tilt of the spectrum.

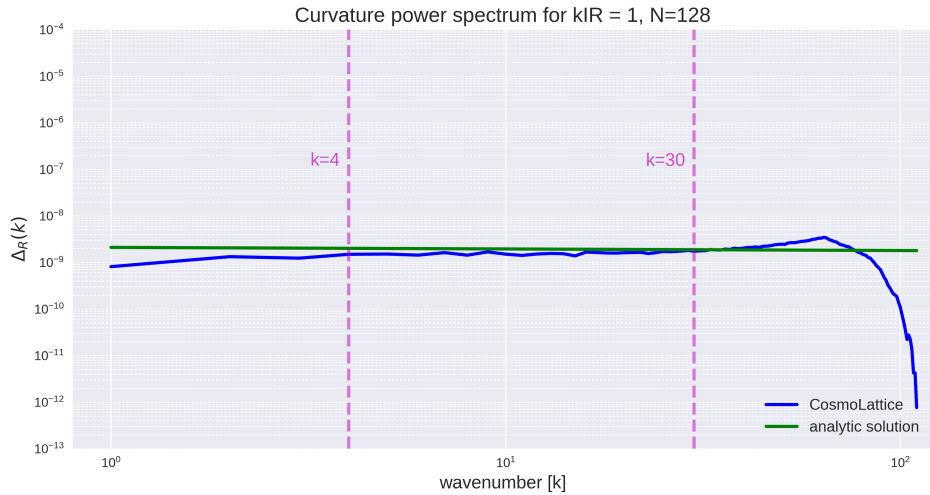


FIGURE 4.3: Comparison of the power spectrum simulated with *CosmoLattice* and the theoretical prediction. In the range from $k = 4$ to $k = 30$, where k describes the dimensionless wave number, the simulation matches the analytic solution quite well. The scalar tilt cannot be reproduced by the simulation, as can be observed from the decreasing differences between simulation and theory with increasing k .

Figure 4.3 clearly shows that the simulation underestimates the power spectrum in the regions of small k near k_{IR} and very large k near k_{max} . This is due to how the power spectrum is determined in Fourier space for each mode k . Since the modes are discrete, the contribution to the power spectrum for a given value of k is obtained by counting all modes within a band between the radii k and $k + \Delta k$. However, due to the cubic geometry, this provides a poor approximation for the smallest and largest modes, as is especially evident in Figures 4.4. The simulations thus demonstrate impressively which parameters and range allow *CosmoLattice* to provide a good approximation of the power spectrum. As a result, the outcomes of the simulation of the quadratic potential serve as the foundation for simulating other more complex models, one of which will be introduced in the next chapter.

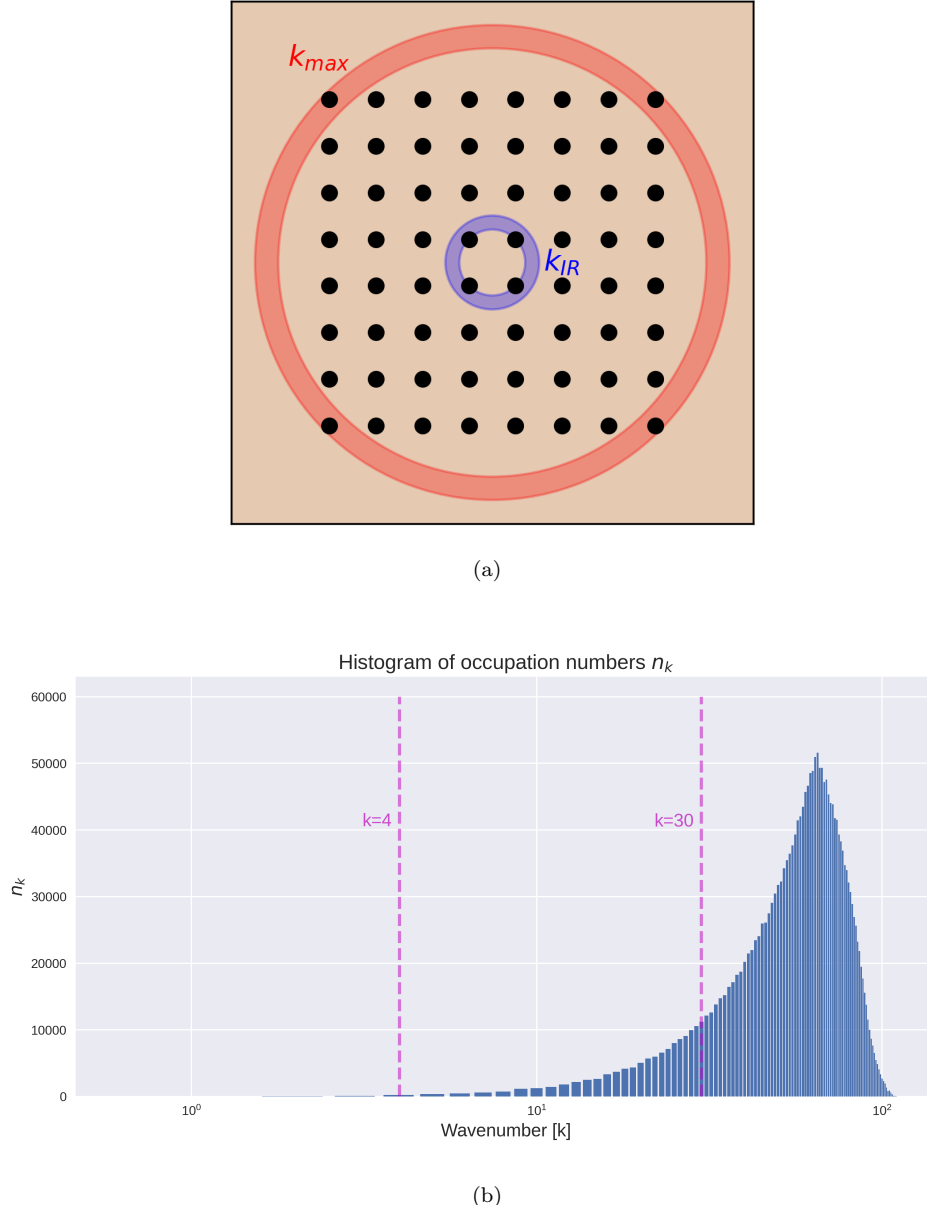


FIGURE 4.4: (a): Graphical representation of a 2D lattice showing how the contributions to the power spectrum for the modes k_{IR} and k_{max} are calculated. (b): Occupation numbers n as a function of the wave number k for the simulation in Figure 4.3. For a classical description, $n_k \gg 1$ is required.

Chapter 5

Theory and simulation of hybrid inflation model

In standard inflationary models, predictions such as scale-invariant, Gaussian, and adiabatic perturbations align well with current cosmic microwave background (CMB) observations [15]. However, future high-precision data, like that from PLANCK, may reveal deviations, such as non-Gaussianity, which could challenge many single-field inflation models.

Local features in the power spectrum, motivated by irregularities in the CMB at specific angular scales, can arise from processes like particle creation or field interactions during inflation. Typically, these features result from temporary violations of the slow-roll conditions, although many existing models use arbitrary mechanisms to achieve this.

In this work, a dynamic mechanism is introduced within a chaotic inflation framework, where the inflaton field φ with its quadratic potential couples to a heavy field χ . When φ reaches a critical value φ_c , χ becomes tachyonic and a rapid phase transition occurs, creating local features in the power spectrum. Unlike hybrid inflation, the potential in this model is not vacuum dominated and therefore the chaotic inflation continues after the phase transition. For observable CMB effects, this transition must occur 50-60 e-folds before inflation ends.

This model, which is taken from [16], presents a natural way to explain local features in the CMB, providing new insights into inflationary dynamics.

The inflationary process in this model can be divided into three distinct stages:

- **Stage 1:** During the first stage, when $\varphi > \varphi_c$, inflation proceeds according to the standard chaotic inflation scenario, driven by the inflaton field φ .

- **Stage 2:** Once φ drops below the critical value φ_c , the second stage begins. This phase is brief in this model, lasting approximately up to 1 e-fold for most parameter choices. During this period, the secondary field χ becomes tachyonic, triggering a waterfall phase transition. As a result, χ settles into its global minimum, leading to a slight shift in the effective mass of the inflaton:

$$m^2 \rightarrow m_+^2 = m^2(1 + C) \quad \text{with} \quad C \ll 1.$$

- **Stage 3:** After the phase transition, the third stage commences. The inflation process resumes, once again following the chaotic inflation dynamics as in Stage 1.

For this purpose, the following potential is considered:

$$\begin{aligned} V(\varphi, \chi) &= \frac{m^2}{2}\varphi^2 + \frac{\lambda}{4}\left(\chi^2 - \frac{M^2}{\lambda}\right)^2 + \frac{g^2}{2}\varphi^2\chi^2 \\ &= \frac{m^2}{2}\varphi^2 + \frac{\lambda}{4}\chi^4 - \frac{1}{2}M^2\chi^2 + \frac{M^4}{4\lambda} + \frac{g^2}{2}\varphi^2\chi^2. \end{aligned} \tag{5.1}$$

The waterfall field χ becomes tachyonic, when its squared effective mass $m_{eff}^2 = g^2\varphi^2 - M^2$ becomes negative, which is given at $\varphi = \varphi_c \equiv M/g$. The waterfall field then quickly rolls down to its local minimum, where also the potential $V(\varphi, \chi)$ has its local minimum. Then, chaotic inflation continues with a slightly shifted mass $m_+^2 = m^2 + g^2\langle\chi\rangle = m^2(1 + C)$ with $C \equiv \frac{g^2M^2}{\lambda m^2}$, where $C \ll 1$ corresponds to the assumption that the potential is dominated by the quadratic inflaton potential.

To ensure the phase transition completes relatively quickly, the inflaton continues driving the expansion after the transition and that this local feature manifests on CMB scales, the following conditions must be met:

$$\alpha \equiv \frac{m^2}{H^2} \ll 1, \quad \beta \equiv \frac{M^2}{H^2} \gg 1, \quad \varphi_c \gtrsim 10 \cdot M_{pl}. \tag{5.2}$$

Here, the smallness of the parameter α ensures that the inflaton remains in the slow-roll regime, β controls the sharpness of the phase transition's duration, and φ_c clearly determines the energy scale at which this process occurs. However, the exact parameters chosen will be discussed in the section where the theoretical calculations are compared with the simulations.

5.1 Inflaton background dynamics

As previously mentioned, the model was taken from source [16], and accordingly, the mathematical aspect of this model also follows that reference. During the first and second phases, the contribution of the field χ can be neglected, and the potential effectively behaves as:

$$V(\varphi, 0) = \frac{1}{2}m^2\varphi^2 + \frac{M^4}{4\lambda}, \quad (5.3)$$

up to the point where the self interaction term $\lambda\chi^4$ becomes important. Just like in the single-field inflation model, in this regime the equation of motion can be solved in the slow-roll approximation, resulting in the following background evolution as a function of the e-fold number $n = N - N_c$:

$$-4M_P^2(N - N_c) = -4M_P^2n = \varphi(n)^2 - \varphi_c^2 \left[1 - C \ln \left(\frac{\varphi}{\varphi_c} \right) \right], \quad (5.4)$$

where N_c describes the e-fold number at the beginning of the phase transition. After the waterfall field settles to its local minimum, driven by the self-interaction term and denoted by the time n_f , it begins rolling across the valley defined by the condition $\partial_\chi V(\varphi, \chi) = 0$, which leads to the following result:

$$\chi^2 = \chi_{\min}^2 \equiv \frac{M^2}{\lambda} - \frac{g^2}{\lambda}\varphi^2. \quad (5.5)$$

The contribution of the waterfall field to the potential in the third phase is therefore determined by the value of φ . As a result, the evolution of the inflaton is influenced by the effective potential:

$$V_{\text{eff}}^+(\varphi) = V(\varphi, \chi(\varphi)) = \frac{1}{2}m^2(1 + C)\varphi^2 - \frac{g^4}{4\lambda}\varphi^4. \quad (5.6)$$

This then gives the following behaviour for the third stage:

$$8M_P^2(N_e - N) = 2\varphi^2(N) - 2\varphi_e^2 + \frac{C}{2} \frac{\varphi^4(N) - \varphi_e^4}{\varphi_c^2} + O(C^2), \quad (5.7)$$

where $\varphi_e \equiv \sqrt{2} \cdot M_{pl}$ marks the end of inflation. In the results section, it will later be demonstrated that Equation 5.4 provides an excellent approximation for all three stages, even though Equation 5.7 represents the exact solution for stage 3. Therefore, equation 5.7 is included for completeness, but beyond its use in calculating the curvature perturbation, it will not play a significant role.

5.2 Waterfall field dynamics

This section explores the dynamics of quantum fluctuations in the waterfall field. Similar to hybrid inflation models, before the waterfall transition, the field χ remains heavy and is fixed at its local minimum $\chi = 0$, meaning there is no classical evolution of the waterfall field during this stage. Following the method outlined in [17], it is assumed that for each horizon-sized patch, the fluctuations χ^2 behave as a homogeneous classical background that varies smoothly on scales larger than the horizon.

On sufficiently large scales, such as the current comoving Hubble horizon, the average value $\langle \delta\chi^2(n) \rangle$ can be computed, and the fluctuation is defined as:

$$\Delta\chi^2(n, x) \equiv \delta\chi^2(n, x) - \langle \delta\chi^2(n) \rangle, \quad (5.8)$$

where $\langle \delta\chi^2(n) \rangle$ represents the homogeneous background, while $\Delta\chi^2(n, x)$ leads to curvature perturbations on super-horizon scales.

With this approach, the background waterfall dynamics and quantum fluctuations are analyzed in further detail. The evolution of the background waterfall field is governed by

$$\chi'' + 3\chi' + \left(-\beta + g^2 \frac{\varphi^2}{H^2} + 3\lambda \frac{\chi^2}{H^2} \right) \chi = 0, \quad (5.9)$$

where the prime here and for the rest of this chapter will denote a derivative with respect to n . As previously mentioned, the waterfall field has no classical evolution during the first stage and remains fixed at $\chi = 0$. During the second stage, the self-interaction term can be neglected, and the solution 5.4 for φ is applied. This leads to an equation that has the following approximate solution:

$$\chi(n) \simeq \chi(n=0) \exp \left[\frac{2}{3} \epsilon_\chi n^{3/2} \right], \quad (5.10)$$

where $\epsilon_\chi \simeq \sqrt{\frac{2}{3}\alpha\beta}$ is assumed to be large. During the second stage, a perturbative treatment of the problem, as discussed in detail in Section 2.2, is still possible. Thus, the following equation for the fluctuations of χ can be formulated in Fourier space:

$$\delta\chi''_{\mathbf{k}} + 3\delta\chi'_{\mathbf{k}} + \left(\frac{k^2}{a^2 H^2} - \beta + g^2 \frac{\varphi^2}{H^2} \right) \delta\chi_{\mathbf{k}} = 0. \quad (5.11)$$

Plugging the background value of φ given by equation 5.4 into this equation leads to

$$\delta\chi''_{\mathbf{k}} + 3\delta\chi'_{\mathbf{k}} + \left(\frac{k^2}{k_c^2} e^{-2n} - \epsilon_\chi^2 n \right) \delta\chi_{\mathbf{k}} = 0, \quad (5.12)$$

where k_c is the comoving momentum of the mode which exits the horizon at the time of waterfall phase transition: $k_c = Ha(n=0)$.

The term inside the parentheses can be understood as the effective tachyonic mass $m_{k,eff}^2(n)$, the magnitude of which quantifies the sharpness of the phase transition. Therefore, in this context, a sharp transition is equivalent to $\epsilon_\chi \gg 1$. For large and negative n , $m_{k,eff}^2(n)$ varies only slowly with n and therefore equation 5.12 can be solved by the WKB approximation by setting $\delta\chi_{\mathbf{k}} \propto \exp[S_0 + S_1 + \dots]$. This leads to the following solution in first order

$$\delta\chi_k(n) = \frac{H}{\sqrt{2k_c^3}} \frac{e^{-3n/2}}{\left(\left(\frac{k}{k_c}\right)^2 e^{-2n} - \epsilon_\chi^2 n\right)^{1/4}} e^{\left[-i \int_{-\infty}^n \left(\left(\frac{k}{k_c}\right)^2 e^{-2n'} - \epsilon_\chi^2 n'\right)^{1/2} dn'\right]}, \quad (5.13)$$

where the standard Minkowski positive frequency in the limit $n \rightarrow -\infty$ was chosen and the normalization of $\delta\chi_{\mathbf{k}}$ is given by the following canonical commutation relation, when the field is quantized:

$$\delta\chi_{\mathbf{k}} \overline{\delta\chi'_{\mathbf{k}}} - \overline{\delta\chi_{\mathbf{k}}} \delta\chi'_{\mathbf{k}} = \frac{iH^2}{k_c^3 e^{3n}}. \quad (5.14)$$

Before examining solution 5.13 in more detail, it is useful to determine the moment when a mode k becomes tachyonic. This is given by the value n_t , at which the term inside the parentheses of equation 5.12 vanishes:

$$n_t(k)e^{2n_t(k)} = \left(\frac{k}{\epsilon_\chi k_c}\right)^2 \Rightarrow n_t(k) = \frac{1}{2} W\left(2\left(\frac{k}{\epsilon_\chi k_c}\right)^2\right), \quad (5.15)$$

where the solution to this algebraic equation is described by the Lambert W function.

Before and shortly after the waterfall phase transition, some quanta of the waterfall field with low k values become tachyonic and behave like classical random fields, while modes with large k still behave like perturbations. Therefore, it is useful to categorize the modes into long- and short-wavelength modes based on their behavior at the horizon crossing.

Long-wavelength modes are those that exit the horizon before the phase transition occurs at $n = 0$. Once these modes cross the horizon, their amplitude decays exponentially, following a profile proportional to $\exp(-3n/2)$, as one can directly see when looking at equation 5.13. At the time of the phase transition, although the WKB approximation fails, their amplitude remains approximately the same up to a factor of order unity. After the phase transition, these long-wavelength modes evolve similarly to

their classical trajectory, shown in equation 5.10, and their growth is described by:

$$|\delta\chi_{\mathbf{k}}^L(n > 0)| \simeq \frac{H}{\sqrt{2\epsilon_\chi k_c^3}} \exp\left(\frac{2}{3}\epsilon_\chi n^{3/2}\right). \quad (5.16)$$

This occurs because once a mode becomes tachyonic, the spatial gradient term in its equation becomes insignificant compared to the tachyonic mass term. As a result, the evolution of these modes $\delta\chi_{\mathbf{k}}^L$ mirrors that of the background field's solution.

On the other hand, **short-wavelength modes** are those that are still sub-horizon at $n = 0$. In their mathematical treatment, the time $n_t(k)$, when a mode becomes tachyonic, is of particular interest. Since $n_t(k) \lesssim 1$ for the relevant parameters, an approximate solution is sufficient. For $n < n_t(k)$, the mode follows the WKB approximation, evolving as:

$$\delta\chi_{\mathbf{k}}^S(n) = \frac{H}{\sqrt{2k}k_c} e^{-n}; \quad n < n_t(k). \quad (5.17)$$

This time $n_t(k)$ is also referred to as the "classicalization" time, after which the short-wavelength modes evolve similarly to the long-wavelength modes. The implication is that for $n > n_t(k)$, they also behave like the classical background and must, therefore, reproduce the same behavior. Thus, by comparing with equation 5.10, one approximately obtains:

$$\delta\chi_{\mathbf{k}}^S(n) = \frac{H}{\sqrt{2k}k_c} e^{-n_t} \exp\left[\frac{2}{3}\epsilon_\chi \left(n^{3/2} - n_t^{3/2}\right)\right]; \quad n > n_t(k). \quad (5.18)$$

By using equations 5.10, 5.18 and 5.15 one can calculate the power spectrum $\mathcal{P}_{\delta\chi}$ of the waterfall field at $n = 0$. The calculation yields

$$\mathcal{P}_{\delta\chi}(k; 0) = \frac{k^3}{2\pi^2} P_\chi(k; 0) \equiv \begin{cases} \frac{H^2}{4\pi^2\epsilon_\chi} \left(\frac{k}{k_c}\right)^3; & k < k_c, \\ \frac{H^2\epsilon_\chi^2}{4\pi^2} n_t(k) \exp\left[-\frac{4}{3}\epsilon_\chi n_t^{3/2}(k)\right]; & k > k_c. \end{cases} \quad (5.19)$$

This result will be of particular importance in the next section, as it is required for the calculation of the curvature power spectrum \mathcal{P}_R .

5.3 Calculation of curvature perturbation

In some inflation models, it is possible to treat the system perturbatively due to the fact that the background value of physical quantities provides the dominant contribution. The previously discussed model with a quadratic potential is one such example where this perturbative approach is applicable. However, this is not the case for the hybrid inflation model, where the waterfall fluctuations $\delta\chi^2$ undergo exponential growth during the phase transition. As a result, the assumption that the background dominates no longer holds.

In this case, the δN formalism is more suitable for calculating physically measurable quantities, such as the curvature power spectrum $\mathcal{P}_{\mathcal{R}}$. The δN formalism uses the separate universe approach [18], where spacetime geometry is assumed to vary smoothly over super-horizon scales, while each region of size comparable to the Hubble horizon is treated as a homogeneous and isotropic universe. This framework is used to describe fluctuations and calculate the power spectrum on super-Hubble scales. The process involves the following steps: First, at a time t_1 , on a flat hypersurface, smoothing is applied on a scale larger than the Hubble radius. This ensures that different regions, though locally homogeneous, may still have varying averages. These regions then evolve independently, each as a separate FLRW universe. At a later time t_2 , the regions are evaluated on a comoving hypersurface, where the perturbation \mathcal{R} is defined. The change in the curvature perturbation between the initial and final time slices is determined by how much the expansion (or the number of e-folds) differs between regions. This difference in expansion histories allows the curvature perturbation to be calculated. For example, at time t_2 , two regions of size λ_s , separated by a distance λ , will give the curvature perturbation \mathcal{R} on the scale λ . An illustration of this process can be seen in Figure 5.1.

To apply the δN -formalism properly, it is necessary to trace the number of e-folds from the end of inflation to the time of horizon crossing for each mode. To avoid confusion, the number of e-folds counted backward from the end of inflation is denoted by \mathcal{N} , defined as $\mathcal{N} \equiv N_{end} - N$. The objective is to express \mathcal{N} in terms of the fields $\varphi(n)$ and $\chi^2(n)$, smoothed over each Hubble patch. Since the relation $R = \delta\mathcal{N}$ holds on scales where small inhomogeneities have minimal impact on the geometry, the smoothing scale is chosen to be slightly larger than the comoving scale corresponding to the wavelength of the last mode that becomes tachyonic.

The calculations are rather tedious and offer little new physical insight, which is why reference is made to [16] for further details. In summary, the background equations for both fields are perturbed and traced back to the Hubble crossing of the respective mode.

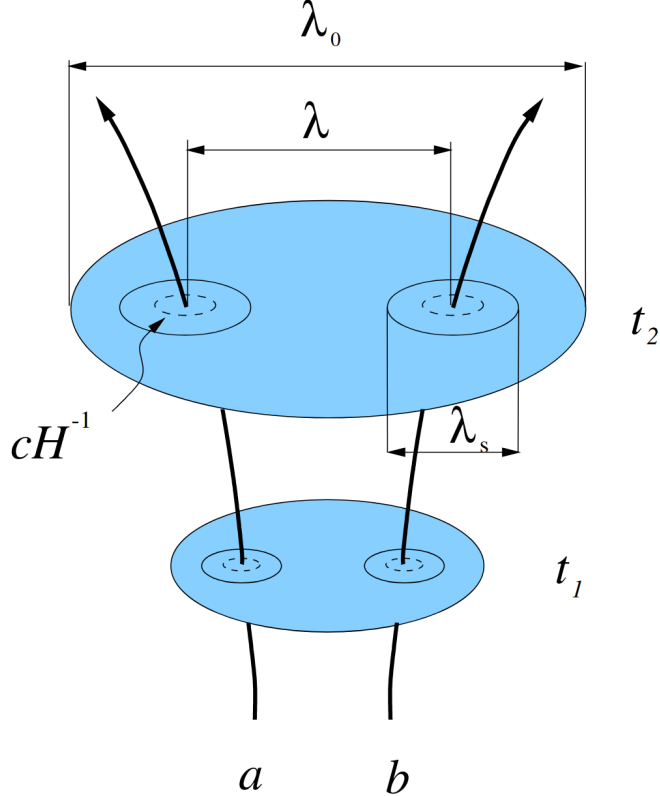


FIGURE 5.1: A schematic illustration of the δN formalism with symbols given in the text. The graphic was taken from [18].

From this, $\delta\mathcal{N}$ can be derived, which to leading order in both fields is given as follows:

$$\mathcal{R} = \delta\mathcal{N} = -\frac{C\epsilon n_f}{f'(n_f) \langle \delta\chi^2(0) \rangle} \frac{\delta\chi^2(0)}{\langle \delta\chi^2(0) \rangle} + \left[1 + \frac{C}{2} + C\epsilon(n - 2n_f) \right] \frac{\varphi\delta\varphi}{2m_{pl}^2}, \quad (5.20)$$

where $\epsilon = 2m_{pl}^2/\varphi_c^2$, $f(n) \equiv \frac{2}{3}\epsilon_\chi n^{3/2}$ and n_f describes the duration of the phase transition. For this result, it was utilized that the phase transition is very sharp. In this approximation one obtains the following estimate for n_f

$$n_f = \Gamma \epsilon_\chi^{-2/3}; \quad \Gamma \simeq \left(\ln \left[\frac{32\pi^2 \epsilon_\chi^{2/3}}{6\lambda} \right] \right)^{2/3}. \quad (5.21)$$

From equation 5.20, the following expression for the curvature power spectrum can then be derived:

$$\begin{aligned} \mathcal{P}_{\mathcal{R}} &= \mathcal{P}_{\mathcal{R}}^{wf} + \mathcal{P}_{\mathcal{R}}^\varphi \\ &= \frac{C^2 \epsilon^2 n_f^2}{f'^2(n_f)} \mathcal{P}_{\delta\chi^2/\chi^2} + \left[1 + \frac{C}{2} + \mathcal{O}(C\epsilon) \right]^2 \frac{\varphi^4}{4m_{pl}^4} \mathcal{P}_{\delta\varphi/\varphi}, \end{aligned} \quad (5.22)$$

with $\mathcal{P}_{\delta\chi^2/\chi^2}$ defined by:

$$\mathcal{P}_{\delta\chi^2/\chi^2}(k) \equiv \frac{1}{\langle \delta\chi^2(0) \rangle} \mathcal{P}_{\delta\chi^2}(k). \quad (5.23)$$

Here, $\langle \delta\chi^2(0) \rangle$ denotes the expectation value of the waterfall fluctuations at time $n = 0$, which, as shown in [16], is dominated by small-scale fluctuations:

$$\langle \delta\chi^2(0) \rangle \simeq \langle \delta\chi^2(0) \rangle_S \simeq \frac{3\epsilon_\chi^{4/3} H^2}{16\pi^2}. \quad (5.24)$$

In [16], the following approximate expressions are found for both contributions $\mathcal{P}_{\mathcal{R}}^{wf}$ and $\mathcal{P}_{\mathcal{R}}^\varphi$:

$$\mathcal{P}_{\mathcal{R}}^\varphi(k) = \frac{1}{96\pi^2} (1+C)^2 \left(1 - \frac{C}{2} \frac{\varphi^2}{\varphi_c^2} \right) \frac{m^2 \varphi^4}{m_{pl}^6} \Big|_{n=n_k}, \quad (5.25)$$

$$\mathcal{P}_{\mathcal{R}}^{wf}(k) \simeq \begin{cases} \frac{16}{9} C^2 \epsilon^2 n_f \epsilon_\chi^{-20/3} \xi^3 \left(\frac{k}{k_c} \right)^3; & k < k_c, \\ \frac{16}{9} C^2 \epsilon^2 n_f \epsilon_\chi^{-8/3} \xi^3 n_t(k) \exp \left[-\frac{4}{3} \epsilon_\chi n_t^{3/2}(k) \right]; & k > k_c, \end{cases} \quad (5.26)$$

with $\xi \simeq e$. It can be observed from the first contribution $\mathcal{P}_{\mathcal{R}}^\varphi$ that, apart from corrections of $\mathcal{O}(C)$, it reproduces the power spectrum for the quadratic potential in the slow-roll limit. Meanwhile, the second contribution $\mathcal{P}_{\mathcal{R}}^{wf}$ enhances the power spectrum through a peak feature on scales that became super-Hubble during the phase transition.

5.4 Results

5.4.1 Results for background

This section is dedicated to comparing the theoretical predictions discussed in the previous chapter with the results from the simulation using *CosmoLattice*. However, suitable model parameters must first be set. Since the potential $V(\varphi, \chi)$ is dominated by the quadratic potential of the inflaton, the slow-roll parameters can be defined to a good approximation as in the single-field model:

$$\epsilon \approx \frac{M_{pl}^2}{2} \left(\frac{V_\varphi}{V} \right)^2, \quad \eta \approx M_{pl}^2 \frac{V_{\varphi\varphi}}{V}. \quad (5.27)$$

In order to obtain the correct amplitude and scalar tilt for the power spectrum as in Equations 3.21 and 3.22, φ_{ini} and m must be set as in the single-field model. This leads to $m \approx 1.46 \cdot 10^{13}$ GeV, which corresponds to $\alpha \ll 1$, and $\varphi_{ini} \approx 3.68 \cdot 10^{19}$ GeV. The remaining parameters must be chosen such that the phase transition is relatively short, i.e., $\beta = \frac{M^2}{H^2} \gg 1$. This means that the waterfall field must be very heavy, while still ensuring $C = \frac{g^2 M^2}{\lambda m^2} \ll 1$, so that the inflaton can continue driving the expansion even after the phase transition. Additionally, φ_c should be set so that the phase transition begins 1 e-fold after the start of the simulation, ensuring that the resulting peak in the power spectrum falls within the region captured by *CosmoLattice*. The following parameters meet these three requirements:

$$g^2 = 3 \cdot 10^{-8}, \quad \lambda = 0.07, \quad \varphi_c = \frac{M}{g} = 15 \cdot M_{pl}. \quad (5.28)$$

φ'_{ini} is given by the derivative of the slow-roll equation 5.4, while χ_{ini} and χ'_{ini} are set to zero. To cover the largest possible range in Fourier space while ensuring that back-reaction effects remain negligible, $N = 256$ and $k_{IR} = 0.1$ were chosen. The simulation duration was set to $N_e = \mathcal{O}(10)$ to ensure that all modes in the considered range eventually become super-Hubble.

It is crucial to first compare the background evolution of the inflaton and waterfall field with corresponding simulations, as they are essential for the explicit form of the curvature power spectrum. For the background dynamics of the inflaton, a comparison between Equation 5.4 and the *CosmoLattice* simulation can be seen in Figure 5.2. It is clear that the simulation and the theoretical prediction align remarkably well, even though Equation 5.4 is strictly valid only for an e-fold number of $N < 1$.

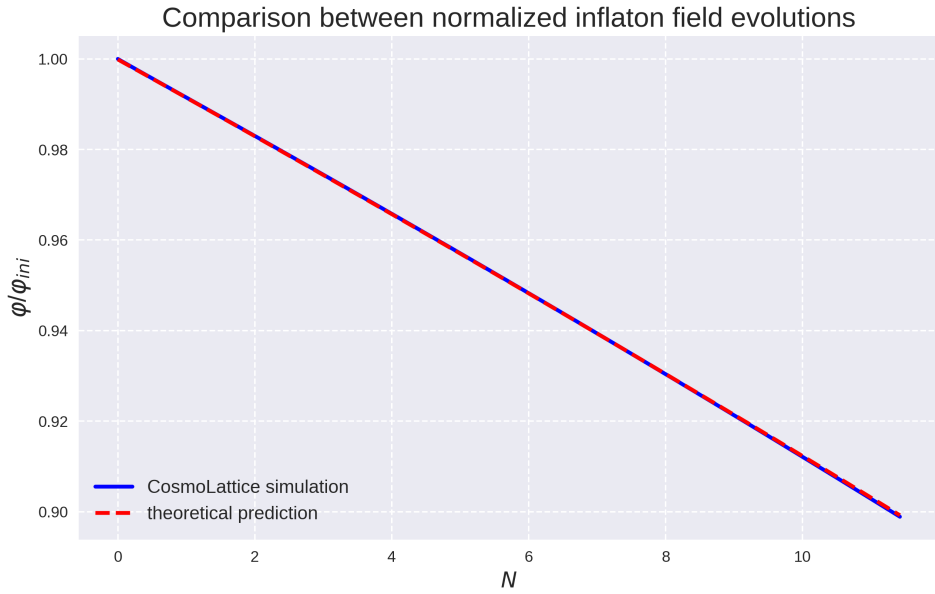


FIGURE 5.2: Comparison between the theoretical evolution of the inflaton and the *CosmoLattice* simulation. All parameters were chosen as mentioned in the text, and both functions were normalized by φ_{ini} .

Furthermore, the background evolution of the waterfall field can be compared for each stage with the *CosmoLattice* simulation, as illustrated in Figure 5.4. It becomes immediately clear that during the first stage, there are significant discrepancies between the theory and the simulation. However, this is expected because the background value of the waterfall field in this stage is set to zero, and it is thus dominated by perturbations, which initially do not follow a classical evolution. Therefore, the simulation cannot follow the blue curve in the first stage, which assumes a hypothetical starting value of $\chi_{ini} \neq 0$.

Additionally, it is evident that the phase transition occurs later than the e-fold number $N = 1$ set by the choice of φ_{ini} , as the background value only begins to grow exponentially at $N \approx 1.7$. The back-reactions in stage 1 thus delay the onset of the phase transition, which is also visible in Figure 5.3. In that figure, it is shown that the domains typical for this type of phase transition, with positive and negative field values of χ , only begin to form around $N \approx 1.6$.

In contrast, during the second and third stages, there is greater agreement between the simulation and the theoretical calculation, with the discrepancy in stage 2 being attributed to the approximate solution of the background equation 5.10, which in general also contains a damping term $\propto e^{-3n/2}$, which mitigates the rapid growth of the theoretical curve and was neglected in the analysis.

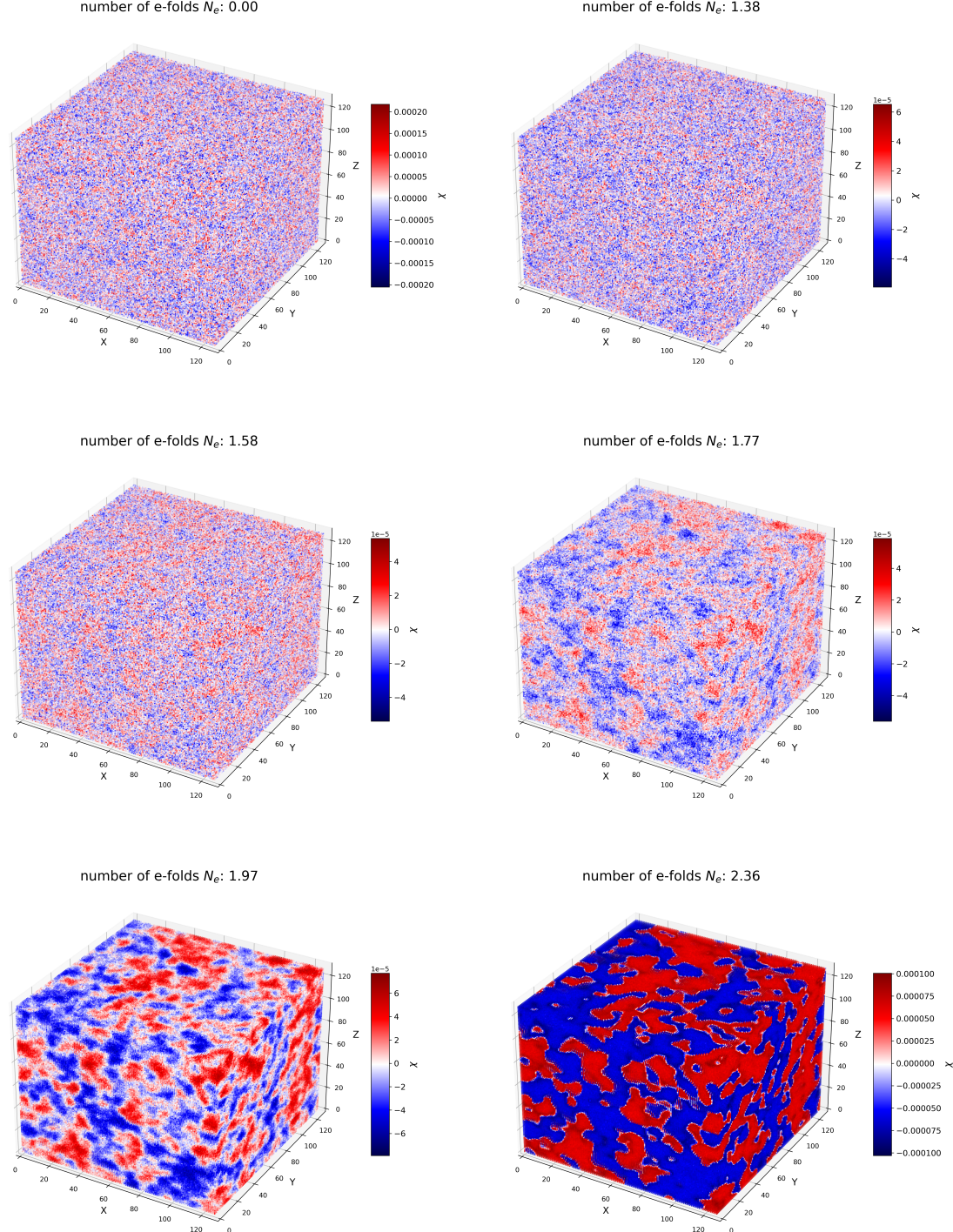


FIGURE 5.3: Time evolution of the waterfall field in a quarter section of the lattice. The plots clearly illustrate the formation of domains, where χ falls either into the minimum with a positive field value $+\chi_{min}$ or into the one with a negative field value $-\chi_{min}$. Here, $N_e = 0$ marks the start of the simulation, with the phase transition occurring after approximately 1.6 e-folds.

The oscillations seen in the simulation curve at the start of stage 3 are due to the waterfall field oscillating around its local minimum, a physical effect that is not accounted for in the theoretical calculations, in which, after the phase transition is completed, it simply takes the value given in equation 5.5. However, at this point, the two curves match perfectly.

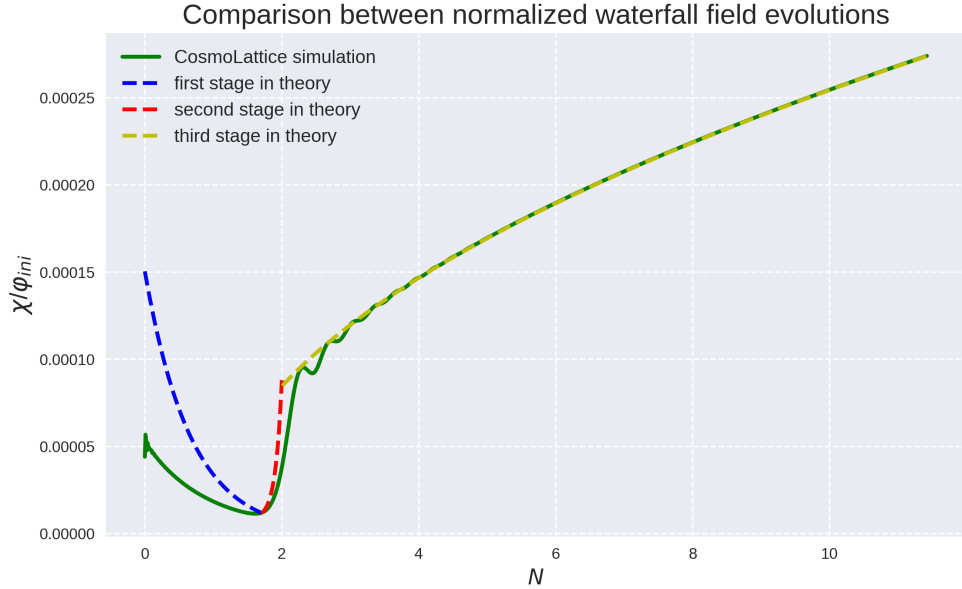


FIGURE 5.4: Comparison between the theoretical evolution of the waterfall field for all three stages with the *CosmoLattice* simulation. These stages are divided as follows: **stage 1** describes the classical evolution of the waterfall field before the phase transition, **stage 2** occurs during the phase transition, and **stage 3** takes place after the phase transition, when the waterfall field settles in the local minimum.

The analysis of the background equations shows that *CosmoLattice* effectively reproduces the background evolution of both fields. It can be assumed that any discrepancies arise due to the approximate analytical expressions on the theoretical side. The next and final subsection will focus on comparing the power spectra from both theory and simulation.

5.4.2 Results for curvature power spectrum

In this final section of the chapter, the focus will primarily be on comparing the previously calculated curvature power spectrum with *CosmoLattice* simulations. For this, a formula for \mathcal{R} adapted for two fields must first be derived. The linearized equation for \mathcal{R} in the context of the hybrid model is given by, as shown in Appendix C:

$$\mathcal{R} = H \frac{\dot{\varphi}\delta\varphi + \dot{\chi}\delta\chi}{\dot{\varphi}^2 + \dot{\chi}^2}. \quad (5.29)$$

Just like in Chapter 4, metric perturbations were neglected here as they play a minor role. From this, by disregarding cross-correlations, the following formula for $\mathcal{P}_{\mathcal{R}}$ can be determined:

$$\mathcal{P}_{\mathcal{R}} = H^2 \frac{\dot{\varphi}^2}{(\dot{\varphi}^2 + \dot{\chi}^2)^2} \mathcal{P}_{\delta\varphi} + H^2 \frac{\dot{\chi}^2}{(\dot{\varphi}^2 + \dot{\chi}^2)^2} \mathcal{P}_{\delta\chi}. \quad (5.30)$$

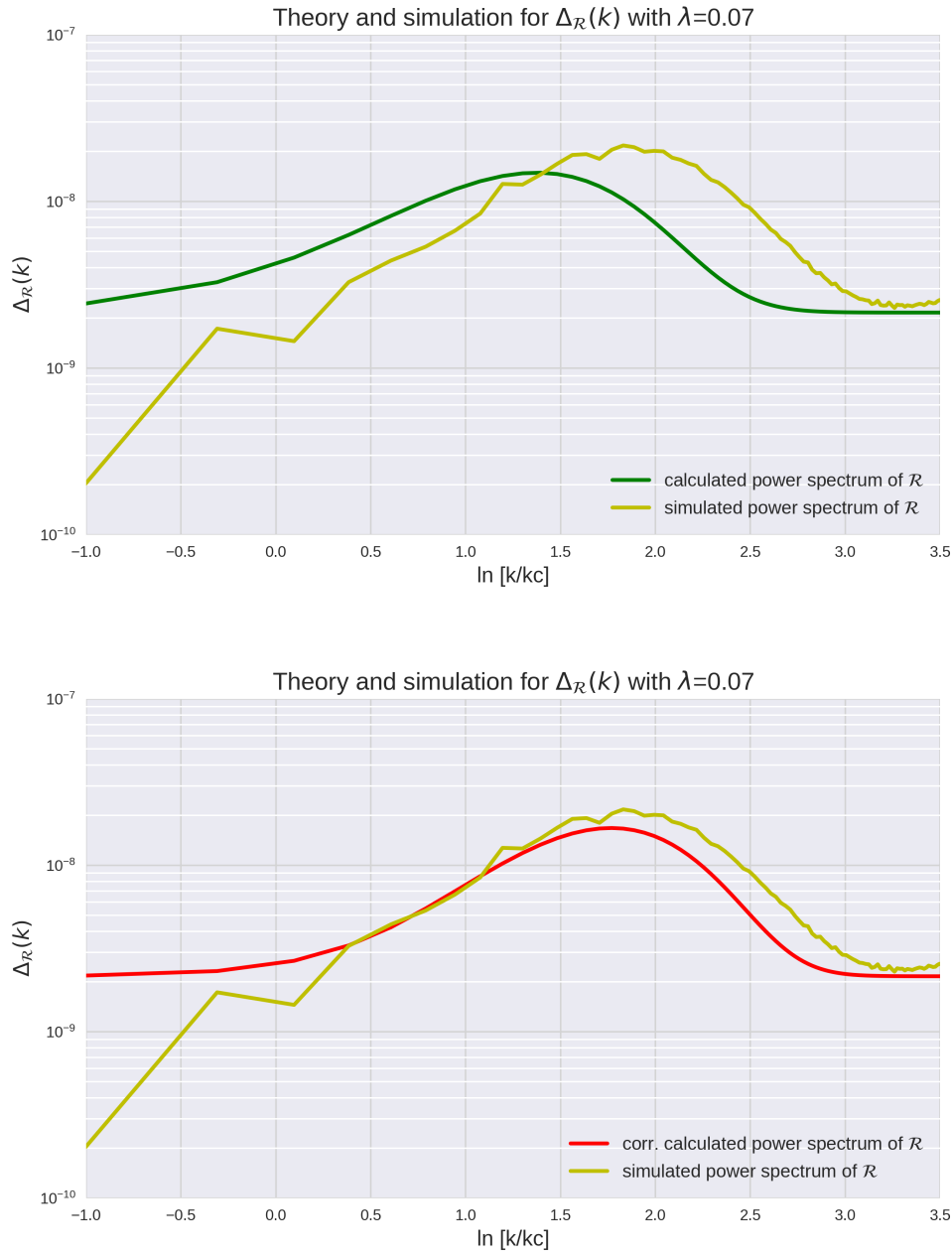


FIGURE 5.5: Comparison between the simulated and theoretical power spectrum after 12 e-folds. **Top:** Using the approximated value of $\mathcal{P}_{\delta\chi^2/\chi^2}$ from Source [16] for the theoretical curve. **Bottom:** Numerically integrated solution of $\mathcal{P}_{\delta\chi^2/\chi^2}$ for the theoretical curve.

Since **CosmoLattice** outputs both the background evolution and the power spectra of both fields, $\mathcal{P}_{\mathcal{R}}$ from equation 5.30 can be compared to the theoretical curve from equation 5.22. This comparison is shown in the upper plot of Figure 5.5, where it becomes evident that the theoretical curve and the simulation do not align. The peak of the theoretical curve is shifted towards smaller k and also has a lower amplitude.

These differences are significant and stem from the fact that in equation 5.22, the power spectrum was estimated in a simplified way to obtain the following analytical expression:

$$\mathcal{P}_{\delta\chi^2/\chi^2}(k) \equiv \frac{1}{\langle \delta\chi^2(0) \rangle} \mathcal{P}_{\delta\chi^2}(k) \approx \frac{1}{\langle \delta\chi^2(0) \rangle} \frac{\xi^3 H^2}{4\pi^2} \mathcal{P}_{\delta\chi}(k), \quad (5.31)$$

where $\xi \simeq e$ is the same numerical factor as in the last chapter. The approximation shows that $\mathcal{P}_{\delta\chi^2}$ is proportional to $\mathcal{P}_{\delta\chi}$. However, to obtain an exact result, the following loop integral must be solved:

$$\left\langle (\delta\chi^2)_k (\delta\chi^2)_q \right\rangle = 2 \int \frac{d^3 q}{(2\pi)^3} |\delta\chi_{|\mathbf{k}-\mathbf{q}|}|^2 |\delta\chi_q|^2 (2\pi)^3 \delta^3(\mathbf{k} + \mathbf{q}). \quad (5.32)$$

The calculation of this correlation function is proportional to $P_{\delta\chi^2}$ in the following way:

$$\left\langle (\delta\chi^2)_{\mathbf{k}} (\delta\chi^2)_{\mathbf{q}} \right\rangle \equiv P_{\delta\chi^2}(k) (2\pi)^3 \delta^3(\mathbf{k} + \mathbf{q}). \quad (5.33)$$

By evaluating the loop integral in Equation 5.32, the contribution of the waterfall field fluctuations to $\mathcal{P}_{\mathcal{R}}$ in leading order is obtained. Since this integral does not have an analytical solution, it was numerically solved within the relevant k -interval using a Python script.

The lower plot in Figure 5.5 shows the effect of this numerical solution, and in comparison to the upper plot, it emerges that the theoretical and simulation curves match much more closely. The overall behavior is quite similar, though the peak amplitude and width of the theoretical curve appear slightly smaller.

The steep decline in the power spectrum from the **CosmoLattice** simulation for small k values can be attributed to two factors. First, as mentioned in Chapter 4, the occupation numbers n_k in the boundary regions are quite low, making a classical treatment unjustifiable. Additionally, the fluctuations at the beginning of the simulation are always Gaussian-distributed for each mode according to the Bunch-Davies vacuum. This is a good approximation when all modes in the considered interval are deep within the sub-Hubble regime. However, to prevent back-reaction effects, k_{IR} was set to 0.1, which places it at the Hubble crossing for the chosen parameters. As a result, this program's approximation is not valid for the smallest modes in this case.

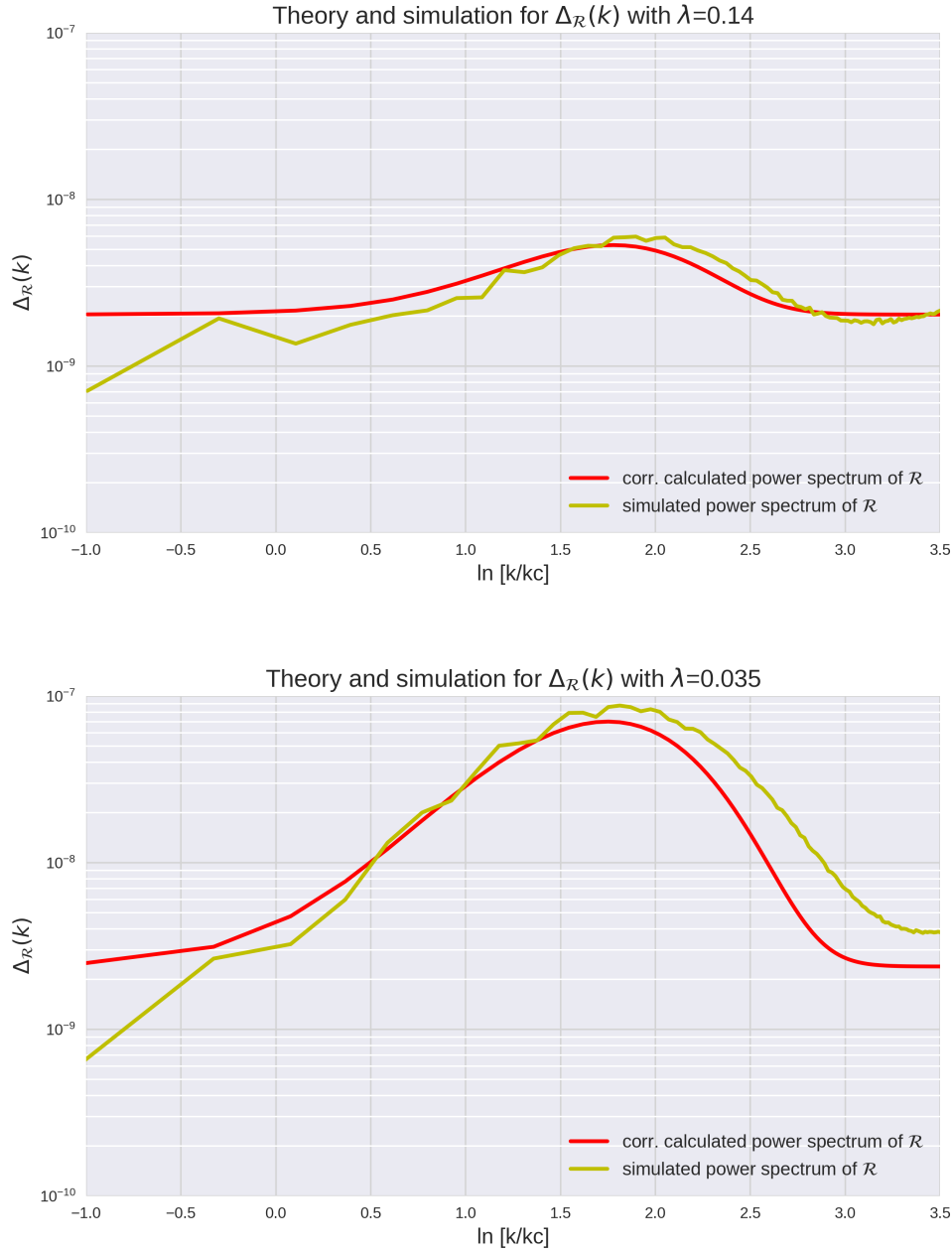


FIGURE 5.6: Comparison between the simulated and theoretical power spectrum after 12 e-folds. This time, λ was increased to 0.14 in the upper plot, while the lower plot shows the comparison between theory and simulation for $\lambda = 0.035$.

In Figure 5.6, the comparison between simulation and theory is illustrated for both a smaller and a larger value of λ . These values serve as a reference to ensure that `CosmoLattice` can largely reproduce the functional behaviour of the theoretical curve for various parameters. The results indicate a solid agreement for both λ values, with slightly better alignment observed for the larger values. This can be attributed to the fact that a higher λ increases the parameter ϵ_χ , which controls the sharpness of the phase

transition. Since most equations were derived under the approximation of a sharp phase transition, the agreement for corresponding parameters is naturally greater. Additional plots for comparison can be found in [Appendix C](#).

Furthermore, potential higher-order loop corrections could account for the difference between the trajectory of the theoretical curve and the simulation curve for larger k values and may slightly correct the amplitude upward. To consider these, the contribution of the waterfall fluctuations to \mathcal{R} in equation [5.20](#) must be expanded as follows [16]:

$$\frac{\delta\chi^2(0)}{\langle\delta\chi^2(0)\rangle} \longrightarrow 2\frac{\delta\chi^2(0)}{\langle\delta\chi^2(0)\rangle} - \frac{1}{2}\frac{\delta\chi^4(0)}{\langle\delta\chi^2(0)\rangle^2}. \quad (5.34)$$

This expands the contribution to the power spectrum at the next order as follows:

$$\frac{k^3}{2\pi^2} \frac{\langle(\delta\chi^2)_{\mathbf{k}}(\delta\chi^2)_{\mathbf{q}}\rangle}{\langle\delta\chi^2\rangle^2} \longrightarrow \frac{k^3}{2\pi^2} \left[4\frac{\langle(\delta\chi^2)_{\mathbf{k}}(\delta\chi^2)_{\mathbf{q}}\rangle}{\langle\delta\chi^2\rangle^2} - 2\frac{\langle(\delta\chi^2)_{\mathbf{k}}(\delta\chi^4)_{\mathbf{q}}\rangle}{\langle\delta\chi^2\rangle^3} + \frac{1}{4}\frac{\langle(\delta\chi^4)_{\mathbf{k}}(\delta\chi^4)_{\mathbf{q}}\rangle}{\langle\delta\chi^2\rangle^4} \right],$$

where the correlation functions were calculated with the help of basic principles for the calculation of loop integrals in [16] and are given by the following equations:

$$\begin{aligned} \langle(\delta\chi^2)_{\mathbf{k}}(\delta\chi^4)_{\mathbf{q}}\rangle &= 8 \int \frac{d^3\mathbf{p}}{(2\pi)^3} \int \frac{d^3\mathbf{l}_1}{(2\pi)^3} |\delta\chi_{|\mathbf{k}-\mathbf{l}_1|}|^2 |\delta\chi_{|\mathbf{l}_1|}|^2 |\delta\chi_{|\mathbf{l}_1+\mathbf{p}|}|^2, \\ \langle(\delta\chi^4)_{\mathbf{k}}(\delta\chi^4)_{\mathbf{q}}\rangle &= 56 \int \frac{d^3\mathbf{p}}{(2\pi)^3} \int \frac{d^3\mathbf{s}}{(2\pi)^3} \int \frac{d^3\mathbf{l}_1}{(2\pi)^3} |\delta\chi_{|\mathbf{k}-\mathbf{p}-\mathbf{l}_1|}|^2 |\delta\chi_{|\mathbf{l}_1|}|^2 \\ &\quad \times |\delta\chi_{|\mathbf{l}_1+\mathbf{p}|}|^2 |\delta\chi_{|\mathbf{p}+\mathbf{l}_1-\mathbf{k}-\mathbf{s}|}|^2. \end{aligned} \quad (5.35)$$

The prefactors 8 and 56 represent the number of possible contractions that lead to a connected graph. The individual contributions of all these graphs are identical for each integral. However, these correlation functions do not have an analytical expression and must therefore also be numerically integrated. Since this process is computationally expensive, they could not be evaluated due to time constraints. They are intended as a basis for a more in-depth analysis of the hybrid model in future research.

Lastly, attention is given to the Gaussian nature of the fluctuations. Paper [16] suggests that the so-called non-Gaussianity parameter, f_{NL} , is very large around the peak of the power spectrum $\mathcal{P}_{\mathcal{R}}$ in this model. The relationship is given by:

$$\frac{6}{5}f_{NL}(\mathbf{k}_1, \mathbf{k}_2, \mathbf{k}_3) \propto B_{\mathcal{R}}(\mathbf{k}_1, \mathbf{k}_2, \mathbf{k}_3) \quad (5.36)$$

with $B_{\mathcal{R}}$ being the so-called bispectrum given by the three-point correlation function $\langle\mathcal{R}_{\mathbf{k}_1}\mathcal{R}_{\mathbf{k}_2}\mathcal{R}_{\mathbf{k}_3}\rangle$. Generally, the approach would involve calculating all contributions to $B_{\mathcal{R}}$ and comparing them to the bispectrum of the simulation data to verify the simulation

results. However, since `CosmoLattice` does not compute the bispectrum, and implementing such functionality would exceed the scope of this work, the only feasible option is to fit the distribution of the curvature perturbation and identify non-Gaussianity based on this fit.

For this purpose, equation 5.29 is utilized, as `CosmoLattice` can output both the background quantities and the field distributions in real space. From this, as shown in Figure 5.7, the distribution of the curvature perturbation \mathcal{R} on the lattice is obtained.

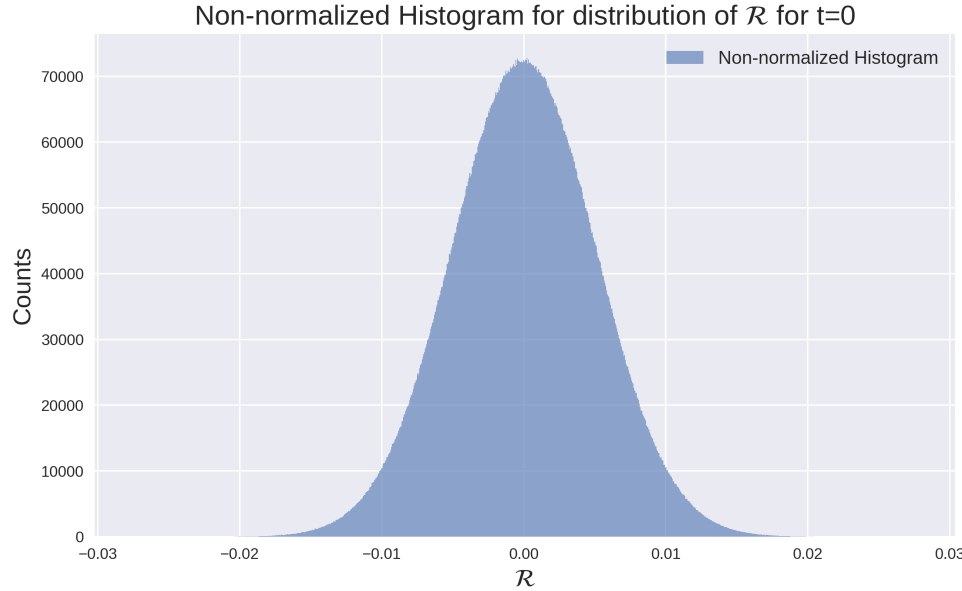


FIGURE 5.7: Distribution of the curvature perturbation in real space at $t=0$. The field fluctuations are set according to the Bunch-Davies vacuum, meaning \mathcal{R} should be distributed in a Gaussian manner.

The distribution can be evaluated at different times and then be logarithmized. For Gaussian-distributed fluctuations, the logarithmic distribution of \mathcal{R} should follow a parabola. By comparing a quadratic and quartic fit to these data, non-Gaussianities in the distribution of \mathcal{R} can be identified. This was done as an example in Figure 5.8, for the beginning and end of the simulation, as well as during the phase transition.

It shows that both fits initially and during the phase transition reproduce the data equally well, even though non-Gaussian effects should be most prominent at the time of the phase transition. At the end of the simulation, both fits yield equally poor results, indicating that a non-Gaussian feature has emerged in the distribution of \mathcal{R} , which suppresses the probability of finding larger \mathcal{R} values in comparison with both fits.

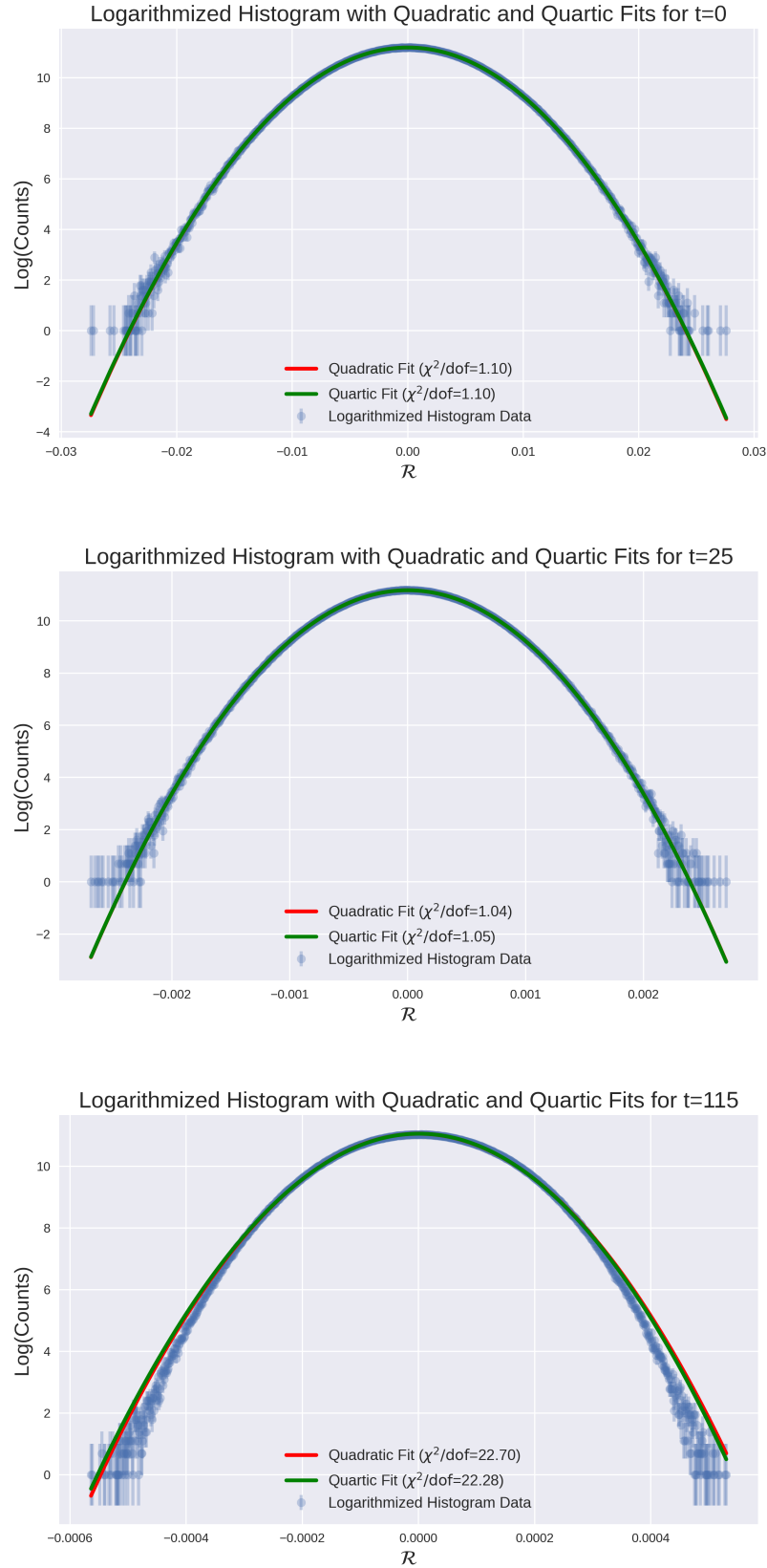


FIGURE 5.8: Logarithmic distributions with quadratic and quartic fits for different times. **Top:** the beginning of the simulation. **Middle:** during the phase transition. **Bottom:** at the end of the simulation.

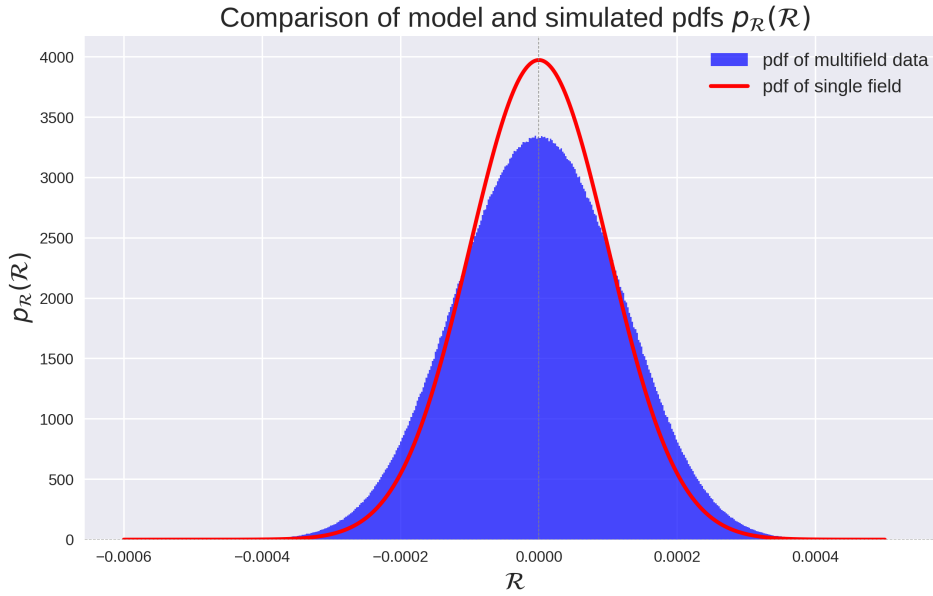


FIGURE 5.9: Comparison of the probability density functions (PDFs) between the single-field model and the simulated hybrid inflation model at the end of the simulation.

Furthermore, as seen in Figure 5.9, the distribution or probability density function (PDF) of \mathcal{R} in the hybrid model is wider than the Gaussian-shaped PDF of the single field model. This clearly demonstrates the influence of waterfall field fluctuations on the distribution of \mathcal{R} .

In summary, it can be concluded that the curvature perturbation follows a broader, non-Gaussian distribution compared to the single field model. The exact form of this distribution is not straightforward to calculate, as the curvature perturbation depends non-trivially on both the inflaton perturbation $\delta\phi$ and the waterfall field perturbation $\delta\chi$, which also develop non-trivial PDFs throughout the simulation.

The theoretical derivation and analysis of the pdf of \mathcal{R} is beyond the scope of this thesis and can be explored in future research by subsequent students. It therefore appears that calculating $B_{\mathcal{R}}$ and $p_{\mathcal{R}}(\mathcal{R})$ and comparing it with the simulation data is essential to fully determine the non-Gaussian behaviour of this stochastic inflation model.

Chapter 6

Conclusion and outlook

In this master’s thesis, the essential foundations of cosmic inflation were mathematically explored using two specific models and compared with the simulation program *CosmoLattice*. Chapter one introduced the concept of inflation as a phase of exponential expansion in the early universe driven by a homogeneous scalar field. In chapter two, this idea was extended by considering perturbations in both the scalar field and the metric. These perturbations were categorized as scalar, vector, and tensor, based on their behavior under rotations in 3D space.

It was found that, for the models studied in this work, only the scalar perturbation \mathcal{R} was relevant, as it is closely related to many cosmological observations like the CMB. The equations of motion for all relevant perturbations were derived, and in chapter three, the curvature perturbation \mathcal{R} was found for a quadratic model. From this, the dimensionless power spectrum $\mathcal{P}_{\mathcal{R}}$, a key measurable quantity in cosmology, was determined.

Chapter four introduced the simulation software *CosmoLattice* and focused on comparing its outputs with the theoretical results for the quadratic model. It was found that *CosmoLattice* can largely reproduce both the theoretical background and $\mathcal{P}_{\mathcal{R}}$ for a suitable choice of parameters. In chapter five, an extended inflation model, the hybrid inflation model, was discussed, and it was similarly found that data and theory, despite the fact that the theoretical results are not exactly solvable, showed good agreement.

This thesis thus serves as a foundation for further investigation into the validity of *CosmoLattice* as a simulation software for inflation. Specifically, in the context of the hybrid inflation model, where analytical solutions are challenging, theoretical results can be improved through more precise solutions of the background equations and taking into account higher-order loop corrections to $\mathcal{P}_{\mathcal{R}}$. *CosmoLattice* could also be modified to allow for variable initial conditions according to the Mukhanov-Sasaki equation,

enabling analysis for small modes. Furthermore, a more general relationship than the linear one between curvature perturbation and field fluctuations could be used for the *CosmoLattice* data, as the linear description appears at least questionable during the phase transition. Finally, the effect of non-Gaussianities in this model can be examined more qualitatively.

In conclusion, while *CosmoLattice* has some limitations, it has the potential to serve as a software to validate calculations for certain theoretical inflation models, thereby contributing to further knowledge about the early universe.

Appendix A

Scalar perturbations

A.1 Gauge transformation of scalar perturbation

By employing equations 2.27 and 2.28 for general perturbations, one can readily observe that a general scalar perturbation of the scalar s can be expressed as follows in different gauges:

$$\delta\tilde{s}(x_b^\alpha) = \tilde{s}(\tilde{p}) - s^{(0)}(p_b), \quad (\text{A.1})$$

$$\delta s(x_b^\alpha) = s(p) - s^{(0)}(p_b). \quad (\text{A.2})$$

In order to relate $\delta\tilde{s}$ to δs , one has to expand \tilde{s} around the point \tilde{p} :

$$\tilde{s}(\tilde{p}) = s(p) + \frac{\partial s}{\partial x^\alpha} [x^\alpha(\tilde{p}) - x^\alpha(p)] = s(p) - \frac{\partial s^{(0)}}{\partial x^\alpha}(p_b) \xi^\alpha. \quad (\text{A.3})$$

Since the background is homogeneous but time dependent, the last term reduces to

$$\frac{\partial s^{(0)}}{\partial x^\alpha}(p_b) \xi^\alpha = \frac{\partial s^{(0)}}{\partial \eta}(p_b) \xi^0 = s'^{(0)} \xi^0. \quad (\text{A.4})$$

Thus one obtains the following relation

$$\tilde{s}(\tilde{p}) = s(p) - s'^{(0)} \xi^0, \quad (\text{A.5})$$

and the final result for the gauge transformation of δs is

$$\delta\tilde{s} = s(p) - s'^{(0)} \xi^0 - s^{(0)}(p_b) = \delta s - s'^{(0)} \xi^0. \quad (\text{A.6})$$

A.2 Conservation of curvature perturbation

Using Equation 2.90, the derivative of the curvature perturbation \mathcal{R} with respect to conformal time is given by:

$$\mathcal{R}' = \Phi' + \frac{\mathcal{H}'}{\bar{\varphi}'} \delta Q - \frac{\mathcal{H}\bar{\varphi}''}{\bar{\varphi}'^2} \delta Q + \frac{\mathcal{H}}{\bar{\varphi}'} \delta Q'. \quad (\text{A.7})$$

In this context, both δQ and $\delta Q'$ can be eliminated using the intermediate equation from Equations 2.86, yielding the following expression for \mathcal{R} :

$$\begin{aligned} \mathcal{R}' = & \Phi' + \frac{2M_{pl}^2 \mathcal{H}'}{\bar{\varphi}'^2} (\mathcal{H}\Phi + \Phi') - \frac{4M_{pl}^2 \mathcal{H}\bar{\varphi}''}{\bar{\varphi}'^3} (\mathcal{H}\Phi + \Phi') \\ & + \frac{2M_{pl}^2 \mathcal{H}}{\bar{\varphi}'^2} (\mathcal{H}'\Phi + \mathcal{H}\Phi' + \Phi''). \end{aligned} \quad (\text{A.8})$$

Now, using the relation $\frac{1}{2M_{pl}^2} \bar{\varphi}'^2 = \mathcal{H}^2 - \mathcal{H}'$ for the background in conformal time, the factor \mathcal{H}' in the second term of equation A.8 can be replaced. This then leads to following expression:

$$\mathcal{R}' = -\mathcal{H}\Phi + \frac{2M_{pl}^2 \mathcal{H}}{\bar{\varphi}'^2} \left[\mathcal{H}^2\Phi + \mathcal{H}\Phi' - 2\frac{\bar{\varphi}''}{\bar{\varphi}'} \mathcal{H}\Phi - 2\frac{\bar{\varphi}''}{\bar{\varphi}'} \Phi' + \mathcal{H}'\Phi + \mathcal{H}\Phi' + \Phi'' \right]. \quad (\text{A.9})$$

The relation for the background can now be applied to the first term within the parentheses. After simplifying various terms, this yields the following expression:

$$\mathcal{R}' = -\mathcal{H}\Phi + \mathcal{H}\Phi + \frac{2M_{pl}^2 \mathcal{H}}{\bar{\varphi}'^2} \left[\Phi'' + 2\left(\mathcal{H} - \frac{\bar{\varphi}''}{\bar{\varphi}'}\right)\Phi' + 2\left(\mathcal{H}' - \frac{\bar{\varphi}''}{\bar{\varphi}'}\mathcal{H}\right)\Phi \right]. \quad (\text{A.10})$$

If one now compares the term in the brackets with the evolution equation 2.87 of Φ , it reduces to just a Laplacian of Φ leaving the following final expression for \mathcal{R}' :

$$\mathcal{R}' = \frac{2M_{pl}^2 \mathcal{H}}{\bar{\varphi}'^2} \Delta\Phi. \quad (\text{A.11})$$

Finally, by applying a Fourier transformation from real space to k-space, the operator Δ becomes $-k^2$. Additionally, when transitioning from conformal time to cosmic time, all time derivatives in the above equation are transformed as follows: $\frac{d}{d\eta} \rightarrow a\frac{d}{dt}$. The final expression is therefore given by:

$$\dot{R}_k = -\frac{2M_{pl}^2 H}{\dot{\varphi}^2} \frac{k^2}{a^2} \Phi = -\frac{2M_{pl}^2 H^3}{\dot{\varphi}^2} \left(\frac{k}{aH} \right)^2 \Phi. \quad (\text{A.12})$$

This relation clearly illustrates that the time derivative of R_k decays exponentially as the corresponding mode k transitions into the super-Hubble regime.

Appendix B

Single field model

B.1 Plots for single field

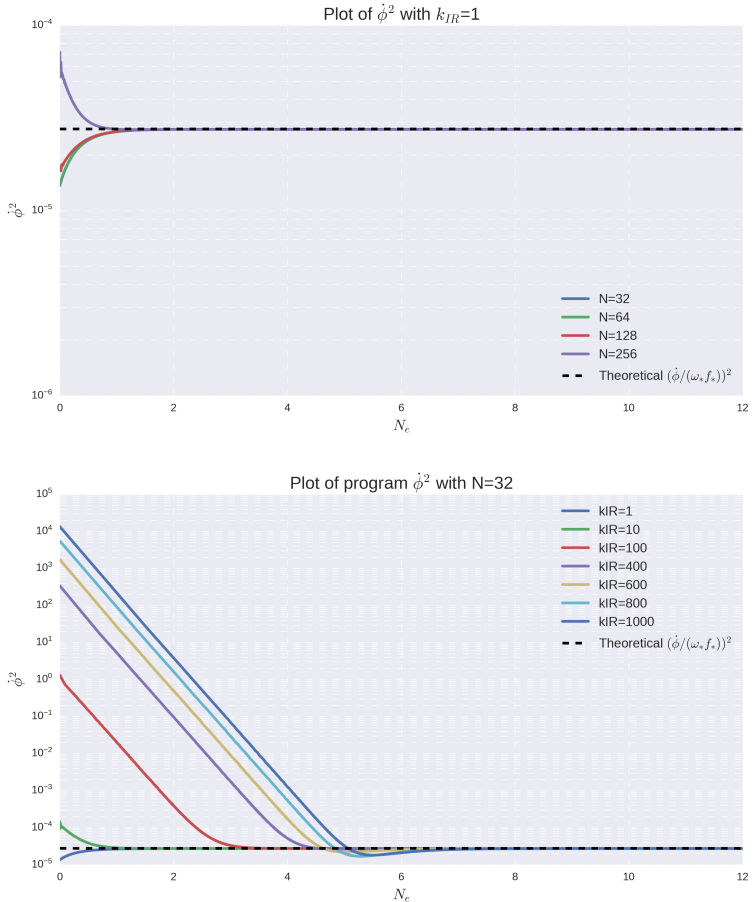


FIGURE B.1: Simulation of the evolution of $\dot{\phi}^2$ over 12 e-folds, showing comparisons for different values of N (**top**) and k_{IR} (**bottom**). The behavior mirrors that observed for H , though with a slight underestimation by the simulation relative to the theoretical curve for small values of both N and k_{IR} .

Appendix C

Hybrid inflation model

C.1 Curvature perturbation for multiple fields

The general expression for the curvature perturbation (without metric perturbations) is defined as [7]:

$$\mathcal{R} = -\frac{H}{\rho + p}\delta q, \quad (\text{C.1})$$

where δq is defined as the scalar part of the 3-momentum density $\delta T_i^0 \equiv \partial_i \delta q$. In the case of multiple fields, the stress-energy tensor 2.4 can be modified such that, instead of a single kinetic term, it includes a sum over the kinetic terms for each field. This leads to the following generalisations of Equations 2.5 and 2.6 for ρ and p :

$$\rho = \frac{1}{2} \sum_a \dot{\varphi}_a^2 + V(\varphi_1, \varphi_2, \dots), \quad (\text{C.2})$$

$$p = \frac{1}{2} \sum_a \dot{\varphi}_a^2 - V(\varphi_1, \varphi_2, \dots). \quad (\text{C.3})$$

The generalisation of the equation for δT_i^0 (with respect to t) in Equations 2.80 can also be determined very easily:

$$\delta T_i^0 = - \sum_a \dot{\varphi}_a \delta \varphi_{a,i} \equiv \partial_i \delta q, \quad (\text{C.4})$$

where δq was defined as $\delta q \equiv - \sum_a \dot{\varphi}_a \delta \varphi_a$. Putting everything together gives the final result for the multi field case:

$$\mathcal{R} = H \frac{\sum_a \dot{\varphi}_a \delta \varphi_a}{\sum_a \dot{\varphi}_a^2}. \quad (\text{C.5})$$

Finally, summing over only two fields gives the desired result for the hybrid inflation model:

$$\mathcal{R} = H \frac{\dot{\varphi} \delta \varphi + \dot{\chi} \delta \chi}{\dot{\varphi}^2 + \dot{\chi}^2}. \quad (\text{C.6})$$

In this context, φ represents the inflaton field and χ denotes the waterfall field.

C.2 Simulations versus 1-loop power spectra

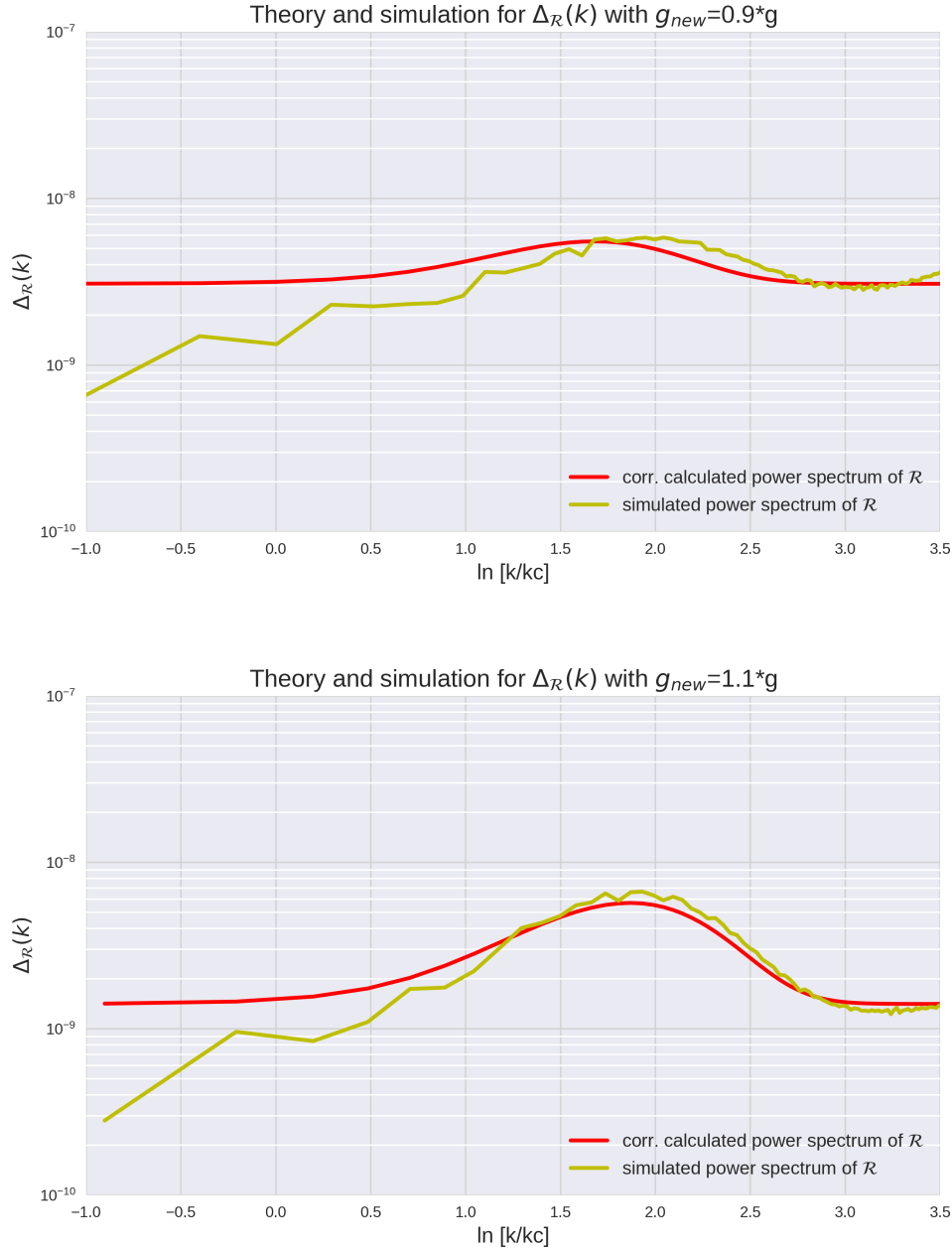


FIGURE C.1: Plots with $\lambda = 0.14$ and varying values of M : The parameters for M were selected based on those used in 5.28. It is evident that the agreement between the theoretical and simulated power spectrum at the peak is stronger for smaller values of M . This can be explained by the fact that for smaller M , ϵ_χ reaches approximately 11.2. In contrast, for larger M , ϵ_χ is only around 7.3. This demonstrates that sharper phase transitions, as expected, lead to a better fit between the theory and simulation.

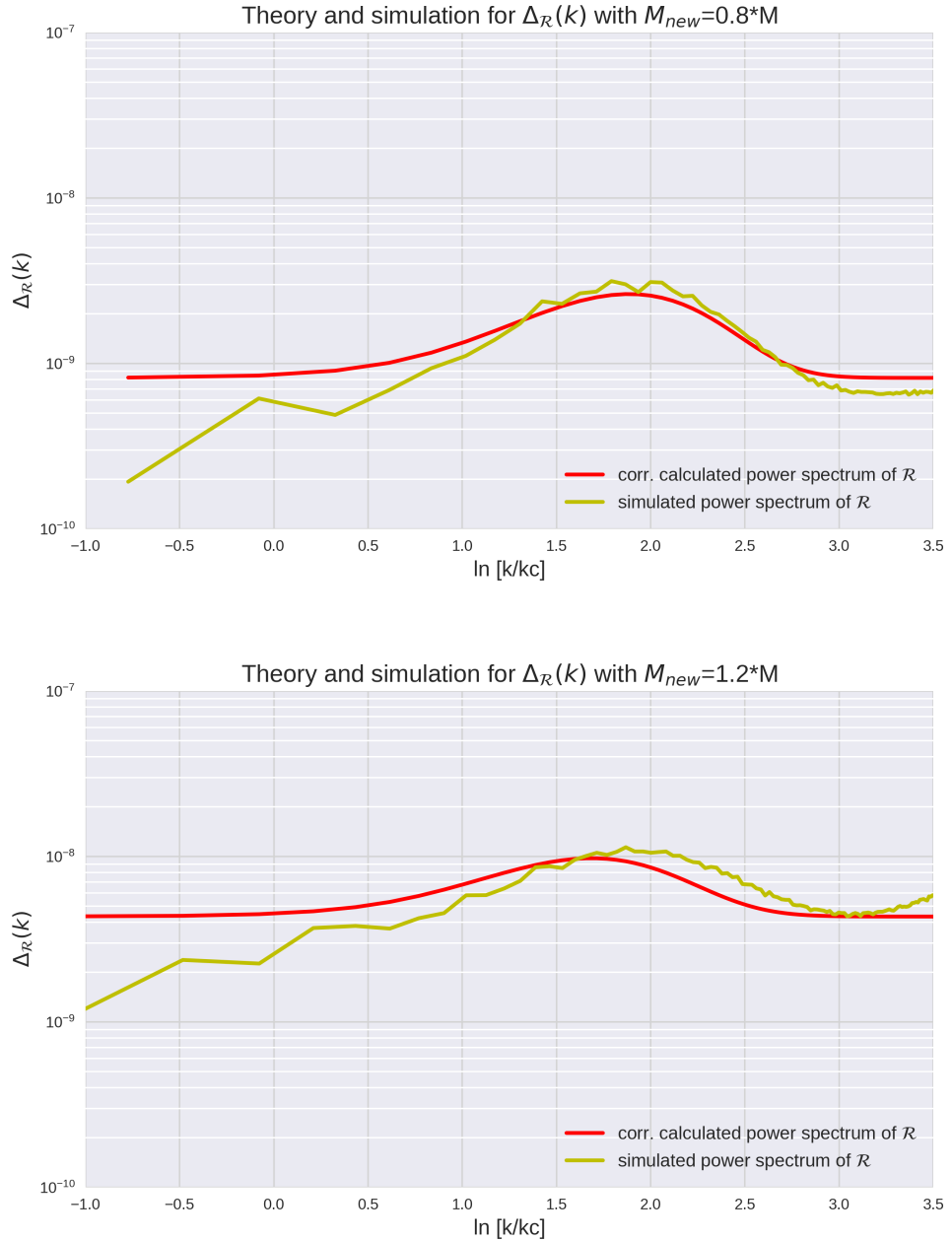


FIGURE C.2: Plots with $\lambda = 0.14$ and varying values of g : The parameters for g were adjusted according to those used in 5.28. It becomes clear that larger values of g result in better agreement between the theoretical and simulated power spectrum at the peak, with ϵ_χ reaching 10.7 for larger g , compared to only 7.3 for smaller g . This confirms that the mathematical approximation provides better results for sharper phase transitions.

Bibliography

- [1] A.A. Starobinsky. A new type of isotropic cosmological models without singularity. *Physics Letters B*, 91(1):99–102, 1980. ISSN 0370-2693. doi: [https://doi.org/10.1016/0370-2693\(80\)90670-X](https://doi.org/10.1016/0370-2693(80)90670-X). URL <https://www.sciencedirect.com/science/article/pii/037026938090670X>.
- [2] Alan H. Guth. The Inflationary Universe: A Possible Solution to the Horizon and Flatness Problems. *Phys. Rev. D*, 23:347–356, 1981. doi: 10.1103/PhysRevD.23.347.
- [3] A.D. Linde. A new inflationary universe scenario: A possible solution of the horizon, flatness, homogeneity, isotropy and primordial monopole problems. *Physics Letters B*, 108(6):389–393, 1982. ISSN 0370-2693. doi: [https://doi.org/10.1016/0370-2693\(82\)91219-9](https://doi.org/10.1016/0370-2693(82)91219-9). URL <https://www.sciencedirect.com/science/article/pii/0370269382912199>.
- [4] Sean M. Carroll. Lecture notes on general relativity, 1997. URL <https://arxiv.org/abs/gr-qc/9712019>.
- [5] Robin Booth. The exochronous universe: a static solution to the einstein field equation, 2023. URL <https://arxiv.org/abs/2201.13120>.
- [6] A. Friedman. On the Curvature of space. *Z. Phys.*, 10:377–386, 1922. doi: 10.1007/BF01332580.
- [7] Daniel Baumann. Tasi lectures on inflation, 2012. URL <https://arxiv.org/abs/0907.5424>.
- [8] N. Aghanim. Planck2018 results: I. overview and the cosmological legacy of planck. *Astronomy & Astrophysics*, 641:A1, September 2020. ISSN 1432-0746. doi: 10.1051/0004-6361/201833880. URL <http://dx.doi.org/10.1051/0004-6361/201833880>.
- [9] Patrick Peter. Cosmological perturbation theory, 2013. URL <https://arxiv.org/abs/1303.2509>.

- [10] Hannu Kurki-Suonio. Cosmological perturbation theory i, 2024. URL <https://www.mv.helsinki.fi/home/hkurkisu/cpt/CosPer.pdf>.
- [11] V.F. Mukhanov, H.A. Feldman, and R.H. Brandenberger. Theory of cosmological perturbations. *Physics Reports*, 215(5):203–333, 1992. ISSN 0370-1573. doi: [https://doi.org/10.1016/0370-1573\(92\)90044-Z](https://doi.org/10.1016/0370-1573(92)90044-Z). URL <https://www.sciencedirect.com/science/article/pii/037015739290044Z>.
- [12] Daniel G. Figueroa, Adrien Florio, Francisco Torrenti, and Wessel Valkenburg. A modern code for lattice simulations of scalar and gauge field dynamics in an expanding universe. *Computer Physics Communications*, 283:108586, February 2023. ISSN 0010-4655. doi: 10.1016/j.cpc.2022.108586. URL <http://dx.doi.org/10.1016/j.cpc.2022.108586>.
- [13] Daniel G. Figueroa, Adrien Florio, Francisco Torrenti, and Wessel Valkenburg. The art of simulating the early universe. part i. integration techniques and canonical cases. *Journal of Cosmology and Astroparticle Physics*, 2021(04):035, April 2021. ISSN 1475-7516. doi: 10.1088/1475-7516/2021/04/035. URL <http://dx.doi.org/10.1088/1475-7516/2021/04/035>.
- [14] Robert H. Brandenberger. *The Early Universe and Observational Cosmology*. Springer Berlin Heidelberg, 2004. ISBN 9783540409182. doi: 10.1007/b97189. URL <http://dx.doi.org/10.1007/b97189>.
- [15] E. Komatsu. Seven-year wilkinson microwave anisotropy probe(wmap) observations: Cosmological interpretation. *The Astrophysical Journal Supplement Series*, 192(2):18, January 2011. ISSN 1538-4365. doi: 10.1088/0067-0049/192/2/18. URL <http://dx.doi.org/10.1088/0067-0049/192/2/18>.
- [16] Ali Akbar Abolhasani, Hassan Firouzjahi, Shahram Khosravi, and Misao Sasaki. Local features with large spiky non-gaussianities during inflation. *Journal of Cosmology and Astroparticle Physics*, 2012(11):012, nov 2012. doi: 10.1088/1475-7516/2012/11/012. URL <https://dx.doi.org/10.1088/1475-7516/2012/11/012>.
- [17] Ali Akbar Abolhasani and Hassan Firouzjahi. No large scale curvature perturbations during the waterfall phase transition of hybrid inflation. *Physical Review D*, 83(6), March 2011. ISSN 1550-2368. doi: 10.1103/physrevd.83.063513. URL <http://dx.doi.org/10.1103/PhysRevD.83.063513>.
- [18] David Wands, Karim A. Malik, David H. Lyth, and Andrew R. Liddle. New approach to the evolution of cosmological perturbations on large scales. *Physical Review D*, 62(4), July 2000. ISSN 1089-4918. doi: 10.1103/physrevd.62.043527. URL <http://dx.doi.org/10.1103/PhysRevD.62.043527>.